Universidade Federal do Rio Grande do Norte
Centro de Ciências Exatas e da Terra
Programa de Pós-Graduação em Geodinâmica e Geofísica

TESE DE DOUTORADO

Medium change monitoring using ambient seismic noise and coda wave interferometry: examples from intraplate NE Brazil and the Mid-Atlantic Ridge.

Autora:
VIRGINIE D'HOUR

Orientador:
Prof. Dr. ADERSON FARIAS DO NASCIMENTO
DGEF / PPGG / UFRN

Co-orientador:
Dr. MARTIN SCHIMMEL
ICTJA-CSIC, Barcelona, Espanha

Tese n.º 45 /PPGG.

Natal-RN, Agosto de 2015

UNIVERSIDADE FEDERAL DO RIO GRANDE DO NORTE
CENTRO DE CIÊNCIAS EXATAS E DA TERRA
PROGRAMA DE PÓS-GRADUAÇÃO EM GEODINÂMICA E GEOFÍSICA

TESE DE DOUTORADO

Medium change monitoring using ambient seismic noise and coda wave interferometry: examples from intraplate NE Brazil and the Mid-Atlantic Ridge.

Autora:

VIRGINIE D'HOUR

Tese apresentada em 01 de setembro de dois mil quinze, ao Programa de Pós-Graduação em Geodinâmica e Geofísica – PPGG, da Universidade Federal do Rio Grande do Norte - UFRN como requisito à obtenção do Título de Doutora em Geodinâmica e Geofísica, com área de concentração em Geofisica.

Comissão Examinadora:

Aderson Farias do Nascimento – UFRN – orientador

Jordi Julià Casas – UFRN

Francisco Hilário Rego Bezerra – UFRN

Marcelo Assumpção – USP

Lucas Vieira Barros – UnB

Natal-RN, Agosto de 2015.

UFRN / Biblioteca Central Zila Mamede.
Catalogação da Publicação na Fonte.

D´Hour, Virgine.

Medium change monitoring using ambient seismic noise and coda wave interferometry: examples from intraplate NE Brazil and the Mid-Atlantic Ridge / Virgine D´Hour. – Natal, RN, 2015.

141 f. : il.

Orientadora: Prof. Dr. Aderson Farias do Nascimento.
Co-Orientador: Prof. Dr. Martin Schimmel.

Tese (Doutorado) – Universidade Federal do Rio Grande do Norte. Centro de Ciências Exatas e da Terra. Programa de Pós-Graduação Geodinâmica e Geofísica.

1. Ruído sísmico - Tese. 2. Auto correlação e correlação cruzada - Tese. 3. Interferometria de cauda da onda - Tese. 4. Intraplaca - Tese. 5. Dorsal meso-oceânica – Tese. I. Do Nascimento, Aderson Farias. II. Schimmel, Martin. III. Universidade Federal do Rio Grande do Norte. IV. Título.

RN/UF/BCZM CDU 621.391.822

AGRADECIMENTOS

Fica difícil citar todos que, de alguma forma, contribuíram e incentivaram a conclusão desta Tese de Doutorado. As chances de cometer injustiças existem, mas alguns nomes não podem deixar de ser citados nestes sinceros agradecimentos

Ao Dr. Aderson Farias do Nascimento pela consideração, competência e sinceridade no seu trabalho de orientação. Obrigada por ter me escutado e ajudado durante os momentos difíceis e por ter me apoiado durante esses 4 anos.

Ao Dr. Martin Schimmel pelas prestimosas sugestões e ajuda nos assuntos pertinentes a sua alçada, buscando sempre a clareza, objetividade e perfeição no aprimoramento das idéias.

Au Dr. Eloenore Stutzmann pour m'avoir si bien accueilli à l'IPGP et pour son aide et suggestions precieuses au cours de l'année passée.

Ao Pr. Zorano do PPGG pelo apoio e pelo empenho na liberação dos recursos financeiros necessários para o desenvolvimento deste trabalho de pesquisa.

À Secretária Nilda (PPGG) pela inegável competência e eficiência com que desenvolve suas funções.

À equipe técnica do Laboratório Sismológico: Eduardo Alexandre, Regina Spineli, Neymar Pereira e Rodrigo Pessoa, pela disponibilidade em ajudar.

Ao PPGG / UFRN pela oportunidade de realização do trabalho..

À CAPES pela bolsa concedida. Ao Programa Ciência sem Fronteiras pela bolsa sanduíche em Barcelona.

Ao INCT - Estudos Tectônicos (CNPq) e Peg- BR.

Ao LabSis, pelos dados cedidos.

A special thanks for my husband Jorge who stood by my side during these 4 years and supported me in the most difficult moments.

Un grand merci à mes parents Florence et Alain ainsi qu'à ma soeur Caroline, pour m'avoir toujours soutenu dans mes choix.

Aos companheiros do PPGG e do LabSis e pelas sugestões, pelos momentos de alegria e descontração: Rafaela, Rosana, Ygor, Heleno, Daniel, Guilherme, Esteban e Flodoaldo.

Resumo

Esta tese apresenta e discute os resultados de correlação do ruído sísmico em dois contextos distintos: Regiões intraplaca e Dorsal Meso-oceânica. O método de interferometria de cauda da onda também foi utilizado para os dados da região intraplaca.

A correlação do ruído sismico é um método que permite obter a resposta estrutural entre dois receptores à partir de registros de ruido sismico, como se uma das estações atuasse como uma fonte virtual. Esta técnica é amplamente utilizada em sismologia para obter a imagem do subsolo e para monitorar mudanças estruturais associadas principalmente com erupções vulcânicas e terremotos de grande magnitude.

No estudo da região intraplaca, foi possivel detectar mudanças estruturais localizadas relacionadas com esta pequena sequência de terremotos, cujo evento principal é de m_R 3.7, no Nordeste do Brasil. Nós também mostramos que a normalização de 1-bit e o branqueamento spectral provoca perdas de detalhes na forma da onda e que a auto-correlação de fase, que não é sensível à amplitude, parece ser mais sensível e robusta para a nossa análise de uma sequencia de pequenos terremotos. A análise de 6 meses de dados usando correlações cruzadas detecta claramente alterações do meio logo após o evento principal, enquanto as auto-correlações detectam alterações após 1 mês. Isso pode ser explicado pela redistribuição da pressão do fluido ocasionada pelas mudanças hidromecânicas e novos caminhos preferenciais mais rasos, devido a terremotos que ocorrem mais tarde.

No estudo da Dorsal Meso-oceânica, investigamos as mudanças estruturais associadas a um terremoto de m_b 4.9 ao longo da falha transformante de São Paulo. Os dados foram registrados pela única estação sísmica localizada a menos de 200 km da Dorsal Meso-oceânica. Os resultados da auto-correlação de fase por um período de 5 meses, mostram uma forte mudança de meio co-sísmica seguido por uma recuperação pós-sísmica relativamente rápida. Esta mudança do meio provavelmente está relacionada aos danos causados pelo terremoto de m_b 4.9. O processo de cicatrização (enchimento das novas fissuras) que durou 60 dias pode ser decomposto em duas fases, uma recuperação rápida na fase pós-sísmica precoce (70% em ~30 dias) e uma recuperação relativamente lenta depois (30% em ~30 dias).

No estudo de interferometria de cauda da onda, monitoramos mudanças temporais do subsolo causada pela sequência de pequenos terremotos intraplaca mencionado anteriormente. Primeiro, o método foi validado com dados sintéticos. Fomos capazes de detectar uma mudança de posição da fonte de 2.5% e uma redução de 15% da quantidade dos espalhadores. Depois, a partir dos dados reais, observamos uma decorrelação rápida de cauda da onda após do evento sísmico m_R 3.7. Isso indica uma mudança rápida do subsolo na região da falha induzida pelo terremoto.

Palavras-chave: ruído sísmico, auto-correlação e correlação cruzada, interferometria de cauda da onda, intraplaca, Dorsal Meso-Oceânica.

Abstract

This thesis presents and discusses the results of ambient seismic noise correlation for two different environments: intraplate and Mid-Atlantic Ridge. The coda wave interferometry method has also been tested for the intraplate data.

Ambient noise correlation is a method that allows to retrieve the structural response between two receivers from ambient noise records, as if one of the station was a virtual source. It has been largely used in seismology to image the subsurface and to monitor structural changes associated mostly with volcanic eruptions and large earthquakes.

In the intraplate study, we were able to detect localized structural changes related to a small earthquake swarm, which main event is m_R 3.7, North-East of Brazil. We also showed that the 1-bit normalization and spectral whitening result on the loss of waveform details and that the phase auto-correlation, which is amplitude unbiased, seems to be more sensitive and robust for our analysis of a small earthquake swarm. The analysis of 6 months of data using cross-correlations detect clear medium changes soon after the main event while the auto-correlations detect changes essentially after 1 month. It could be explained by fluid pressure redistribution which can be initiated by hydromechanical changes and opened path ways to shallower depth levels due to later occurring earthquakes.

In the Mid-Atlantic Ridge study, we investigate structural changes associated with a m_b 4.9 earthquake in the region of the Saint Paul transform fault. The data have been recorded by a single broadband seismic station located at less than 200 km from the Mid-Atlantic ridge. The results of the phase auto-correlation for a 5-month period, show a strong co-seismic medium change followed by a relatively fast post-seismic recovery. This medium change is likely related to the damages caused by the earthquake's ground shaking. The healing process (filling of the new cracks) that lasted 60 days can be decomposed in two phases, a fast recovery (70% in ~30 days) in the early post-seismic stage and a relatively slow recovery later (30% in ~30 days).

In the coda wave interferometry study, we monitor temporal changes of the subsurface caused by the small intraplate earthquake swarm mentioned previously. The method was first validated with synthetics data. We were able to detect a change of 2.5% in the source position and a 15% decrease of the scatterers' amount. Then, from the real data, we observed a rapid decorrelation of the seismic coda after the m_R 3.7 seismic event. This indicates a rapid change of the subsurface in the fault's region induced by the earthquake.

Key words: ambient seismic noise, auto- and cross-correlation, coda wave, interferometry, intraplate, Mid-Atlantic Ridge.

Table of Contents

ÍNDICE DE FIGURAS

ÍNDICE DE TABELAS

LISTA DE SÍMBOLOS E ABREVIATURAS

m_R	Regional Magnitude
m_b	Body-wave Magnitude
C_{cc}	Classical cross-correlation
C_{pcc}	Phase cross-correlation
u	Seismic noise records
t	Time lag
T	Correlation window length
τ_0	Time lag at 0
$\varphi(\tau)$	Instantaneous phases of u_1
$\gamma(\tau)$	Instantaneous phases of u_2
ϑ	Factor used to control the sensitivity of the C_{pcc}
R	Correlation coefficient
t_s	Time shifted
u_{unp}	Unperturbed wave field
u_{per}	Perturbed wave field

Chapter 1

Introduction

In this introduction, I give general information concerning this thesis. I expose the objectives of my work, and introduce the methods and the two different studied areas present in this thesis.

1.1 Objectives

The main objective of this thesis is to detect small structural changes related to small magnitude earthquake ($m_b < 6$) in particular geological context such as intraplate and Mid-Atlantic Ridge. We used two set of data:

- One related to an intraplate sequence of events in São Caetano, NE Brazil in which the main event had a magnitude of m_R 3.7.
- One related to a m_b 4.9 earthquake in Saint Peter and Saint Paul archipelago (SPSPA) that is located at less than 200 km from the equatorial Mid-Atlantic Ridge.

Another objective of this work is to compare different techniques and determine the one that gives the most refined results in São Caetano and SPSPA. We compared the following techniques: coda wave interferometry, ambient seismic noise classical auto- and cross-correlation and phase auto- and cross-correlation.

Finally, from these analysis we can extract important information that help us to understand better:

- The behavior of an intraplate medium submitted to a seismic swarm of a small intensity.
- The post-seismic behavior of a medium located near the Mid-Atlantic Ridge.
- The type of healing process that take place near the Mid-Atlantic Ridge.

1.2 Ambient seismic noise

1.2.1 What is "ambient seismic noise"?

Ambient seismic noise can be defined as a signal without recognizable seismic signature (Figure 1.1) and that is not reproducible (Scales et al., 1998). It can be produced by industries, wind, ocean tides, teleseismic earthquakes, etc. There are three main advantages of using ambient seismic noise to monitor the subsurface. First, the seismic noise is recorded continuously so it is possible to obtain an everyday analysis. Second, this method is non-invasive so the studied medium is not anthropologically modified. Third, we do not need information about the source as in the case of multiplets analysis.

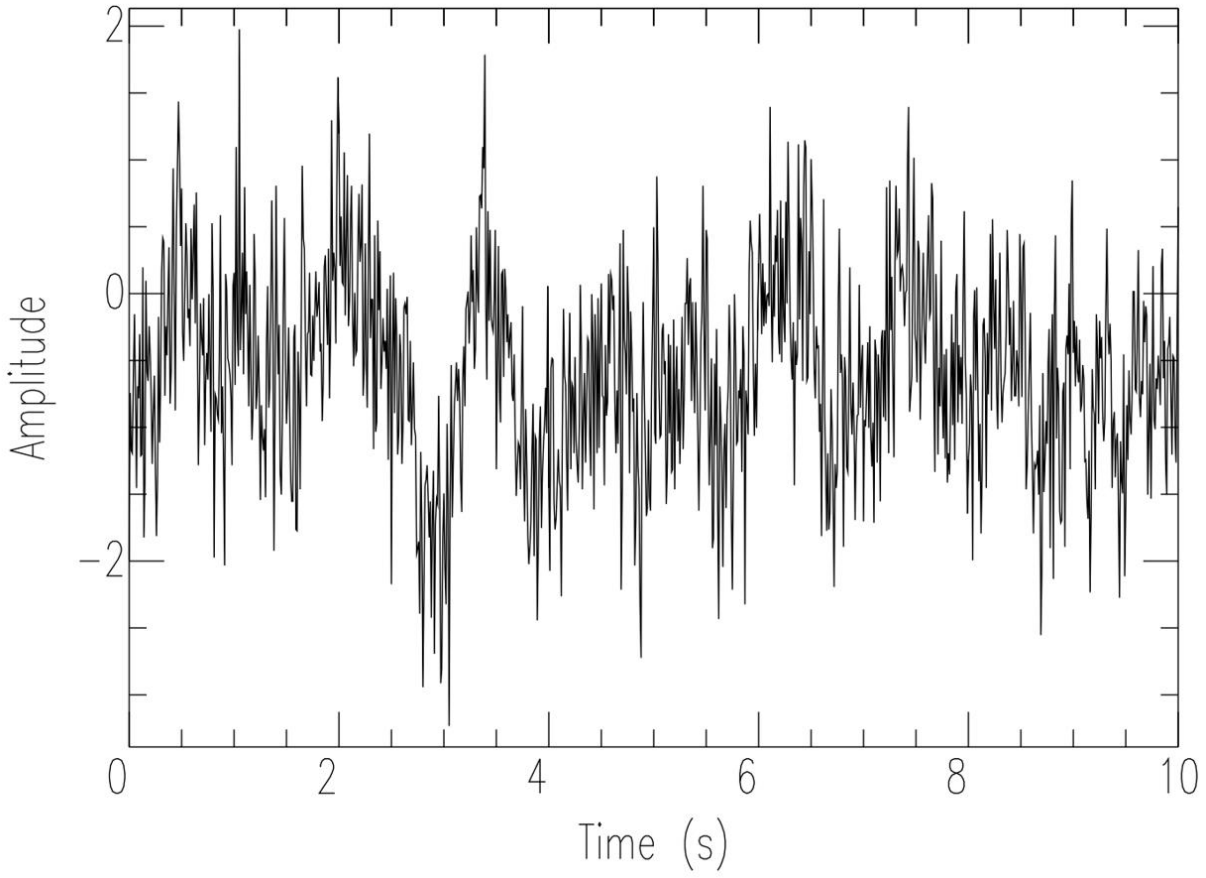

Figure 1.1: Plot of 10 seconds of raw seismic noise (data from São Caetano - Chapter 2) after removing the mean and the trend.

Ambient seismic noise is a signal obtained from a superposition of simultaneously uncorrelated sources that propagated through a same medium (Wapenaar et al., 2010). So, the correlated responses of this signal correspond to the reflection response of the medium. Early successful results of seismic responses retrieval from noise correlations were obtained in the field of acoustics (Weaver and Lobkis, 2001, 2002).

Also, the convergence of the correlations to the reflection response is strongly influenced by the variations in the spatial distribution of the noise sources and the spectral content of the noise (Roux, 2005). For this reason, ambient seismic noise correlation is computed for data filtered in a chosen frequency band.

1.2.2 Ambient seismic noise interferometry

Interferometry is an investigation's technique based on the superposition of two signals in a way that it will give meaningful information about the medium. In ambient seismic noise interferometry, we correlate the seismic noise to obtain reflection responses of the medium at different time. So, we can measure the temporal evolution of the medium.

1.2.2.1 Principles

Interferometry techniques have been first used in the domain of astronomy (Michelson and Morley, 1887). It arrived later in geophysics with the study of Claerbout (1968) that drew up the hypothesis of using seismic noise interferometry to investigate the shallow subsurface.

The principle of interferometry is to compare quantitatively two signals by cross-correlating them at different time lag (arrow in Figure 1.2). In Figure 1.2 a and b, we can observe ambient noise recorded at the same time by two different stations. From the cross-correlation of these two signals, we obtain two important measures: the correlation's coefficient (cc) and the time shift (ts).

The correlation's coefficient is a diagnosis of the resemblance between the two investigated signals. The time shift represents the time it takes to a source in a) to be recorded in b).

Figure 1.2 c represents the results of the cross-correlation between the signals a and b. We can note that the cross-correlation is not symmetric, which means that the noise source is not entirely equipartitioned.

In addition, the correlation coefficient of one hour of signal is low. It shows that the noise is uncorrelated for a small period of time (Wapenaar et al., 2010) and that it is necessary to average the correlations over weeks or months of data (Sabra et al., 2005; Larose et al., 2008). However, we have to be aware that the longest the averaging time-window is, the lowest is our temporal resolution. The result of this stack is called correlogram. By comparing the correlograms from one day to another, we can obtain the temporal evolution of the medium. We can use the correlation from one station (auto-correlation) or/and two stations (cross-correlation). So, the auto-correlation is a particular case of cross-correlation where a signal is correlating with itself.

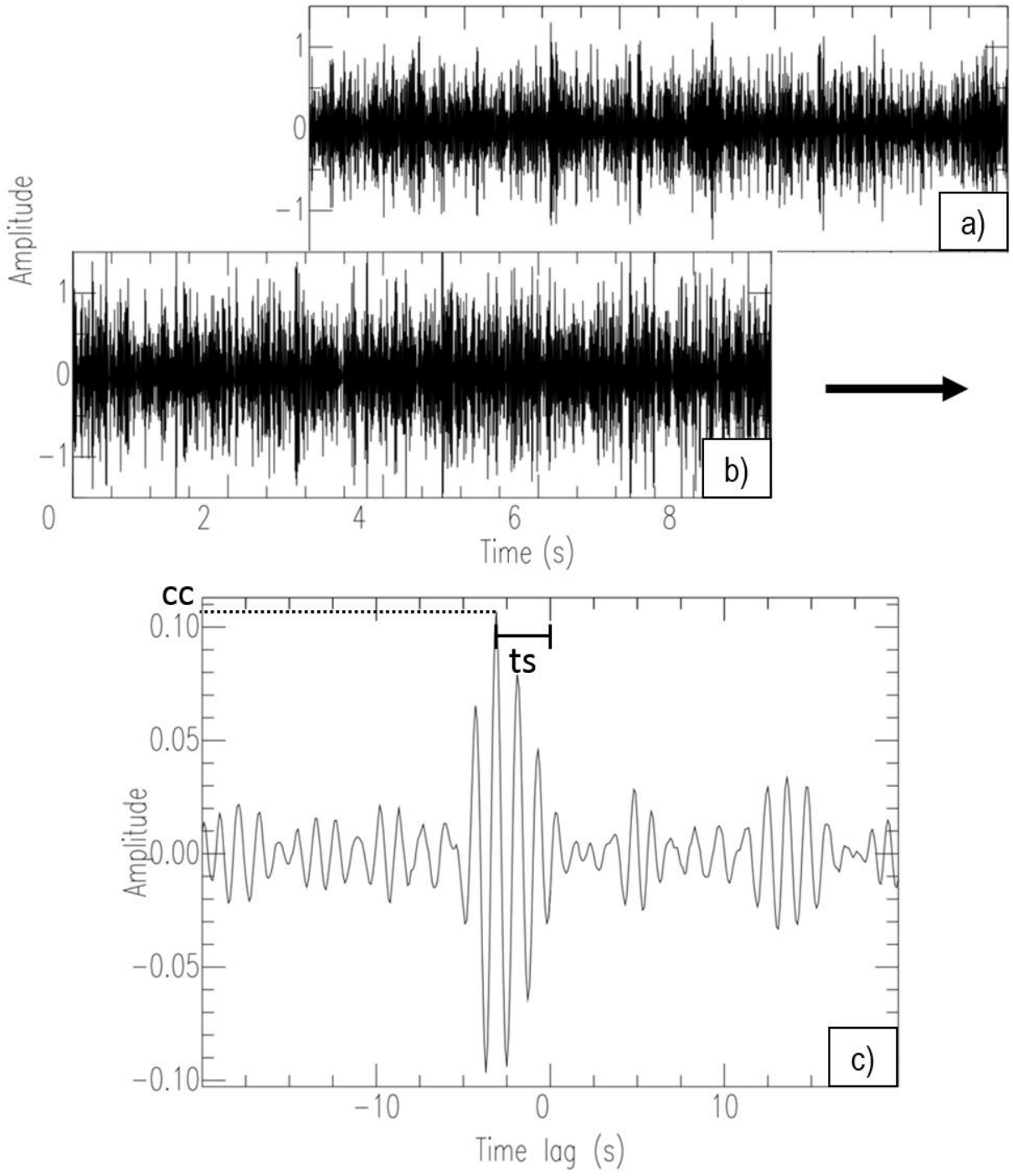

Figure 1.2: 10 seconds of two seismic noise filtered 0.7-1.4 Hz (a and b) recorded by two different seismometers. c) Result of their cross-correlation highlighting the correlation's coefficient (cc) and the time shift (ts). The arrow show that after each measure, the signal b is shifted to get a measure at a different time lag. These data are from São Caetano 2007 (Chapter 2).

In this method, earthquakes, with their high amplitude and characteristic signature, are regarded as anomalies and the noise sources needs to be sufficiently diffuse (e.g., Lobkis and Weaver, 2001). For these reasons, absolute amplitude normalization (1-bit) and spectral whitening (Bensen et al., 2007) are generally applied in order to suppress high amplitude earthquakes and isolated noise sources with a defined frequency. These normalizations are illustrated Figure 1.3. Figure 1.3 a and b show a 2-8 Hz band-passed data and its frequency contents, respectively. The 1-bit normalization divides, at each time, the recorded amplitude by its absolute amplitude. The purpose of this preprocessing is to eliminate the strong amplitudes of isolated sources. The spectral whitening equalizes the spectrum of the signal by enhancing low level spectral components and attenuating high level ones, making it similar to the white noise spectrum (spectral amplitude equal to one). Its aim is to remove the influence of signals which manifest in amplitude spectra such as frequency-localized noise sources. The downside of these normalizations is that we lose waveform details, manifests in a less sensitive signal extraction. Figure 1.3 c and d show the data after 1-bit normalization and spectral whitening in the time and frequency domain, respectively. We can see that the signal has become more uniform in both time and frequency domain.

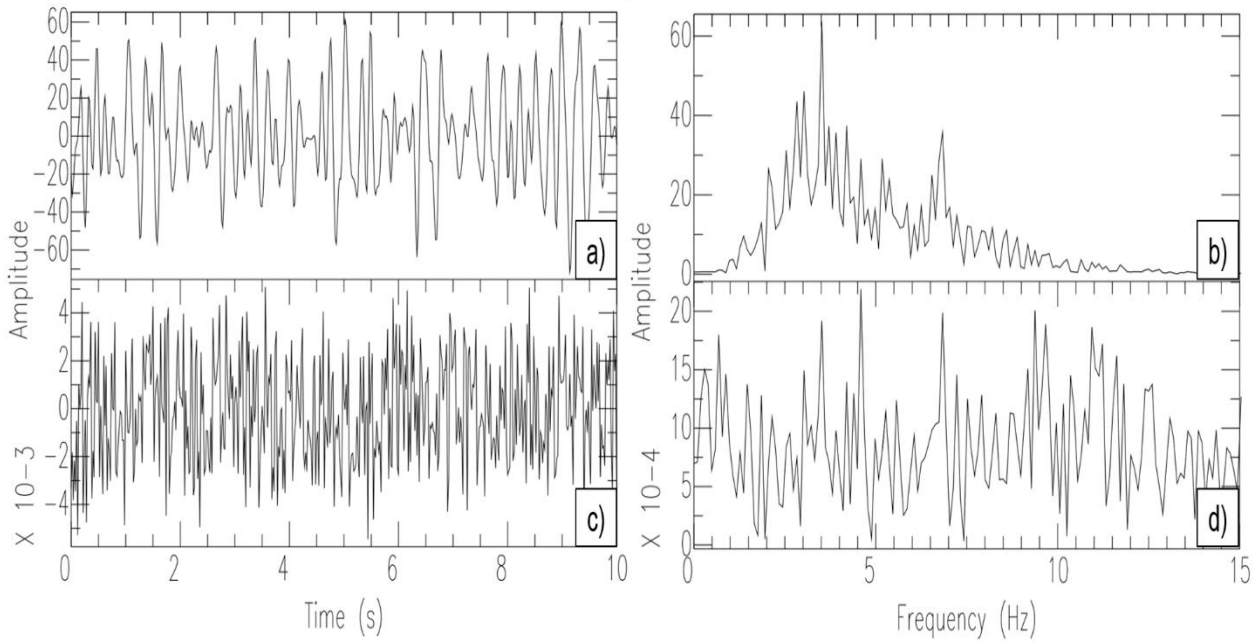

Figure 1.3: 2-8 Hz data in the time (a) and frequency (b) domain. Data after 1-bit normalization and spectral whitening in the time (c) and frequency (d) domain. These data are from São Caetano 2007 (Chapter 3).

1.2.2.2 Classical Cross-Correlation and Phase Cross-Correlation

In this thesis, two correlation methods have been used to compute the noise auto-correlation and cross-correlation: the classical cross-correlation (CC) and the phase cross-correlation (PCC) by Schimmel (1999).

The CC method (Wapenaar et al., 2010a and 2010b) corresponds to the reflection response between two receivers convolved with the auto-correlation of the source function.

$$C_{cc}(t) = \sum_{\tau=\tau_0}^{\tau_0+T} u_1(t+\tau)u_2(\tau) \qquad (1.1)$$

where u_1 and u_2 are the two time-series and where t and T are the time lag and correlation window length, respectively. τ_0 is the start time of the correlation window. The time lag t is applied to u_1.

CC needs time (1-bit normalization) and spectral (spectral whitening) normalizations (Figure 1.3) before its computation to not be influenced by abnormally large amplitude signals.

In another hand, PCC is a method that measures the similarity of the instantaneous phases of the analytic traces. So it is amplitude unbiased and does not need temporal and spectral normalizations. It evaluates quantitatively the goodness of waveform fit between two time series as function of lag time (Schimmel, 1999). It equally weights every sample in the correlation window.

$$C_{pcc}(t) = \frac{1}{2T}\sum_{\tau=\tau_0}^{\tau_0+T}\left\{\left|e^{i\varphi(t+\tau)} + e^{i\gamma(\tau)}\right|^{\vartheta} - \left|e^{i\varphi(t+\tau)} - e^{i\gamma(\tau)}\right|^{\vartheta}\right\} \qquad (1.2)$$

where $\varphi(\tau)$ and $\gamma(\tau)$ are the instantaneous phases of u_1 and u_2 (eq. 1.1), t is the lag time, as for the classical cross-correlation and ϑ is a factor which allowed to increase the sensitivity when $\vartheta>1$.

When the signals are perfectly correlated, the last term in the summation becomes 0 at all samples τ ($C_{pcc}(t) = 1$). For anti-correlated signals, this term becomes 2 while the first term has 0 amplitude ($C_{pcc}(t) = -1$). If there is no correlation, both terms almost equal ($C_{pcc}(t) \approx 0$). So PCC measures the waveforms similarity between two data sets as function of lag time with an amplitudes ranging between - 1 and 1.

Then, the correlations from any of both methods are stacked linearly to obtain stable correlograms. Here stable correlograms means that the results do not change significantly by adding more data. It means also that the correlograms converge to the reflection response of the studied medium.

1.2.3 Different applications

Ambient seismic noise correlation has been used in numerous studies. It has been largely used for crustal tomography. The first crustal tomography studies were realized by Sabra et al. (2005) and Shapiro et al. (2005) for the southern California area. They show

that this method has the unique ability to image crustal structure without using earthquakes or artificial seismic source. Then, several other studies applied this technique to get an image of the crust all over the world: New Zealand (Lin et al., 2007), Spain (Villaseñor et al., 2007), Korea (Cho et al., 2007), Japan (Nishida et al., 2009), U.S.A. (Moschetti et al., 2007; Lin et al.,2007; Yang et al., 2008; Bensen et al., 2008, 2009), Europe (Yang et al., 2007), Australia (Saygin and Kennett, 2010), Tibet (Yao et al. 2006; Yang et al., 2010), Brazil (Dias et al., 2014), among other places.

Other studies showed seasonal variations of the seismic velocity (e.g., Sens-Schönfelder and Wegler, 2006; Meier et al., 2010) induced by changes in the ground-water aquifer. Others showed seismic velocity changes associated with volcanic eruptions (e.g., Ratdomopurbo and Poupinet, 1995; Snieder and Hagerty, 2004; Brenguier et al., 2008a; Obermann et al., 2013).

In this thesis, we show that it is possible to detect small structural changes related to earthquakes of small magnitude ($m_b < 6$) in an intraplate and oceanic ridge environment using ambient seismic noise correlation (Chapter 2 and 3). Previous studies used it to measure structural changes nearby large earthquakes ($m_b > 6$) in different kind of geological context. Some studies has been done in subduction zone, for example in Japan (e.g., Wegler and Sens-Schönfelder, 2007; Wegler et al., 2009; Takagi et al., 2012; Hobiger et al., 2012). Other studies were realized along the San Andreas fault and more particularly near Parkfield (Brenguier et al., 2008b; Zhao et al., 2010; Schaff, 2012). Also, others took interest in zone of plates' collisions as in the Sichuan province (Chen et al., 2010; Liu and Huang, 2010; Liu et al., 2014) or on the contrary in extensional context as in L'Aquila (Zaccarelli et al., 2011).

1.3 Coda waves

1.3.1 What are "coda waves"?

Coda waves correspond to the signal that arrives after the first arrivals. This signal is often considered as noise. However, it has been shown in previous studies that coda waves are repeatable under the same conditions. It proves that they carry information about the medium (e.g., Grêt, 2004; Snieder et al., 2007; Wapenaar et al., 2010). Several situations can illustrate the different mechanisms of coda-wave creation (Figure 1.4): a - the case of a wave guide in which the P wave is bouncing back and forth between two boundaries many times; b - the case of surface waves, in which they can circle the earth many times and c - heterogeneities in the medium of propagation leading P-wave scattering so that the P wave is going to rebound several times within the medium before being recorded.

As the coda waves are repeatable, it means that if the waveforms are different, the medium has changed. So we actually compare two waveforms, one has propagated through an unchanged and one through a changed medium. It is the principle of interferometry.

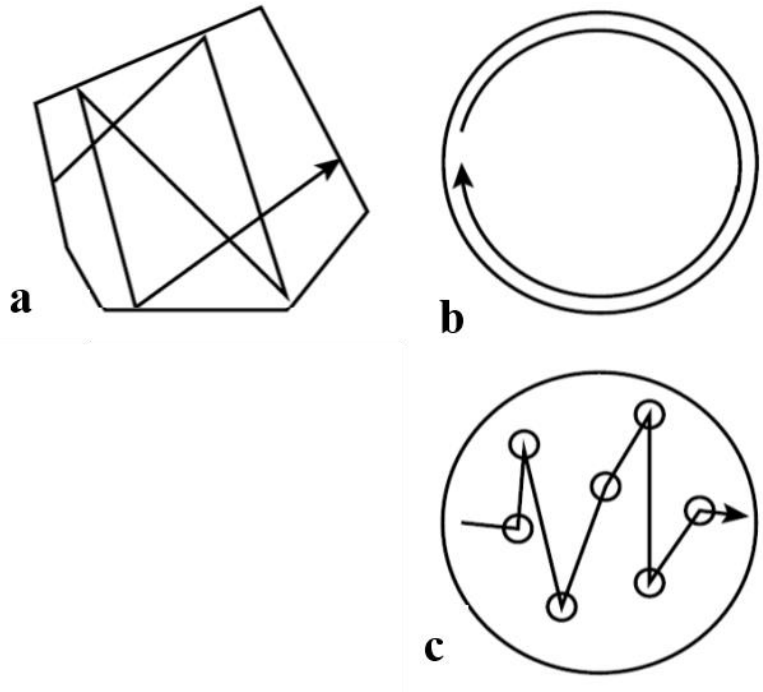

Figure 1.4: After Grêt, 2004. Cartoon of different wave modes that may co-exist in a medium. a) The waves go straight back and forth between two boundaries, as a bouncing ball. b) Surface waves that propagate along the boundary, circling the medium once or more. c) Multiple scattering from small-scale scatterers (small circles) in the medium.

Moreover, the coda waves' propagation path is longer and confined in a limited area making them more sensitive to small changes. It means that a change may not be visible on the P wave, while it is on the coda wave (Figure 1.5). This property is the reason why Coda Wave Interferometry (Snieder et al., 2002; Snieder, 2002) is a good tool for monitoring purposes. However, this technique has a limitation. It requires a repeatable source, active (airgun, explosion) or passive (co-located events or repeatable noise). In Chapter 4, for instance, we used co-located events to detect small medium changes using this technique.

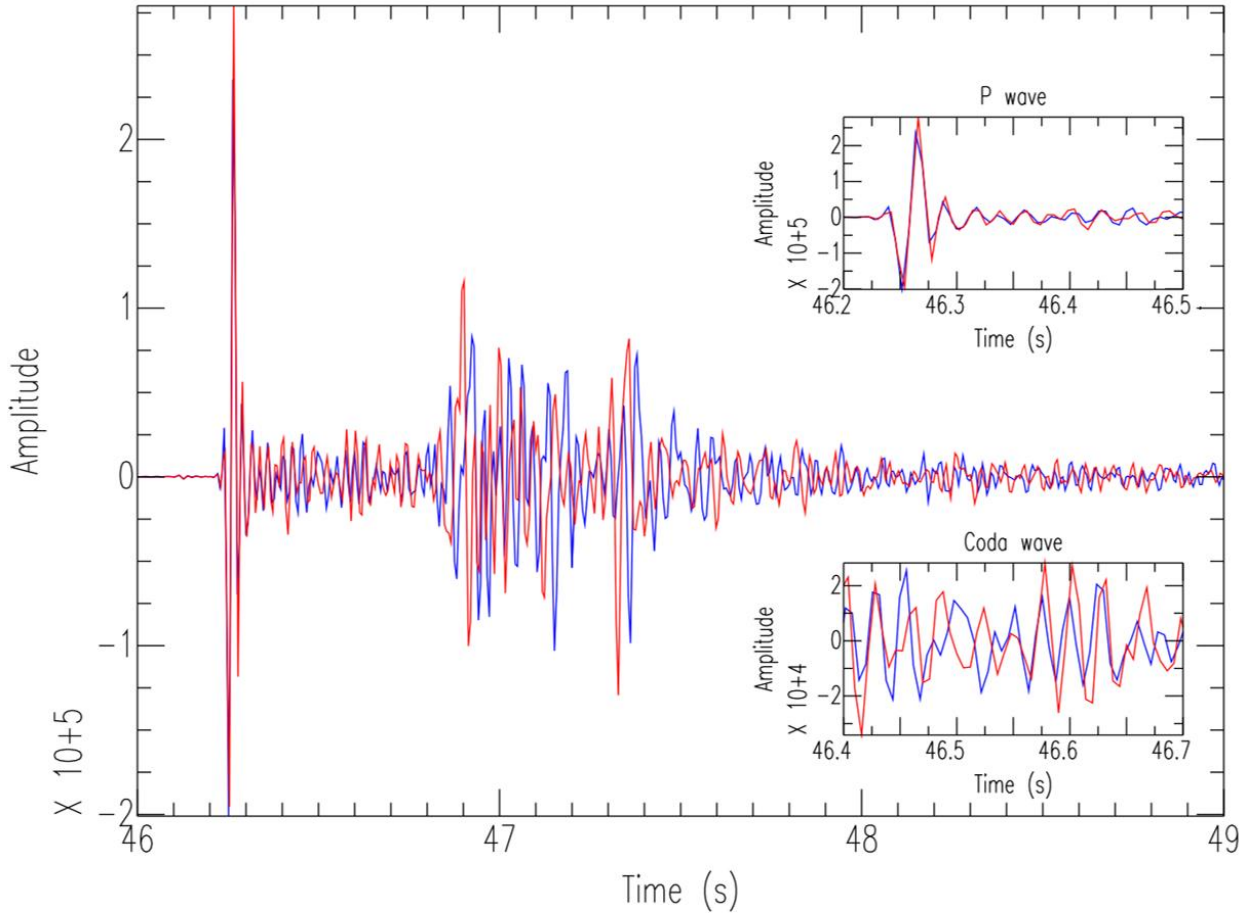

Figure 1.5: Seismic signal of two co-located event from the 2007 São Caetano swarm (Chapter 4). On the top right is a zoom on the P wave and on the bottom right a zoom on the coda wave. The P wave of the co-located events are similar while the coda wave changed. The signals have been filtered 1-30 Hz.

1.3.2 Coda wave interferometry

The basic principles of CWI remain the same than for the ambient seismic noise interferometry (Chapter 1 - 2.2). However, in Coda Wave Interferometry (CWI) method, the two signals used in the correlation correspond to the coda waves of two co-located events (multiplets) that occurred at different time. In this case, we can study the temporal evolution of the medium by measuring their subtle differences on the waveforms. This method, unlike the ambient seismic noise interferometry, is dependent of the source

characteristics (localization, focal mechanism, magnitude). So a preliminary characterization of the source is needed to establish groups a similar events, called clusters.

If we use two co-located events recorded by the same station, we can consider that both waves have travelled across the same ray path. As they occur at two different date, any travel-time differences (time shift) between the two signals can be interpreted as a change in the medium that occurred between the first and the second event. By consequence, CWI gives information on how much the medium has changed in a certain period of time.

CWI is based on the correlation of two signals (equation 1.1), an unperturbed signal (before the medium change) and a perturbed signal (after the medium has changed). This principle is described by the following equation from Snieder (2002):

$$C_{up}^{(t,t_w)}(t_s) \equiv \int_{t-t_w}^{t+t_w} u_{unp}(t')u_{per}(t'+t_s)dt' \qquad (1.3)$$

where the window is centered at time t with duration $2t_w$, t_s is the time shifted used in the cross-correlation, u_{unp} is the unperturbed wave field and u_{per} the perturbed wave field.

Then, we want to obtain a measure of the wave field change, which is the cross-correlation coefficient (R). R characterizes how similar two signals are, when R=1 the signals are identical. The time-windowed cross-correlation's coefficient is defined as:

$$R^{(t,t_w)}(t_s) \equiv \frac{\int_{t-t_w}^{t+t_w} u_{unp}(t')u_{per}(t'+t_s)dt'}{(\int_{t-t_w}^{t+t_w} u_{unp}^2(t')dt' \int_{t-t_w}^{t+t_w} u_{per}^2(t')dt')^{1/2}} \qquad (1.4)$$

Also, the time shift is given by how much the maximum of correlation is shifted. It corresponds to the arrival time difference between the signal recorded before the perturbation and the signal recorded after the perturbation. It is the tool that we use to quantify a change in the medium.

1.3.3 Different applications

As described in the previous paragraphs, coda wave interferometry has been often used to monitor small changes in a medium. In Chapters 4, we monitor medium changes due to an intraplate seismic swarm of small magnitude (m_R < 3.7). In this case, CWI is well indicated as we are dealing with small medium changes.

Because of the high sensitivity of the coda waves, CWI has been used for medium monitoring in order to detect structural changes in volcanoes (Ratdomopurbo and Poupinet, 1995; Baisch and Bokelmann, 2001; Vidale and Li, 2003; Niu et al., 2003; Snieder, 2004).

It has also been used for the monitoring of mines (Grêt et al., 2006), nuclear waste (Grêt, 2004; Snieder et al., 2007) and CO_2 sequestration (Khatiwada et al., 2012).

It has also been used to determine seismic velocity changes in laboratory specimens (Roberts et al., 1992; Snieder et al., 2002; Grêt et al., 2006), volcanoes (Ratdomopurbo and Poupinet, 1995; Grêt et al., 2005) and fault zones (Poupinet et al., 1984; Larose et al., 2010).

1.4 Areas of study

1.4.1 São Caetano

São Caetano is located on the Pernambuco Lineament, in the Borborema province. The Borborema Province is largely responsible for the South American intraplate seismicity. The seismicity in this region is not uniform and is characterized by long-lasting earthquake sequences of small magnitude m_b < 5.0 (Berrocal et al., 1984; Ferreira et al., 1998; Bezerra et al., 2011).

The first historical earthquake (1807) had an estimated magnitude of m_b 4.8 while the largest recorded earthquake had a magnitude of m_b 5.2 and occurred in 1980 in Cascavel, State of Ceará (Assumpção et al., 1985). Earthquakes of approximately m_b 5.0 are really rare (Bezerra et al., 2011) in this region (about 5 in 200 years). The seismicity in this region spread from 20 to 300 km from the coast, at depths between 1 and 12 km (Bezerra et al., 2011).

The Pernambuco Lineament is one of the most active fault of the Borborema province. It is a 700 km long shear fault that was created during the Brasiliano orogeny ~750–500 Ma ago (Brito Neves et al., 2000). It forms an "intercontinental" lineament that continues in Africa as the Garoua/Sanaga shear fault (Trompette, 1994). Nowadays, it is considered as inactive but the feature still represents a weak zone (Lopes et al., 2010) that may break when submitted to the present stress field. Indeed, four main earthquake sequences were identified along the Pernambuco shear zone: in 1991 with normal earthquakes $m_b < 1.8$ (Ferreira et al., 1998; Ferreira et al., 2008) and in 2002 with strike-slip earthquakes $m_b < 3.5$ (Ferreira et al., 2008) near the city of Caruaru, in 2004 with normal earthquake $m_b < 3.1$ (Lopes et al., 2010) near the city of Belo Jardim, and in 2007 with strike-slip earthquakes $m_R < 3.7$ (Lima Neto et al., 2011; Chapter 2 and 5 of this thesis) near the city of São Caetano.

More precisely, in the neighbourhood of São Caetano city (inset Figure 1.6), the major recorded seismic event had a magnitude of m_R 4.0 (Brazilian earthquake magnitude scale as in Assumpção, 1983) and occurred on the 20/05/2006 near Santa Luzia town. Before 2006, no seismic activity has been reported. Since then, the seismicity remains more active with the occurrence of seismic events of smaller magnitude, though. After this m_R 4.0 event, a seismic network was deployed in 2007 in the epicentral area for almost 6 months in order to study this new seismicity (Lima Neto et al., 2011; D'Hour et al., 2015, Chapter 2 and 4).

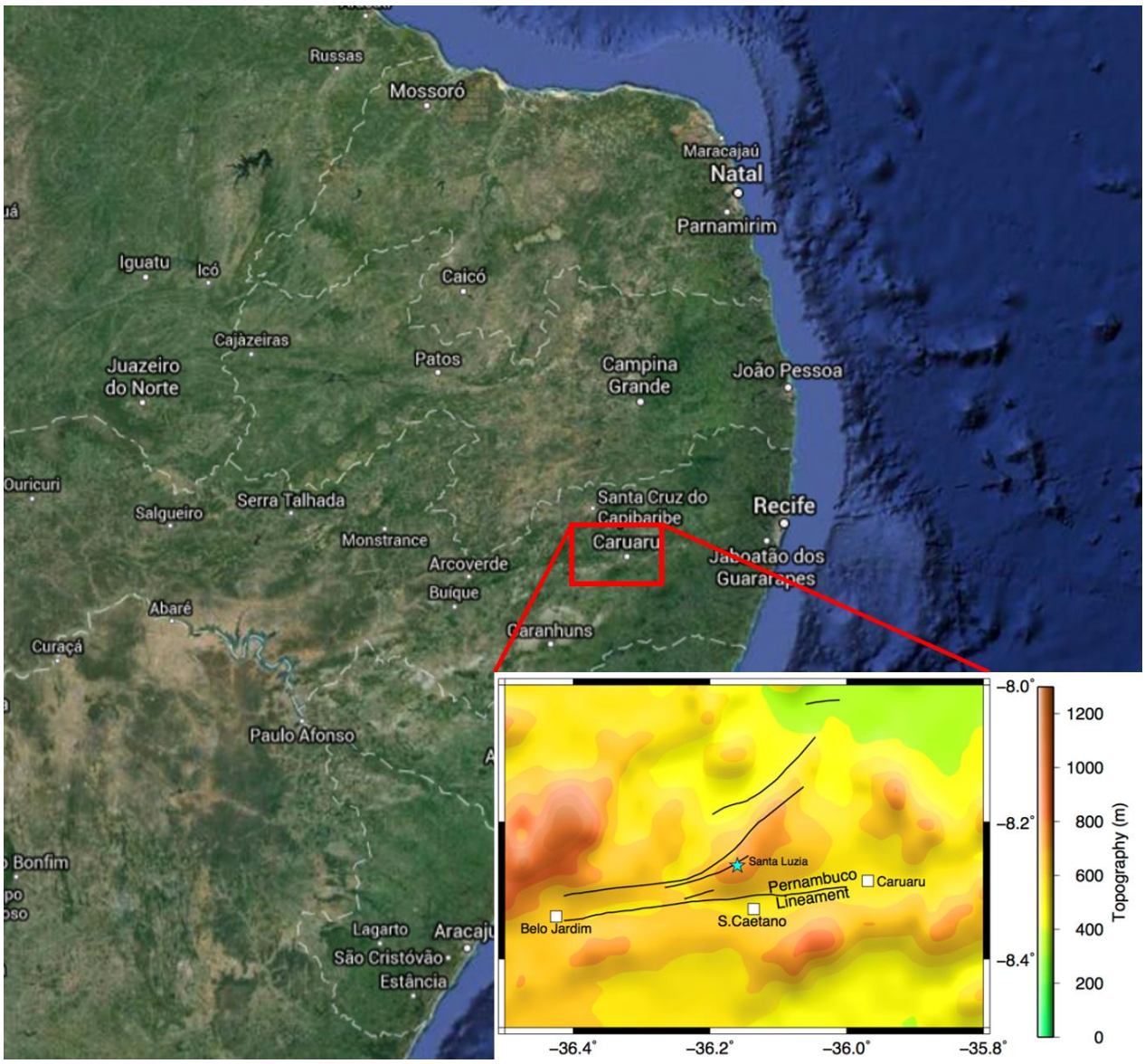

Figure 1.6: Map (from Google Earth) showing the approximate location of the São Caetano region (red rectangle). The inset shows the location of the cities where seismicity was observed and the Pernambuco Lineament. The blue star indicate the epicentres of the 2007 m_R 3.7 seismic event.

1.4.2 Saint Peter and Saint Paul Archipelago

The Saint Peter and Saint Paul Archipelago (SPSPA) is located at about 1,100 km off the coast of north-eastern Brazil (Figure 1.7), slightly on the north of the Equator (00º55.1' N, 29º20.7' W). These small islets belongs to Brazil and consists of six relatively large islands, four smaller ones, and several rock tops. The archipelago has a total emerged area of approximately 17,000 m², a maximum altitude of 18 m and the distance between the extreme points is about 420 km (Miguens, 1995). The archipelago is the emerged part of a submarine mountain chain, which covers an area of over 400 km².

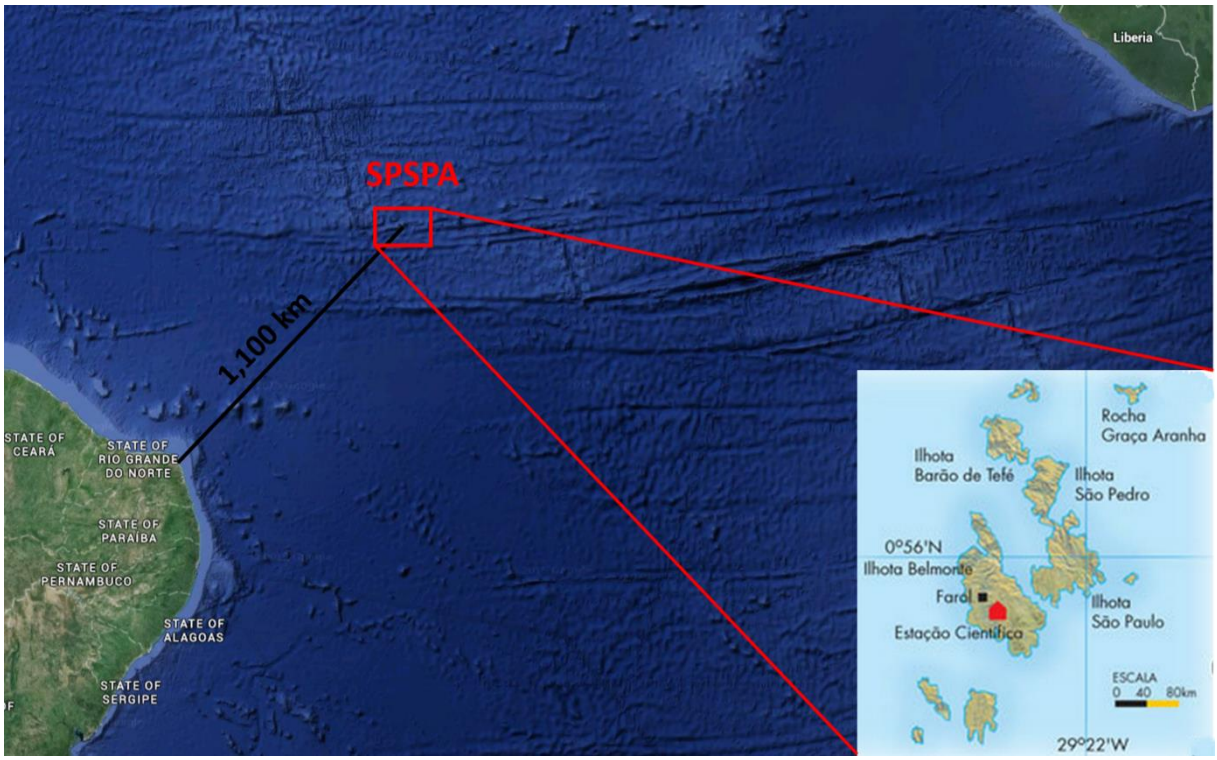

Figure 1.7: Map (from google earth) showing the position of the Saint Peter and Saint Paul archipelago (SPSPA). The SPSPA schematic representation is also shown with the location of the seismic station (from the website "http://horizontegeografico.com.br/exibirMateria/57/-tsunami-no-atlantico", 16/07/2015).

This submarine chain rises from a depth of about -4 km (Figure 1.8). The bathymetry of the archipelago shows that the chain has a sunken relief exhibiting elongated elevations

like a crest, with gentle slope in the EW direction and strong declivity in the NS direction. It stands parallel, north side, to the Saint Paul transform fault at less than 200 km from the Mid-Atlantic Ridge.

Unlike the majority of the islands along accretionary boundaries, the SPSPA does not have a volcanic origin (Palmiotto 2013, Sichel et al. 2008). Also, Bonatti (1990) shows that the SPSPA corresponds to sub-continental mantle that was tectonically uplifted. The SPSPA represents one of the rare case of tectonic formatted islands on the planet.

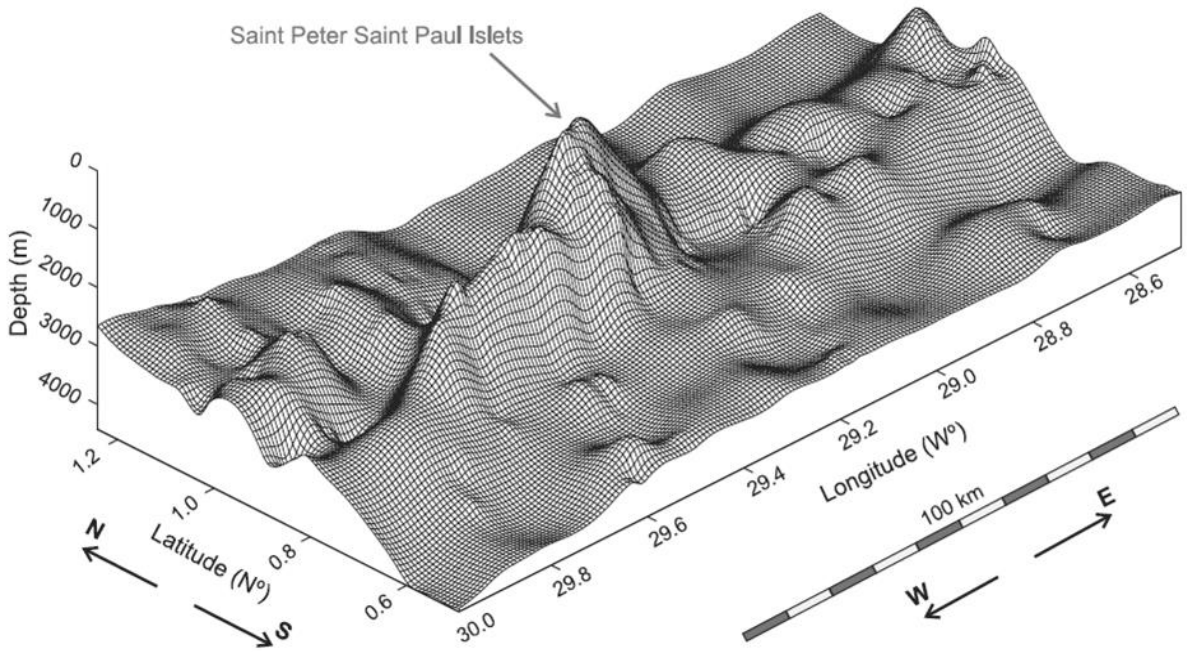

Figure 1.8: View the SPSPA bathymetry, based on predicted bathymetry resolution of 1.8 km, from Motoki et al. (2009). The vertical scale is exaggerated in 12 times the horizontal scale.

A scientific station was established on the SPSPA's largest island (Belmonte) in 1998 and then in 2011 seismic equipment (one broadband sensor and one strong motion sensor)

were added. This area is seismically active and located in a very particular place. It makes this data a really rare occasion to understand better the mechanisms of a transform fault that cut the Mid-Atlantic Ridge.

1.5 Summary of this thesis

This thesis is a collection of three articles, one accepted for publication, two submitted.

Chapter 2 corresponds to an analysis of the medium perturbation related to the 2007 sequence of events $m_R < 3.7$ near São Caetano (Chapter 1.4.1). This analysis was done using ambient seismic noise interferometry (Chapter 1.2). It shows that, using PCC, it was possible to detect small medium changes.

Chapter 3 shows the study of the SPSPA region when submitted to a m_b 4.9 earthquake located at 32 km from the single station of the area. This analyses uses ambient seismic noise to detect temporal changes in the auto-correlations. It also presents the preliminary analyses of medium changes in the SPSPA region related to earthquakes occurring in 2013 and 2014. This work is not finished yet but it is promising for a future submission.

Chapter 4 shows the results of São Caetano medium monitoring during the 2007 swarm using this time CWI.

We will finish this thesis by giving general considerations about this thesis and future works.

Chapter 2

Detection of subtle medium changes, NE Brazil*

2.1 Abstract

Ambient noise correlation analyses are largely used in seismology to map heterogeneities and to monitor the temporal evolution of seismic velocity changes associated mostly with stress field variations and/or fluid movements. Here we analyse a small earthquake swarm related to a main m_R 3.7 intraplate earthquake in North-East of Brazil to study the corresponding post-seismic effects on the medium. So far, post-seismic effects have been observed mainly for large magnitude events. In our study, we show that we were able to detect localized structural changes even for a small earthquake swarm in an intraplate setting. Different correlation strategies are presented and their performances are also shown. We compare the classical auto-correlation with and without pre-processing, including 1-bit normalization and spectral whitening, and the phase auto-correlation. The worst results were obtained for the pre-processed data due to the loss of waveform details. The best results were achieved with the phase cross-correlation which is amplitude unbiased and sensitive to small amplitude changes as long as there exist waveform coherence superior to other unrelated signals and noise. The analysis of 6 months of data using phase auto-correlation and cross-correlation resulted on the observation of a progressive medium change after the major recorded event. The progressive medium change is likely related to the swarm activity through opening new path ways for pore fluid diffusion. We further observed for the auto-correlations a lag time frequency-dependent change which likely indicates that the medium change is localized in depth. As expected, the main change is observed along the fault.

.

*The main content of this chapter has been accepted for publication in *Pure Appl. Geophys.*

2.2 Introduction

Monitoring medium changes is important for a better understanding of the Earth dynamics expressed at the Earth surface through volcanic and seismic activities, and by thus improving prevention systems of these hazards. It is used also for industrial applications to monitor local dynamics as those induced by e.g., gas and petroleum extraction, waste deposits, mine activity, or CO_2 sequestration. Initially, monitoring medium changes consisted in seismological analyses based essentially on the first arrival waves from an artificial source or the analysis of waveform changes in earthquake doublets but which occurred at different times (e.g., Poupinet et al. 1984; Baisch and Bokelmann 2001, Gret et al., 2004).

In the last decade, monitoring medium changes gained increasing interest due to the recent progress in understanding the seismic noise wave field and its usage for monitoring (e.g., Snieder, 2004b; Brenguier et al., 2008a; Hadziioannou et al., 2011) and imaging studies (e.g., Campillo and Paul, 2003; Shapiro et al., 2005). The seismic noise wave field can be used for monitoring structural changes whenever the noise wave field does not change its characteristics (Zhan et al., 2013). The principle of this method is to retrieve signals, which contain the structural response of the medium from noise cross-correlations (Lobkis and Weaver, 2001; Derode et al., 2003; Wapenaar, 2004; Snieder, 2004a; Roux et al., 2005, among others). Besides the cross-correlations between two stations, auto-correlations of the noise wave field recorded at one station can be employed to monitor medium changes (e.g., Sens-Schönfelder and Wegler, 2006; Hobiger et al., 2014; Nakahara, 2015). There are many advantages of using ambient seismic noise to monitor temporal variations of the Earth structure. First, using noise correlations allows to discard source parameters, as its location and focal mechanism. Second, the seismic noise is continuously available, which results in a dense temporal coverage of measurements. And third, it is a non-invasive or destructive monitoring method. For these reasons, this method has been applied in many studies, including earthquake monitoring (Wegler and Sens-

Schonfelder, 2007; Brenguier et al., 2008b; Ohmi et al., 2008; Wegler et al., 2009; Minato et al., 2012; Zaccarelli et al., 2011; Hobiger et al., 2014) and volcano monitoring (e.g., Sens-Schönfelder and Wegler, 2006; Mordret et al., 2010).

In this work, we focus on the detection of medium changes due to a m_R 3.7 (Brazilian earthquake magnitude scale as in Assumpção, 1983) intraplate earthquake using the seismic ambient noise wave field. The hypocentre is located near Sao Caetano town, NE of Brazil, and the main shock was followed by a sequence of low-magnitude seismic and micro seismic events (typically below m_R 1.0). Also, the main event has a low magnitude and the expected impact on the medium is much lower than for larger events (above m_b 6.0) as usually analysed in previous noise-based monitoring studies on earthquake hydromechanical effects on the medium (e.g., Wegler and Sens-Schönfelder, 2007; Wegler et al., 2009; Roux and Ben-Zion, 2013).

All these monitoring studies are based on the classical cross-correlation approach and may differ in the applied data pre-processing. Here, we show that the phase cross-correlation (PCC) by Schimmel (1999) is also suited to detect medium changes. PCC is based on the instantaneous phase coherence concept used in the phase weighted stacks (Schimmel and Paulssen, 1997). The PCC is amplitude unbiased and has been introduced to noise correlation studies in Schimmel et al. (2011). They demonstrated that PCC due to its phase sensitivity is more efficient when there are large amplitude variations which could hide waveform similarities when using the classical cross-correlation.

This manuscript is divided into five parts. Section 2 describes the geological background of the studied area and the data configuration. In section 3, we explain the different methods used for the data processing, show their performances and explain our choice for the subsequent data processing which we present in section 4. Then in section 5, we show the main auto- and cross-correlation analysis and their results. Finally, in section 6, we discuss our results and interpretations.

2.3 Studied area and data configuration

We studied data from São Caetano in the state of Pernambuco, North East of Brazil. This area is cut by the Pernambuco lineament and its ramifications (Fig. 2.1), which appeared during the Brasiliano orogeny (600 Ma). São Caetano is located in the Boborema province, intraplate setting, which means that earthquakes occur rarely and with small magnitude. The largest event recorded during the last 200 years in this region had a magnitude of m_b 5.2 known as Pacajus earthquake, 1980 (Bezerra et al., 2011).

A m_R 3.7 event (dextral strike slip) occurred on the 20/03/2007 in a NE-trending branch of the Pernambuco shear zone. Lima Neto et al. (2013) determined that this event and its aftershocks occurred along a fault ~ 4 km long with a depth ranging between 2 and 8 km, all of them on the same fault plane that have a dip of 60° south. Lopes et al. (2010) proposed that this ramification represents a "weak zone", which, combined with the present-day stress field (N-S tension), led to the reactivation of this fault segment (Sykes, 1978; Ferreira et al., 2008). However, other geological structures under the same conditions have not shown any seismicity, which means that other local factors must be taken into account to explain the observed seismicity cases (Lopes et al., 2010).

In May 2006, a m_R 4.0 event occurred in the same São Caetano area. After this event, a local five-station network (SOJO, SOCA, SOLC, SOMA and SOFI) was deployed in the epicentral area for almost 6 months (01/02/2007 - 21/07/2007). The stations were equipped with short period S13J sensors (three components with 1 Hz frequency) and SMART24® dataloggers recording at 100 sps. A total of 214 events were detected during this period (Lima Neto et al. 2013). The data quality of the stations SOCA and SOFI was not satisfactory for our purposes and we therefore based the following analysis on the data from the stations SOJO, SOLC and SOMA (red triangles on the map Figure 2.1). Unfortunately, the data from the station SOJO has two time gaps from the 25/02/2007 to the 09/03/2007 and from the 15/04/2007 to the 15/05/2007. This station is particularly important for our study because it is located close to the epicentre of the main event (blue star, Fig. 2.1).

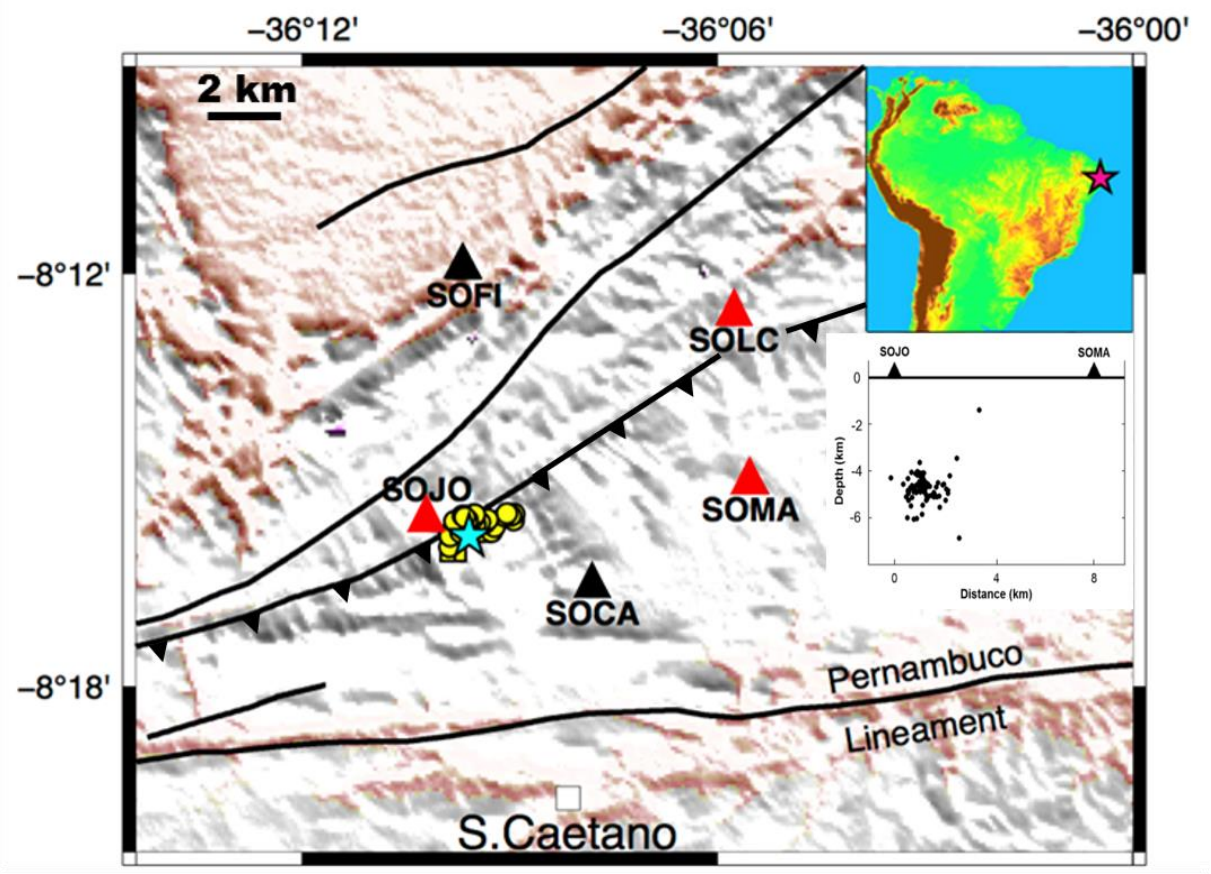

Figure 2.1 : Map showing the fault system of the studied region, the location of the available short-period stations (triangles) and the distribution of the events occurring during the studied period (small yellow circles) including the main event (20/03/2007) of magnitude m_R 3.7 (blue star). The red triangles mark the stations which provided continuous data of satisfactory quality for our study. The bottom inset shows the hypocentres along the trajectory SOJO-SOMA.

2.4 Data processing

The main processing steps are common and consisted in (1) pre-processing, (2) cross-correlation and (3) cross-correlogram stacking (e.g., Bensen et al. 2007; Schimmel et al. 2011). In order to improve the convergence of the noise correlation function, this processing is performed in a selected frequency band (Roux et al. 2005). Throughout this

study, we used the vertical component from the short period stations shown by the red triangles in Figure 2.1. In the following, we briefly outline the different processing steps.

We started data pre-processing by cutting the continuous data into non-overlapping segments of 60 min length and performing a visual inspection of the data to detect data problems. As we used the same seismometer with the same frequency response and a short frequency band, we did not need to remove the instrument response for our monitoring purpose. Further, the data have been band-passed using a zero phase Butterworth filter to reduce the frequency band to the one where we expected to observe the best signal to noise ratio (SNR). We basically worked, for the auto-correlation, in the 2-8 Hz band. These frequencies have also been used in other previous studies (Wegler et al., 2009; Wegler and Sens-Schönfelder, 2007, among others). It is not clear whether in this frequency band the auto-correlations are dominated by surface waves or body waves (e.g. Wegler et al., 2006; Nakahara, 2015) which can cause ambiguous interpretations. For the cross-correlation, we used a 0.7-1.4 Hz frequency band that are expected to contain mainly surface waves, due to the longer wave path between the stations.

After these data preparation steps, we applied a time- and frequency-domain normalization to the data, 1-bit normalization and spectral whitening, respectively. Different strategies can be used (e.g., Bensen et al., 2007) and their purpose is to make the cross-correlation results less sensitive to large amplitude signals, such as the ones caused by earthquakes or isolated strong narrow-band noise sources. The 1-bit normalization divides, at each time, the recorded amplitude by its absolute amplitude. And the spectral whitening is achieved, through a Fourier Transform to the frequency domain, by normalizing the amplitude spectra within the considered frequency band to one, and a back transform to the time domain. The phase spectra have not been manipulated. Both normalizations are frequently used in seismic noise studies and permit to balance the contributions to the cross-correlation results through attenuating the large amplitude signals and enhancing the weak amplitude signals.

The following step is the computation of cross- and auto-correlations. Here we used two different strategies: the classical cross-correlation (CC) and the phase cross-correlation

(PCC) by Schimmel (1999). The classical cross-correlation (eq. 2.1) is the most commonly used in ambient seismic noise monitoring studies.

$$C_{cc}(t) = \sum_{\tau=\tau_0}^{\tau_0+T} u_1(t+\tau)u_2(\tau) \qquad (2.1)$$

u_1 and u_2 are the seismic noise records and t and T are the time lag and correlation window length, respectively. The auto-correlation is a special case with $u_1 = u_2$.

In addition, we use the PCC (eq. 2.2) by Schimmel (1999) which has been introduced to noise studies in Schimmel et al. (2011).

$$C_{pcc}(t) = \frac{1}{2T}\sum_{\tau=\tau_0}^{\tau_0+T}\left\{\left|e^{i\varphi(t+\tau)} + e^{i\gamma(\tau)}\right|^{\vartheta} - \left|e^{i\varphi(t+\tau)} - e^{i\gamma(\tau)}\right|^{\vartheta}\right\} \qquad (2.2)$$

This approach measures the waveform similarity based on the instantaneous phases $\varphi(\tau)$ and $\gamma(\tau)$ of the time series u_1 and u_2, the lag time t, and the correlation window length T, as for the classical cross-correlation. ϑ is a factor which can be used to control the sensitivity. The instantaneous phases are obtained from the analytic signals of u_1 and u_2. This approach is amplitude unbiased and does not need time- and frequency domain normalized data (Schimmel et al., 2011). In fact, these normalizations deteriorate the noise waveforms which lead to poorer results with PCC.

Finally, both auto- and cross-correlations were stacked linearly to obtain robust correlation results with an increased SNR. The amount of correlograms to be stacked had been investigated for each station and for the auto and cross-correlations. Most stacks converge to a stable correlogram using a time window of 1-3 days as shown in the following section.

2.5 Comparison of CC with PCC

In this section we show the performance of the CC on both, with and without time- and frequency domain normalized noise data and compare the results with PCC. An example of stacked correlograms' convergence is also shown.

Figure 2.2 shows an example of noise auto-correlations obtained for station SOJO using the first 2 months of data. The data were band-pass filtered between 2-8 Hz and the auto-correlations (CC and PCC) were stacked using a moving window of 3 days. Figure 2.2a shows the corresponding auto-correlation stacks using CC on pre-processed data, i.e., employing the 1-bit normalization and spectral whitening. The Julian day corresponds to the centre time of the moving window used for the stack. Figures 2.2b and 2.2c show the auto-correlation stacks using respectively CC and PCC on data which have not been normalized, i.e., data that have not been processed using 1-bit normalization and spectral whitening. The red line marks the date of the main event (20/03/2007, Julian day 79) and the beginning of the earthquake swarm.

It is seen already from Figure 2.2a that stacking 3 days of noise auto-correlations is not sufficient to achieve stable auto-correlograms for the 2 months of data. While from Figures 2.2b and 2.2c, we can see that during the pre-event period there exist auto-correlograms which resemble each other for independent, non-overlapping time windows. This indicates that we likely see a structural response caused by heterogeneities rather than climatic changes or other non-stationary features.

The data used to obtain Figure 2.2b were not normalized and one can see that the auto-correlograms are affected by the earthquake swarm. Also, instrumental problems which happened during 2 hours on day 50 (marked with an X) are seemingly detectable as anomalous auto-correlograms which clearly do not resemble to the response we obtain for most of the other days. These features are expected (e.g., Bensen et al. 2007) and they are the main motivation to normalize the noise data during the pre-processing.

PCC were also applied on non-normalized data and it is seen that this approach is indeed amplitude unbiased since the resulting auto-correlograms (Fig. 2.2c) seem not to be affected by the instrumental problems or by larger amplitudes of the earthquakes after day 79. A visual comparison of, for instance the first days of Figures 2.2b and 2.2c show that

the CC and PCC auto-correlograms are quite similar for calm days, that is when CC is not being affected by large amplitude features in the noise data. On the contrary, the 3-day-stack auto-correlograms from Figure 2.2a do not exhibit similar traces. It shows that the noise data normalization, which has the disadvantage of losing waveform details, manifests in a less sensitive signal extraction.

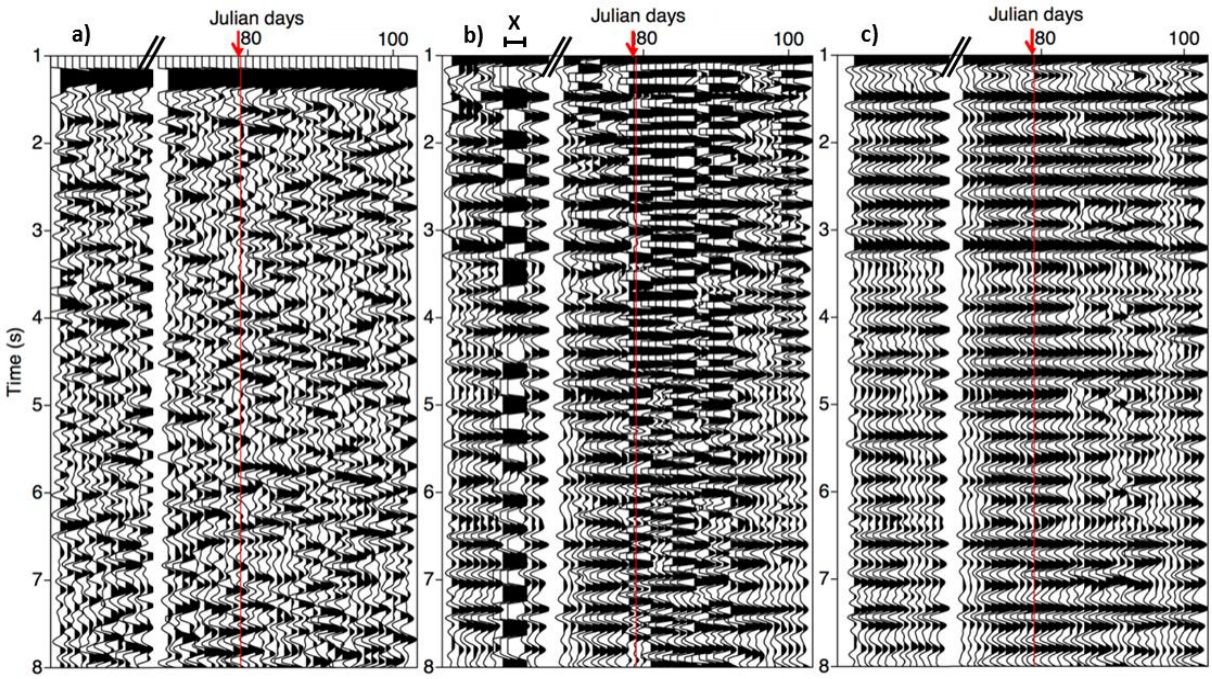

Figure 2.2: Record section of auto-correlations for 2-8 Hz band-passed noise recordings from station SOJO using a) the classical auto-correlation of pre-processed data (1-bit normalization, spectral whitening); b) the classical auto-correlation without pre-processing; and c) the phase cross-correlation. The correlograms were stacked using a moving window of 3 days. The red line shows the main event (Julian day 79) of the 4 months crisis. X marks the effect of anomalous signals due to instrument failure during less than 2h on day 50.

In Figure 2.3, we show the waveform convergence of the auto-correlation stacks (Figure 2.2) to a reference trace as function of time, i.e., as function of stacking length. The

data used for this analysis are from the pre-event period (before 20/03/2007, Julian day 79) and were selected randomly 10 times to show the robustness of the convergence. The waveform similarity was computed using the zero-lag CC geometrically normalized (eq. 6 in Schimmel et al., 1999) with respect to a reference trace which was obtained for each of the three approaches through stacking all available pre-event data. For this analysis, we removed 2 hours (18-20h) of the Julian day 50 to exclude abnormal high amplitudes due to instrument failure.

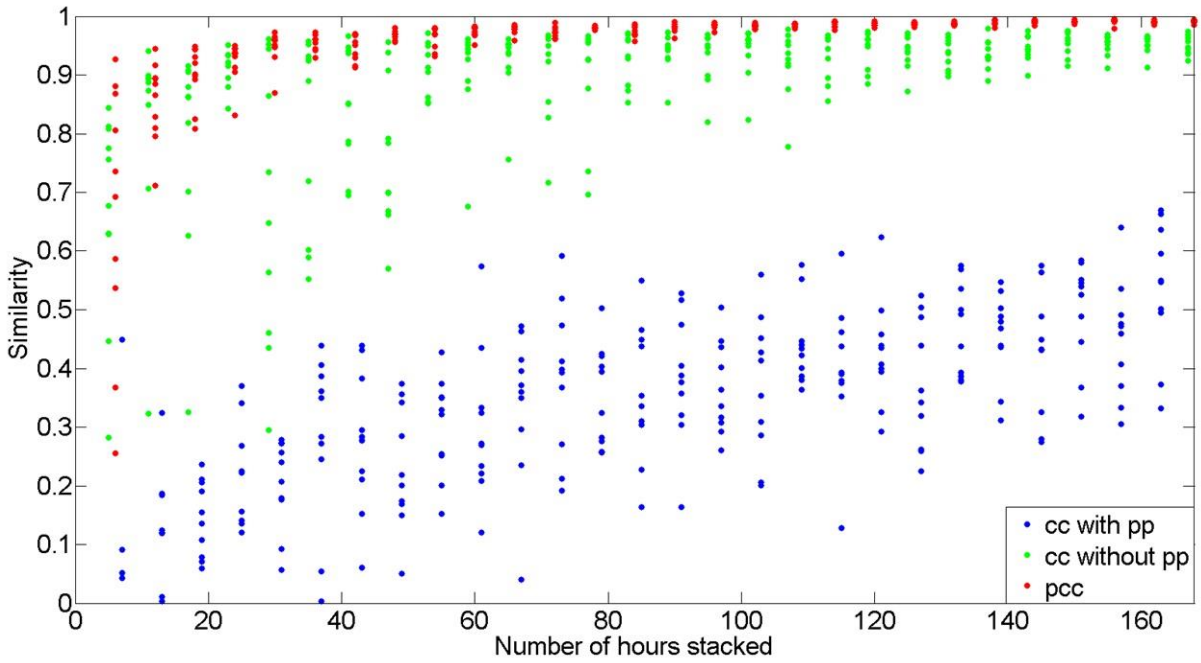

Figure 2.3: Waveform convergence of auto-correlation stacks as function of time, i.e., as function of data used in the stacks. The noise data used are from the pre-event period and have been selected randomly to show the robustness of the convergence. The colours distinguish the three cases: CC with pre-processing in blue, CC without pre-processing in green and PCC without pre-processing in red. Pre-processing here means 1-bit normalization and spectral whitening. A reference trace has been obtained for each method through stacking all available pre-event data.

It can be seen from Figure 2.3 that PCC (red dots) converges already after about 2 days. Also PCC seems to be more stable since the corresponding similarity is less variable

than for the other two methods. The CC applied on non-normalized noise data (Fig. 2.2b and green dots in Fig. 2.3) converges faster than the CC applied on normalized data (Fig. 2.2a and blue dots in Fig. 2.3) which strengthens that the noise data normalization may lead to a less sensitive signal extraction. The 1-bit normalization and spectral whitening are operations which alter in a non-unique manner a complex waveform. For instance, an infinite number of waveforms can have the same 1-bit representation of the data. This loss of information is the price one pays for the amplitude normalization. As consequence, more data is needed to extract signals from the noise. In conclusion PCC seems to be more sensitive and robust for our analysis of a small earthquake swarm.

2.6 Analysis and results of the full data processing using PCC

2.6.1 Auto-correlation

As shown in the previous section, we obtained the best results using PCC. In the following part, we applied PCC to the entire data set to analyse the structural response due to the earthquake swarm. The stations SOJO and SOMA were the only ones converging after stacking over less than five days so the next results will be shown for these two stations.

At the station SOJO, which is the closest from the main event location, a three day stack is enough for the waveforms to converge (red dots, Fig. 2.3). Figure 2.4 shows the auto-correlograms' section of 6 months of data. One can see that until approximately the Julian day 83 the waveforms are stable, which corresponds to three to five days after the main event (red line on Fig. 2.4). Then, the signals get disturbed and it seems that we observe two types of frequency regimes (I and II on Fig. 2.4), beginning somewhere within the data gap from days 103 to 136. It seems that the post event period can be divided into an immediate post-event period and a second period which starts about one month later. Regime II, between approximately 3 and 6.5 s, seems to be different from the rest of the auto-correlogram by showing higher frequency waveforms. A zoom into these regimes is

shown in Figure 2.5 (Figs. 2.5a and 2.5c for regime I and Fig. 2.5b for regime II). This lag time localization is not expected for structural changes which happen everywhere beneath and around the station. It is possibly an indicator of structural changes which are spatially localized. A similar frequency change is observed for station SOMA, but the starting time of regime II is ambiguous. The transition from regime II to I? is at about 7s for this station.

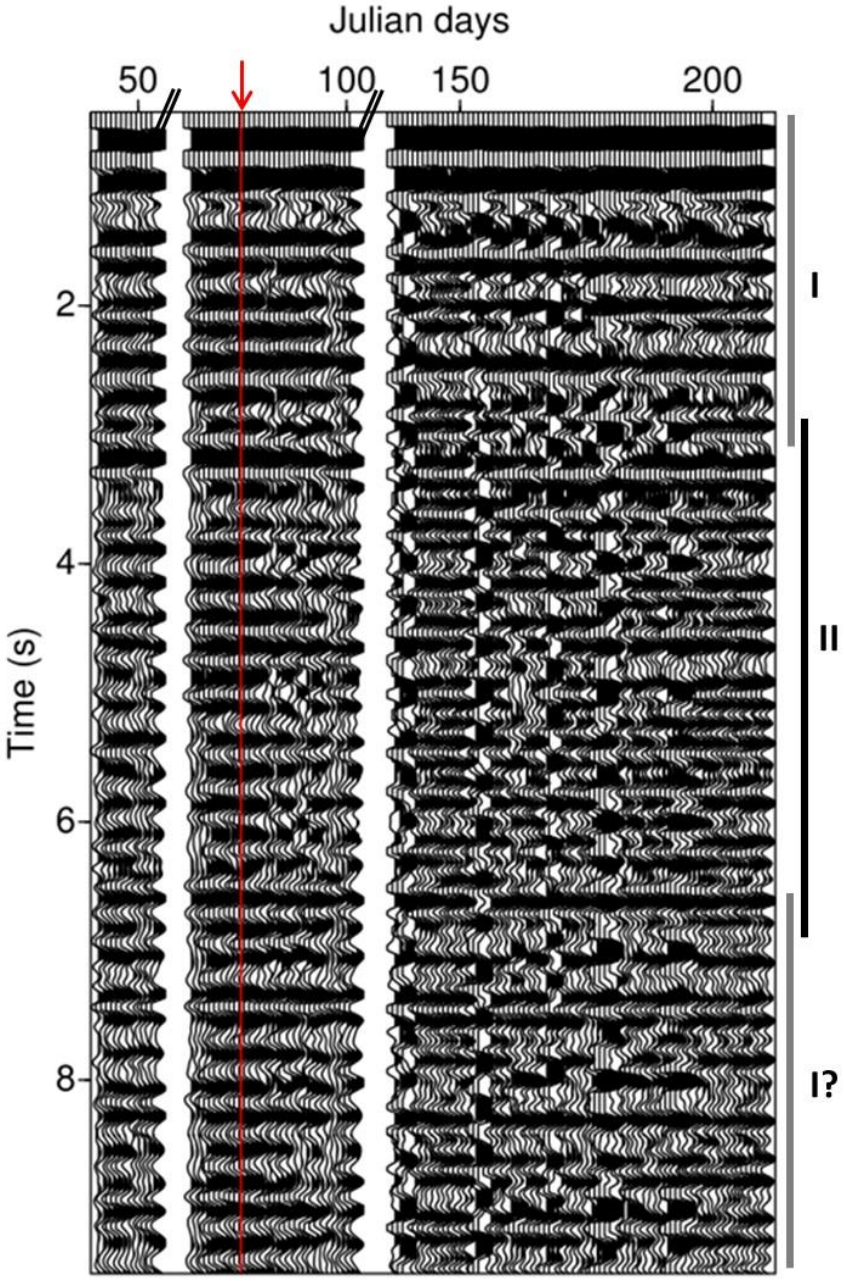

Figure 2.4: Full record section of the auto-correlations using PCC for the station SOJO from 0.5 to 9 s with the approximate delimitation of regimes I and II. The correlograms have been stacked linearly using a 3-day moving window. Data gaps are from days 56 to 69 and 103 to 136, respectively. The main event is marked by the red line.

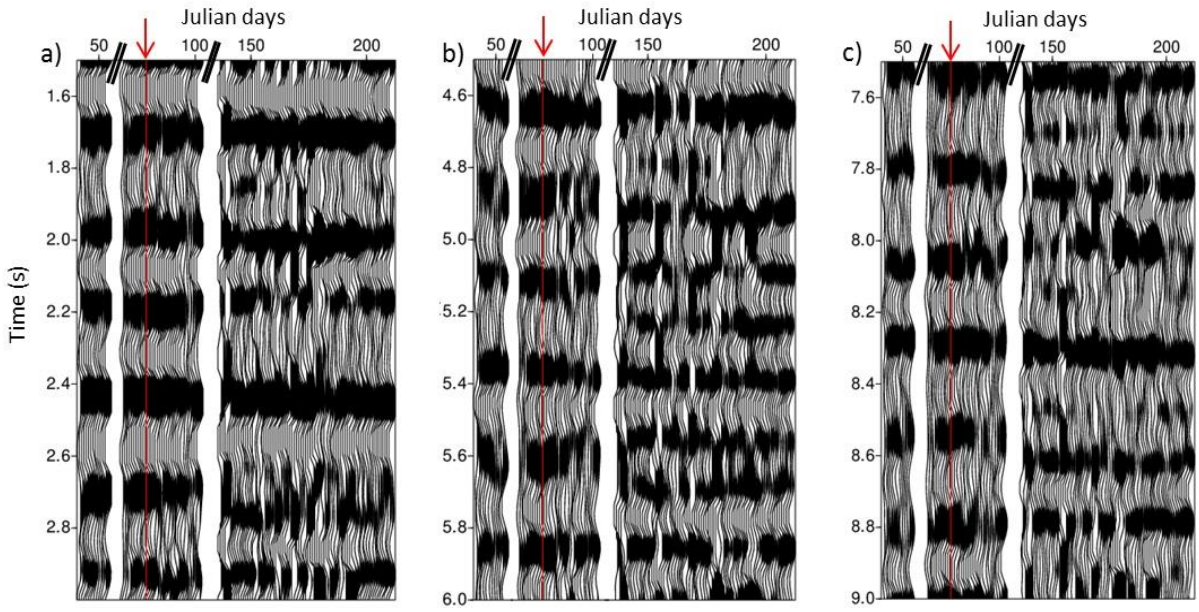

Figure 2.5: a) Zoom from 1.5 to 3 s (regime I), b) zoom from 4.5 to 6 s (regime II), c) zoom from 7.5 to 9 s (regime I?). The correlograms have been stacked linearly using a 3-day moving window. Data gaps are from days 56 to 69 and 103 to 136, respectively. The main event is marked by the red line.

In Figure 2.6, we show the normalized amplitude spectra of the auto-correlograms for the two presumed regimes before (Fig. 2.6a) and after (Fig. 2.6b) the main event for the station SOJO. "After the event" refers here to the 2nd post-event period which starts about 30 days after the main event. We plotted the median spectral amplitudes of the daily auto-correlograms using the 23 days of available data before the event and the month of June after the event. In full analogy, Figures 2.6c and 6d show the same for station SOMA, which has 28 days of available data before the event (Fig. 2.6c). It is clearly visible that there exist a change in the frequency contents for the auto-correlations from both stations.

After the event, the lower frequency components seem to be attenuated with respect to the higher frequencies. We also see that there are differences as function of lag time which are not observed during the pre-event period. It can be seen that after the event the auto-correlations for lag times 4-6.5s contain stronger higher-frequency components than lower-frequency components. This is not the case for the pre-event period at all lag time windows and for the regime I lag time windows after the event. In Figure 2.7, we show the daily relative amplitude change for both stations (SOJO: Figs 2.7a,b, SOMA: Figs 2.7c,d). These relative amplitudes correspond to the maximum amplitudes in the 6-7 Hz frequency band normalized by their corresponding maximum amplitudes from the 3-4.5 Hz frequency band. The median spectral amplitudes and absolute median variations are shown as horizontal and vertical bars, respectively. Median statistics have been used to be less sensitive to amplitude outliers. For station SOJO, it can be observed for the pre-event period that the relative maximum amplitudes are in the same order for the three selected lag time windows. On the contrary, for the post-event period we observe a large difference in the relative maximum amplitudes. Indeed, the relative maximum amplitudes are considerably higher for the 4-6.5 s lag time window than for the other windows, which clearly shows a relative frequency increase for regime II. These observations seem to be also valid for station SOMA but they are not as clear likely because of data quality. This figure further strengthens that there are significant changes in the auto-correlation functions which are localized in lag time. This localization in lag time is difficult to explain by an increase of the event activity or changes in the noise characteristics since they are expected to appear at all lags. Further, these observations are from a long time period. A likely explanation invokes localized structural changes beneath both stations (e.g., Maeda et al., 2010). We did not further investigate the origin of the frequency change which also is beyond the scope of this study, but frequencies are likely related to the characteristics of the structure.

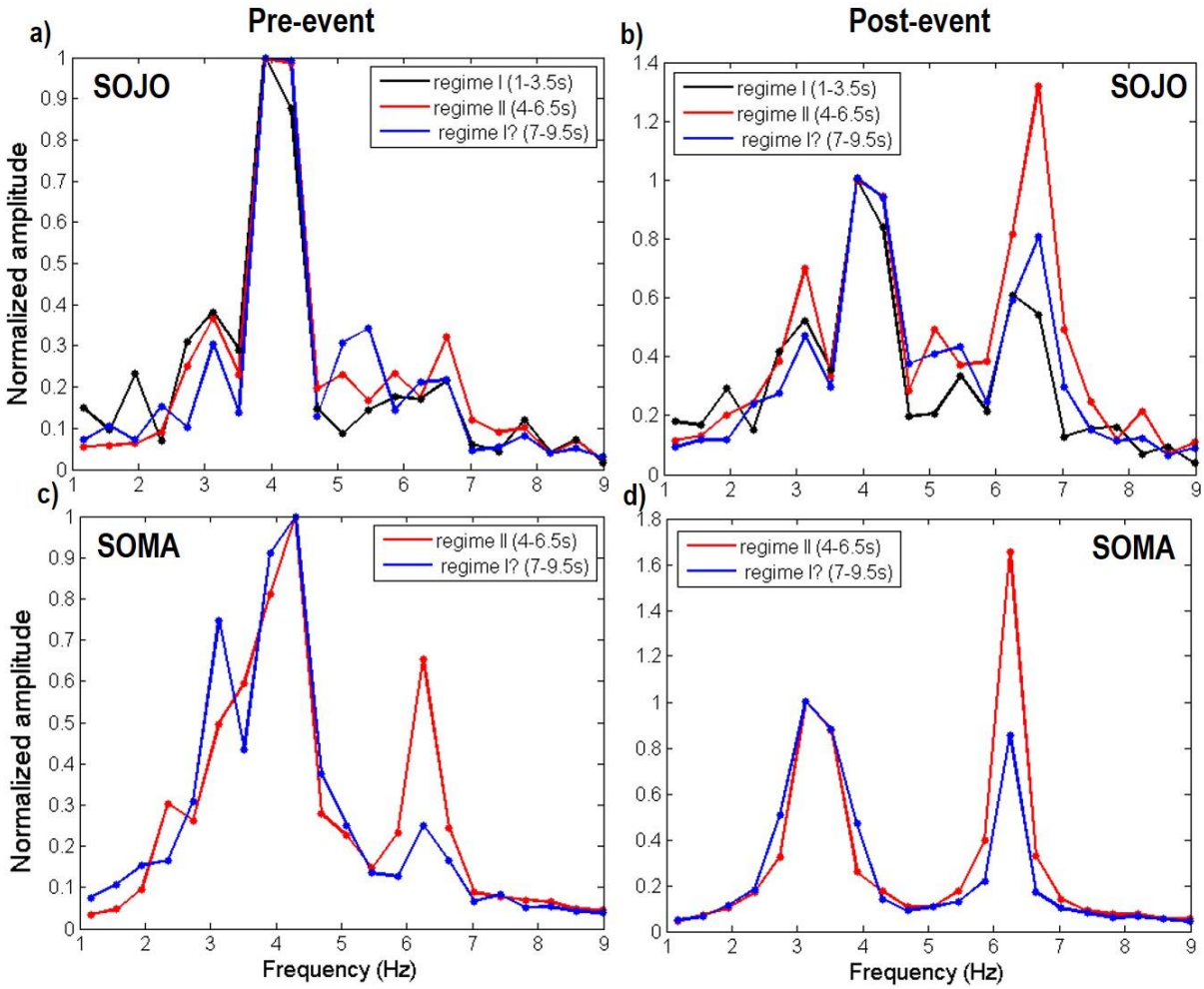

Figure 2.6: Median amplitude spectra for station SOJO a) for the pre-event period (11/02-19/03) and b) for the post-event period (01/06-30/07) and for station SOMA c) for the pre-event period (11/02-11/03) and d) for the post-event period (01/06-30/07). Spectra are plotted as function of lag time windows: 1 to 3.5 s (regime I - black), 4 to 6.5 s (regime II - red) and 7 to 9.5 s (regime I? - blue).

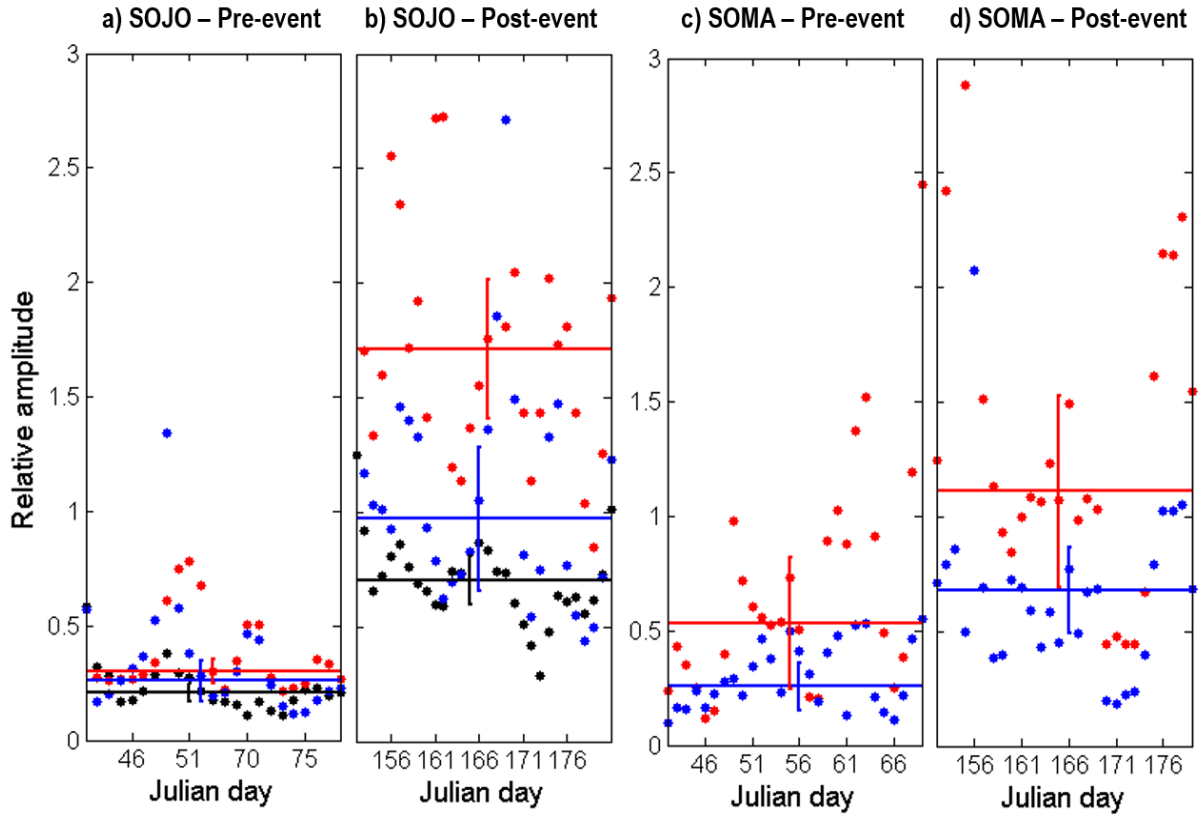

Figure 2.7: Relative amplitudes of the frequency peak at 6-7 Hz with respect to the one at 3-4 Hz for station SOJO a) for pre-event period (from day 41 to 78) and b) for post-event period (from day 151 to 180) and for station SOMA c) before the major seismic event (from day 41 to 70) and d) after the major seismic event (from day 151 to 180), as function of lag time windows: 1-3.5 s (regime I - black), 4-6.5 s (regime II - red) and 7-9.5 s (regime I? - blue). Spectral median amplitudes and median deviations are represented by the horizontal and vertical bars, respectively.

Due to the different frequency contents and severe changes of the waveforms we do not quantify time delays as often done in monitoring studies. Nevertheless, we evaluate the waveform changes by analysing the evolution of the similarity for a 0.5-6.5s lag time window, between a reference trace (stack of all pre-event auto-correlograms) and the auto-correlograms stacked within one day and three days moving window for the station SOJO

(Fig. 2.8c) and for the station SOMA (Fig. 2.8d). As the events' magnitude are unknown, we plotted also the number of aftershocks per day (Fig. 2.8a) and the daily cumulative squared amplitude of the 2-8 Hz band-passed waveforms which were recorded on the vertical components of stations SOJO and SOMA (Fig. 2.8b). The daily cumulative squared amplitude is proportional to the seismic energy recorded on the vertical component at each station. Both measures (Fig. 2.8a and 2.8b) may allow us to identify calm periods and periods with more seismic activity.

It can be seen from the similarity plots in Figure 2.8 that the similarity decreases and that the shape of the curves become rougher with progressive time for both stations. It seems that more medium changes are detected with progressive time. We now may divide the shown time interval into three periods: a pre-event period, an immediate post-event period with small similarity decrease and a second post-event period where the similarity curves become rougher with time. These periods are indicated in Figure 2.8 by the numbers 1, 2, and 3.

The pre-event period (from Julian days 40 to 79), corresponds to a relatively calm period with respect to the swarm starting on Julian day 79 where the similarities at both stations are consistent with the lack of seismic activity. They are characterized by an approximately constant and high correlation coefficient (≥ 0.85). Only few events (from Julian days 42 to 55) break this calm period resulting in a decrease of the similarity at the station SOMA. During the second period (from Julian days 79 to ~110), immediately after the main event (Julian day 79) we can observe a slight but steadily decrease of the similarity at both stations. The third period starts at about day 110 and is characterized with a similarity curve which is rougher than for the immediate post-event period (2). This period coincides with the period of increased frequencies at the 3-6 s lag time window (regime II). It seems that about 1 month after the main event the auto-correlation starts detecting larger medium changes than during period 2, i.e., the first month after the main event. We may interpret this observation as medium changes which come into the sensitivity range of the auto-correlation at each station. The corresponding mechanisms are unknown, but fluid pressure redistribution, for instance to shallower depth levels due to path ways opened by later occurring earthquakes could be a possible explanation.

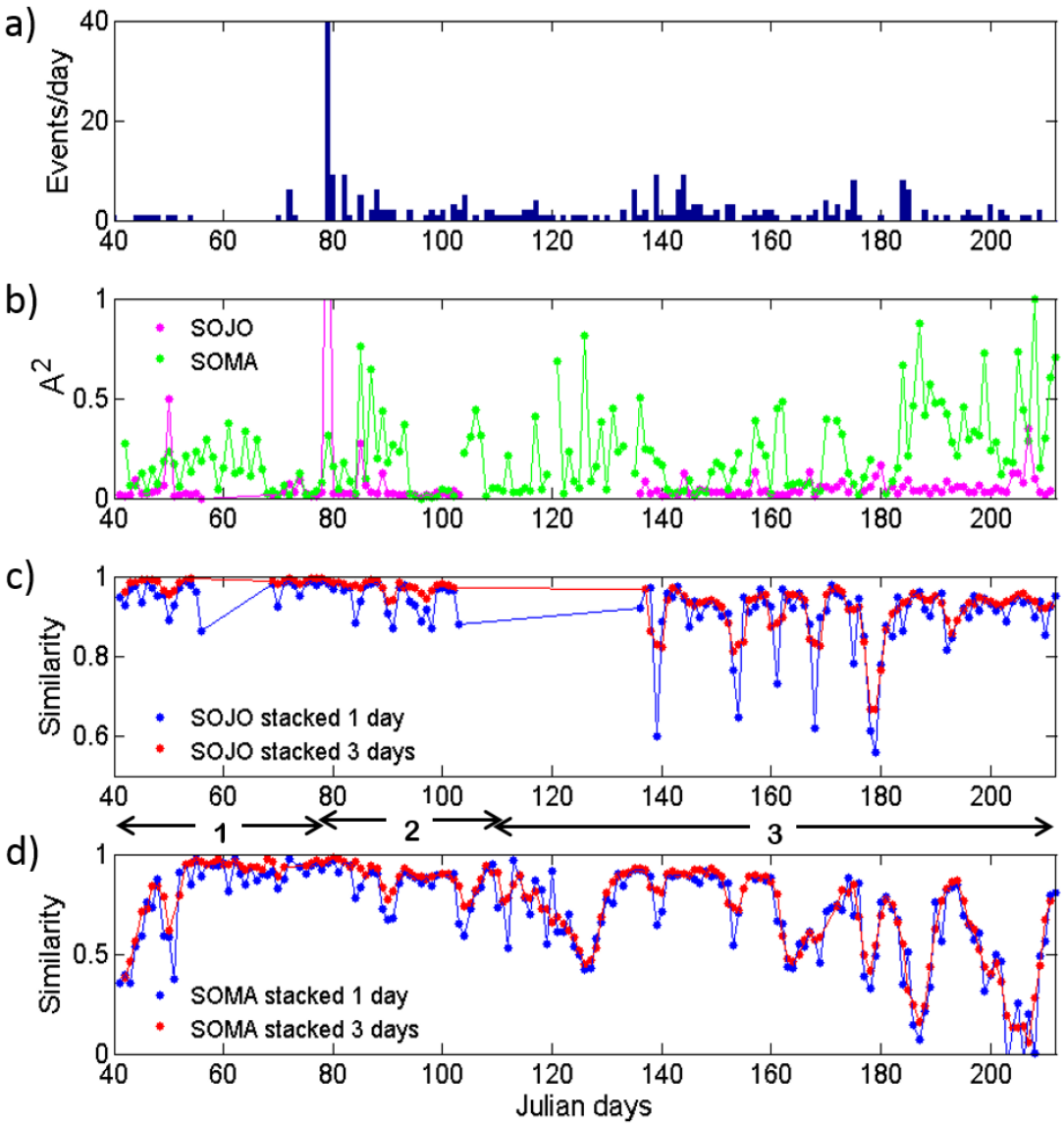

Figure 2.8: Study of the similarity evolution between the every day auto-correlograms within one day (blue) and three days (red) moving window and a reference trace (stack of all the correlograms before the day 79) for the stations SOJO (c) and SOMA (d) as function of the number of events per day (a) and the squared amplitude A (accumulative energy) per day at an arbitrary scale for visual purposes (b).

2.6.2 Cross-correlation

Besides the auto-correlations, we also analysed cross-correlations which are suited to provide information on structural changes between each station pair. The data processing for the cross-correlation is the same as for the auto-correlation. Cross-correlations using PCC were computed for the station pairs SOJO-SOMA, SOJO-SOLC and SOLC-SOMA and a 0.7-1.4 Hz frequency band. The resulting cross-correlations were used to analyse their similarity to a pre-event reference cross-correlation stack which is in full analogy to the auto-correlation analysis of Figure 2.8. The pre-event reference is the linear stack of cross-correlations for the days 40 to 79. The used lag time window is from 0.5 to 6.5 s. We only used the positive (causal) part as the cross-correlations are quite symmetric. The results are plotted in Figure 2.9. It is visible from this figure that the similarity decreases three days after the main event (Julian day 79) for all the station pairs. That is, medium changes are clearly observed for the cross-correlations only three days after the main event while the auto-correlations detect only weak changes which become more pronounced after 1 month.

The most important similarity decrease is observed for station pair SOJO-SOLC (Fig. 2.9c). This is expected since the trajectory between these stations is along the fault system. For station pair SOJO-SOMA (Fig. 2.9b), the interstation trajectory crosses the fault at an angle smaller than 40 degree. Also for this station pair we observe a first important decrease after the main event followed by a continuous decrease, which is similar with the results of the auto-correlations at the stations SOJO and SOMA. For station pair SOLC-SOMA (Fig. 2.9d), the station trajectory is almost perpendicular to the fault line. We observe for SOLC-SOMA a decrease of the similarity which is less important than for the other station pairs. It can be explained by the fact that the detected signals are for waves which propagate dominantly in a region which is less affected by medium changes.

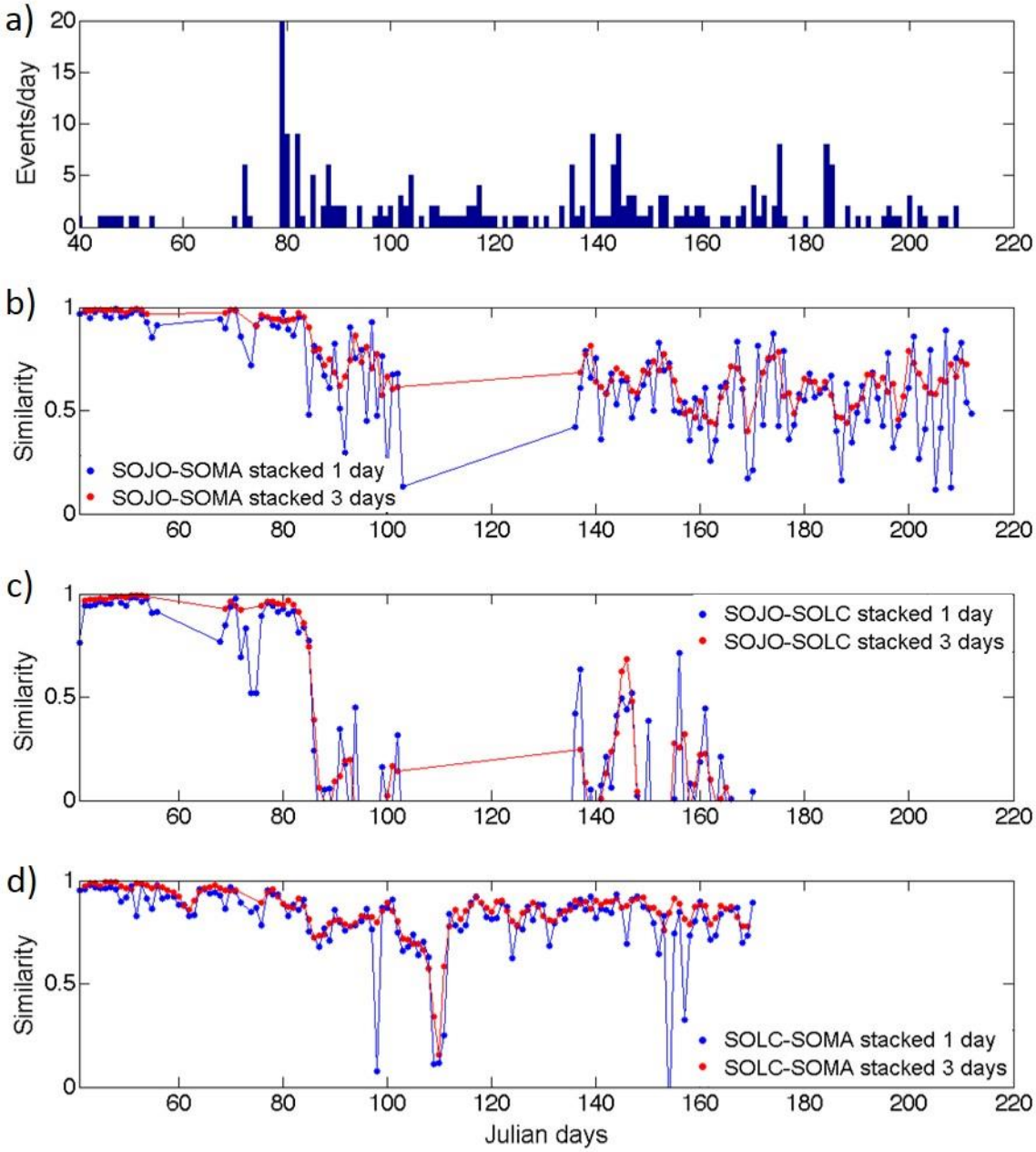

Figure 2.9: Study of the similarity evolution between the every day cross-correlograms within one day (blue) and three days (red) moving window and a reference trace (stack of all the correlograms before the day 79) for the station pairs SOJO-SOMA (b), SOJO-SOLC (c) and SOLC-SOMA (d) as function of the number of events per day (a).

The cross-correlations of the three station pairs evidence the presence of detectable medium changes soon after the main event. The observed decrease in similarity is more pronounced and more abrupt than for the auto-correlations. This makes alternative explanations, such as apparent medium changes due to changes in the characteristics of the ambient noise wave field, unlikely. That is, changes in the ambient noise wave field should be detected simultaneously by the auto-correlations, which is not the case. The cross-correlations are more sensitive to medium changes along the interstation trajectory than the auto-correlations which can explain the different responses of cross-correlations and auto-correlations for stations which are not deployed within the affected areas.

The sketches of Figure 2.10 summarize our observations. The interstation trajectories (Fig. 2.10a) are plotted on a colour scale, which marks the amount of similarity decrease observed for each couple of station after the main event, from day 90. Medium changes are strongest somewhere along the fault and in between the three stations. One month later the auto-correlations start to show a pronounced similarity decrease mainly confined within a lag time window from 3 to 6.5 s for the station SOJO and until 7 s for the station SOMA. If we consider an empirical apparent velocity of 1km/s for scattered waves, as sometimes used to approximate the lag time window (Meier et al., 2010; Zhan et al., 2013), then the observed similarity decrease would be localized roughly to a distance of about 1.5 to 3 km from the station SOJO and until 3 km from station SOMA. If we further assume that we detect mainly surface waves then these waves at 2-8 Hz would be sensitive to medium changes at very shallow depths less than a few hundreds of meters. The distances in Figure 2.10 are only indicative and marked by the circles. We can not determine the precise distances or depths, but we can say that independently of the wave type, the medium changes happen close to the stations.

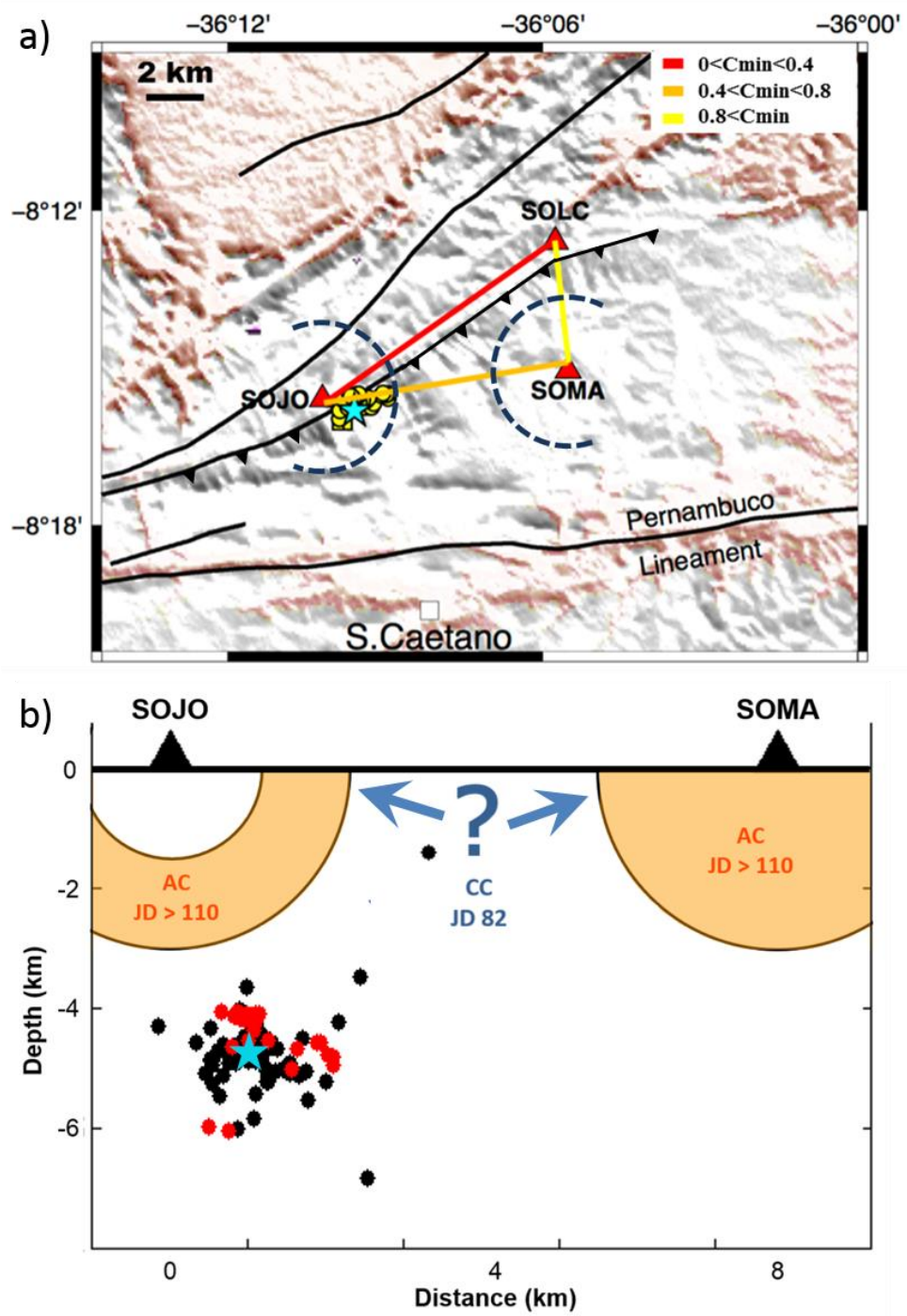

Figure 2.10: a) Map showing the similarity minimum for the interstation trajectories (plotted with colours) and the hypothetical location of the medium changes after Julian day (JD) 110. b) Summary sketch of our interpretation showing the hypothetical temporal evolution of the medium changes and its likely location. Event location before (black) and after (blue) day 110 and m_R 3.7 (blue star). Depth sensitivity of surface waves in the AC (2-8Hz) and CC (0.7-1.4Hz) frequency bands are in the order of few tens of meters to several hundreds of meters.

The pronounced decrease of the similarity after one month and at a small distance from the stations could be explained by fluid pressure redistribution which can be initiated by hydromechanical changes and opened path ways to shallower depth levels due to later occurring earthquakes. This hypothesis can not be proved by other data, since, for instance, there exist no borehole water level measurements for the study area.

2.7 Discussion and conclusions

Our analysis of the m_R 3.7 São Caetano intraplate event and its aftershocks has been based on a new correlation approach, the PCC (Schimmel, 1999) which so far, to our knowledge, has not been presented for monitoring purposes. We compared PCC with the classical approach and showed that with PCC we achieve for our data a robust and fast convergence to a reference trace, obtained through stacking auto- or cross-correlograms over a long time window. This fast convergence means that PCC enables a higher time resolution than CC since one needs to stack fewer days in the moving window of the monitoring analysis. Our pre-analysis also shows that the CC applied on pre-processed (one-bit normalization and spectral whitening) data is not suited for our purposes. It seems that the pre-processing removes too much information from the waveform data to permit a fast convergence. CC without pre-processing, however, provides better results but is sensitive to events and other data anomalies. This sensitivity manifests in the waveforms (Fig. 2.2b) and in the variability of convergence (Fig. 2.3). PCC does not need the pre-processing and does not show the sensitivity to outlying amplitude events (Schimmel et al., 2011) as it can be seen from the waveforms and the small variability in the convergence diagram. Our CC and PCC results are similar when there are no outlying amplitude events in the data.

It seems, from the SOJO auto-correlation's record sections (Figs. 2.4, 2.5) and from the frequency analysis (Figs. 2.6 and 2.7), that we observe a frequency change which is mainly confined to a particular lag time window. The change in frequency contents starts between 20 and 50 days (we can not be more precise due to the data gap) after the main m_R 3.7 event and lasts several weeks. The frequency change, which dominates during a

confined lag time window, strengthens that we likely observe the result of a localized medium change rather than an external cause (e.g., meteorological cause) or an overall medium change. The frequency perturbation is observed from approximately 3 to 6.5 s and consists mainly in a relative frequency increase with respect to earlier and later lag time. A similar relative frequency increase is also observed at station SOMA. However, its beginning lag time is not well defined and its ending lag time is at about 7 s. The corresponding structural changes would be shallow and close to both of the stations. As mentioned before, if we consider an apparent wave velocity of 1km/s, then the structural variations would be located within about 3 km from the stations. If we detect mostly surface waves with the auto-correlations at 2-8 Hz then the medium change should happen at very shallow depth (several tens of meters). An exact depth and distance determination is beyond the scope of this study, but it is generally accepted that the auto-correlations are mostly sensitive to the local shallow structure around each station (e.g., Nakahara, 2015).

The origin of the frequency change has not been analysed. A relative increase of higher frequencies can mean that the structural variations cause a higher reflectivity of the higher frequency waves. The reason can be stronger or sharper discontinuities or an increase in the amount and strength of scatterers (Groenenboom and Snieder, 1995; Snieder, 2002; Larose et al., 2010). There is likely no increase in the amount of scatterers close to the stations, but an increase of reflectivity strength of inhomogeneities, for instance, due to the local water table migration mainly within the fault zone can not be ruled out.

With the cross-correlations, a more pronounced decrease of similarity (Fig. 2.9) is observed already 3 days after the main event of Julian day 79. The cross-correlations are sensitive to the structure along the station trajectory. This strengthens that at the beginning of the crisis the medium changes are further away from the stations since no pronounced decrease of the similarity is observed simultaneously on the auto-correlations. Since diffusivity of fluids increases outwards from the main damage zone the delayed decrease of similarity observed on the auto-correlations is understandable. This could mean that the corresponding structural changes at shallow depth are initiated by some of the aftershocks. This is consistent with the fact that fluids flow is occurring within a zone of young open fractures probably initiated due to the mechanical contrast between the fault core and the

surrounding rock during the earthquake (Pytharoulli et al., 2011; Soden et al., 2014). The aftershocks can cause new opening cracks (Poupinet et al., 1984; Sibson, 1996; Baish and Bokelmann, 2001) which further can enhance the outward diffusion of pore pressure. And then, it can be observed from the auto-correlations of the stations SOJO and SOMA (Fig. 2.8) as a more pronounced decrease of similarity after 21 days (Julian day 110), and until the end of the study.

Gavrilenko (Gavrilenko, 2005; Gavrilenko et al., 2010) studied the complex relation between aftershocks and the fluid flow after an earthquake and showed that they can be due to hydrological (variation of the water level) and mechanical changes (stress transfer) or a hydromechanical coupling. The fluid flows from the compressed area to the dilated area until reaching equilibrium (Nur and Booker, 1972; Bosl and Nur, 2002). The permeability of the medium is a key parameter which determines the temporal dependence of the aftershocks and the pressure redistribution. In our case, the medium, a Precambrian crystalline basement, has a low matrix permeability, which means a very slow pressure redistribution in the host rock and the hydraulic properties are controlled by a discrete set of fractures (do Nascimento et al., 2004; do Nascimento et al., 2005a,b). The series of aftershocks keep on opening cracks increasing the permeability. And by consequence, the fluid migration would increase when the aftershocks create more cracks or even interconnect faults. Fluid migration has often been used to explain observed medium changes with seismic interferometry (e.g., Miller et al., 2004; Snieder et al., 2007; Terakawa et al., 2010).

Other studies of the same type (Wegler et al., 2009; Wegler and Sens-Schönfelder, 2007) used the classical cross-correlation and studied the effect of earthquakes of at least magnitude 6 and showed a sharp wave velocity decrease occurring immediately after the event. The main event of our study has a magnitude of 3.7 and is followed by a sequence of much lower energy aftershocks. We can conclude from our study that medium changes for smaller energy events are also detectable. The corresponding variations are clearly visible and show that monitoring studies can be extended to smaller energy events. We further show that PCC is suited to monitor these little changes. The PCC auto-correlations

detect medium changes later than the cross-correlations which can strengthen our hypothesis of fluid movement as a plausible and likely cause of our observations.

At this stage the interpretations are speculative since no other constraints, as borehole data are available. Also the distance estimation should be taken with care since we have no control whether the published apparent velocity of 1km/s is valid at São Caetano and for the considered frequencies. Further, more stations are needed to better constrain the damage zone. Nevertheless, an analysis of wave propagation is out of the scope of this study which mainly focuses on the detection and clearly shows that the auto-correlations detect strongest medium changes later than the cross-correlations which makes our hypothesis a plausible starting point for further investigations.

2.8 Acknowledgement

The authors thank the Instituto Nacional de Ciência e Tecnologia - Estudos Tectônicos (INCT-ET/CNPq) and the Instituto Nacional de Ciência e Tecnologia – Geofísica do Petróleo (INCT-ET/CNPq). V. D'hour and H. Lima Neto thank CAPES for their PhD grants. A. Nascimento and J. Ferreira thank CNPq for their PQ grants. M. Schimmel thanks the Science without Borders Programme for his PVE grant and CGL2013-48601-C2-1-R. V. D'hour also thanks the Science without Borders Programme for allowing the sponsored period of 1 year in Barcelona, Spain. The authors also thank Eduardo Menezes for this valuable work in the data acquisition period, and the editor and the 2 reviewers for their careful and constructive reviews.

Chapter 3

Temporal medium evolution near the Mid-Atlantic Ridge after a m_b 4.9 earthquake.*

3.1 Abstract

We investigate structural changes associated with a m_b 4.9 earthquake in the region of the Saint Paul transform fault located at less than 200 km from the Mid-Atlantic ridge. We use the phase auto-correlation to compute the structural response from continuous waveforms recorded by a single broadband seismic station located at 32 km from the epicenter. The results obtained, from May to September 2012, show a strong co-seismic medium change followed by a relatively fast recovery in the early post-seismic stage that slows down later. A full recovery is reached after only 60 days. The co-seismic medium change is likely related to the damages caused by the earthquake's ground shaking. The post-seismic recovery can be attributed to the filling of the new fractures by precipitation of secondary minerals or compaction and pressure solution. This result is the first observation of a post seismic healing process in the Mid Atlantic Ridge area.

3.2 Introduction

The Mid-Atlantic Ridge (MAR) is responsible for the occurrence of seismic events of mainly small to moderate magnitude (m_b < 6.0). They are generally difficult to characterize due to the lack of seismic stations in this area. The majority of this seismicity is clustered at the proximity of dyke intrusions (Simão et al., 2010) which means there are

*The main content of this chapter has been submitted for publication in *Geophys. Res. Lett.*

zones of intense seismicity and other zones that lack seismicity (Smith et al., 2003). The MAR is crossed by numerous transform faults that accommodate the ocean floor extension.

In this study, we focus on the Saint Paul transform fault where a seismic station has been installed in 2011 on the Saint Peter and Saint Paul Archipelago (SPSPA, 0º55'N-29º21'W). It is located at approximately 1,010 km from the coast of Brazil (nearest mainland point: Calcanhar Cape, Rio Grande do Norte State), at less than 200 km from the axis of the MAR. The SPSPA is a small group of islets and rocks with a total area of about 0,012 km² and a maximum altitude of 18 m. The proximity to the MAR at these latitudes and the presence of no other islets makes the SPSPA a unique location for seismic data acquisition. On the 07/09/2012, a m_b 4.9 seismic event occurred at 32 km from this station. We are going to analyze if it is possible to detect a medium change due to this m_b 4.9 seismic event.

Ambient seismic noise correlation is a method that allows to retrieve the structural response between two receivers from a diffuse noise wave field (Lobkis and Weaver, 2001; Snieder, 2004; Wapenaar, 2004; among other), as if one of the station was a virtual source. Claerbout (1968) first proposed to use seismic noise auto-correlations, and then cross-correlations (Rickett and Claerbout, 1996) to retrieve the reflection response. This conjecture has then been widely applied in geophysics, particularly for monitoring purposes. For example, it has been used to study auto- or cross-correlogram variations that can be seasonal (e.g., Sens-Schönfelder and Wegler, 2006; Meier et al., 2010) or related to volcanic eruptions (e.g., Ratdomopurbo and Poupinet, 1995; Snieder and Hagerty, 2004; Brenguier et al., 2008a; Obermann et al., 2013) and large earthquakes (e.g., Brenguier et al., 2008b; Wegler et al., 2009; Zaccarelli et al., 2011; Schaff, 2012; Hobiger et al., 2012, 2014; Liu et al., 2014, Nakahara, 2015).

These last studies showed important medium changes caused mainly by earthquakes larger than m_b 6.0 (Li et al., 2006; Zacarelli et al., 2011; Hadziioannou et al., 2011, among others) and only a few under m_b 6.0 (e.g., Poupinet et al., 1984; Rubinstein and Beroza, 2004; Maeda et al., 2010). Moreover, the majority of them used several seismic stations to obtain a good spatial resolution. In this study, we look at a m_b 4.9 earthquake and with the

only broadband seismometer available in this area, we managed to show co-seismic variations in the auto-correlograms followed by a full post-seismic similarity recovery.

Changes in auto-correlograms of seismic noise can be caused by changes in the medium (e.g., Ohmi, 2008; Wegler et al., 2009) as damages in the sub-surface material or changes of the water saturation in the pore space. Monitoring this unique region provides important information about the behavior of the medium located on the Saint Paul transform fault near the MAR in response to a moderate earthquake (m_b 4.9) occurring nearby. This area is not well constraint yet due to the lack of possibility to install seismic stations or OBS. For example, it has never been determined if post-seismic recovery tends to be slow or fast at the MAR.

3.3 Data and Method

The seismic data used in this work were recorded by a single seismic station, located on the largest SPSPA islet (Belmonte Islet: 5,380 m^2) represented by a yellow triangle on Figure 3.1. It has one broadband sensor with a flat velocity response between 120 s and 50 Hz and one strong motion sensor. Due to technical reasons the strong motion sensor has not been working properly for most of the time. We used the vertical-component continuous waveforms recorded from May to September 2012 at a rate of 100 samples per second. During this period of time, more than 70 seismic events were recorded. Here, we study the effect of the main one that had a magnitude of mb 4.9 and occurred on day 191 (09 July) at about 32 km from the SPSPA. Considering that the SPSPA zone is dominated by strike-slip mechanisms (Campos et al., 2010), the focal mechanism of our m_b 4.9 earthquake may be as well strike-slip.

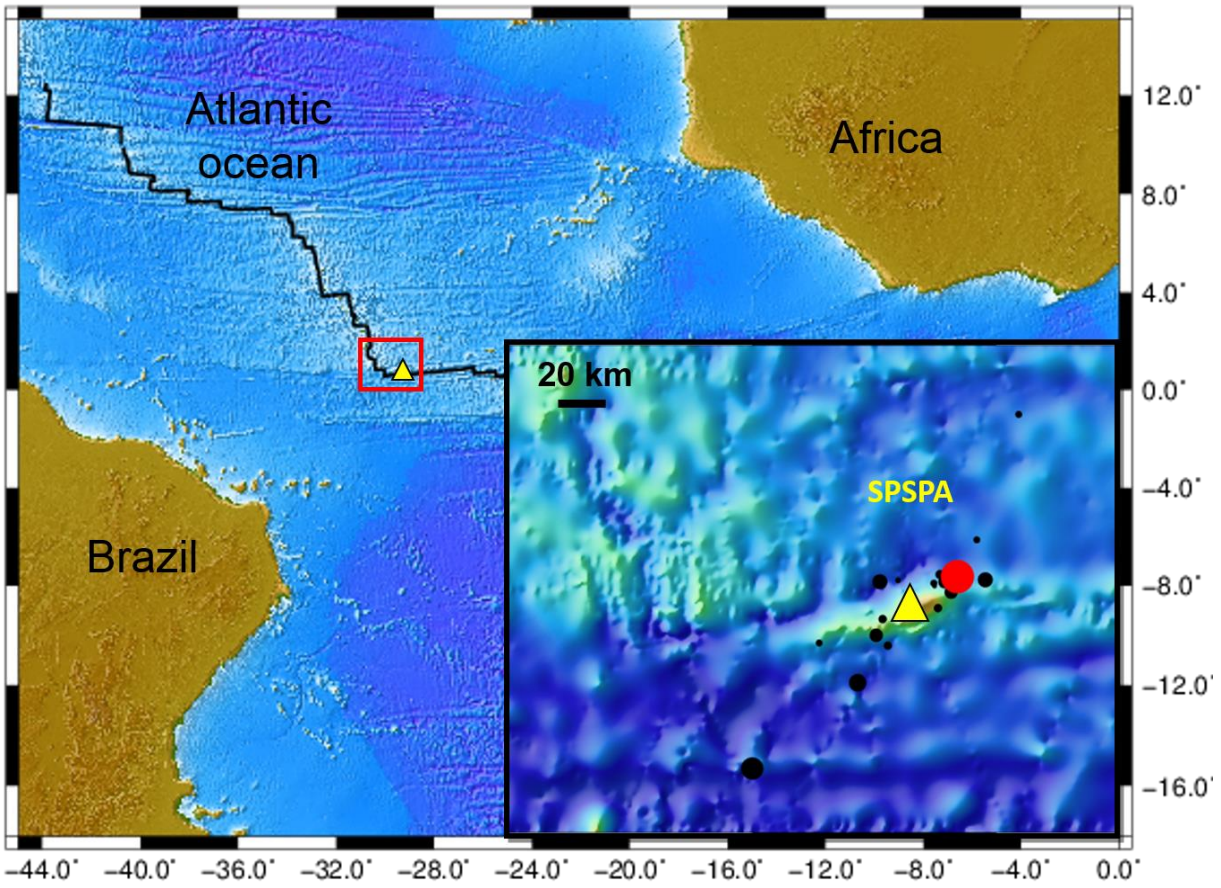

Figure 3.1: Map showing the location of the studied region (red square). The inset shows a zoom on the studied region with the location of the station (yellow triangle) and the earthquakes (circles) within the time window of interest. The red circle show the location of the 4.9 m_b event. The size of the circles is proportional to the earthquakes magnitude.

The analysis procedure consisted of three main steps (1) pre-processing, (2) auto-correlation and (3) auto-correlogram stacking (e.g., Bensen et al., 2007; Schimmel et al., 2011). In the following paragraph, we briefly outline the different processing steps.

We started data pre-processing by cutting the continuous data into non-overlapping segments of 60 min length. Further, the data have been band-passed using a zero phase Butterworth filter (Roux et al., 2005) to reduce the frequency band to the one where we

expected to observe the best signal to noise ratio (SNR). We worked in the 0.1-0.5Hz band corresponding mainly to ocean-generated microseismic noise, since the SPSPA is isolated and we do not virtually have anthropogenic noise (Figure 3.2). This frequency band has also been used in other previous studies (Wegler et al., 2009; Wegler and Sens-Schönfelder, 2007, among others).

Figure 3.2: Photo of the SPSPA where it is possible to see the scientific station on the Belmont islet. Photo taken from http://forum.outerspace.terra.com.br/index.php?threads/arquipélago-de-são-pedro-e-são-paulo-o-local-mais-inóspito-do-brasil-fotos.273255/ (07/10/2015).

After these data preparation steps, we computed the auto-correlations using the Phase Cross-Correlation (PCC) method by Schimmel (1999).

$$C_{pcc}(t) = \frac{1}{2T}\sum_{\tau=\tau_0}^{\tau_0+T}\left\{\left|e^{i\varphi(t+\tau)} + e^{i\gamma(\tau)}\right|^{\vartheta} - \left|e^{i\varphi(t+\tau)} - e^{i\gamma(\tau)}\right|^{\vartheta}\right\} \quad (3.1)$$

This approach measures the waveform similarity (equation 3.1) based on the instantaneous phases $\varphi(t)$ and $\gamma(\tau)$ of two time series, the lag time t and the correlation window length T. ϑ is a factor which can be used to control the sensitivity. This approach is amplitude unbiased and does not need time- and frequency domain normalized data (Schimmel et al., 2011). In fact, these normalizations deteriorate the noise waveforms which lead to poorer results with PCC.

In order to look at the temporal variation of the auto-correlograms, we stacked linearly all the pre-event auto-correlations (from day 126 to 289) to obtain a reference trace. Then we compared this reference trace with each auto-correlogram that corresponds to the linear stack of the auto-correlations within a defined time window. It is done by computing the zero-lag cross-correlation for a chosen lag time. The results of this zero-lag cross-correlation will be referred as “similarity” in this manuscript.

The time window used for the stack of the auto-correlations has a fix size and is chosen to obtain signals with a good SNR. Here, a good SNR means that sufficient auto-correlations have been averaged to obtain a stable structural response, i.e. that does not change significantly by adding more data. Typically a satisfactory SNR is obtained by averaging over weeks or months of data (Sabra et al., 2005; Larose et al., 2008). The downside is that the longest the time window is, the lowest is the temporal resolution.

In order to estimate the optimal length of the moving window, we calculated the similarity between the auto-correlations and a reference trace as function of window length, i.e., as function of data used in the stacks (Figure 3.3). The data used for this analysis were selected randomly 10 times to show the robustness of the convergence. That way, we were able to determine that the auto-correlations should be stacked at least 15 days to obtain a satisfactory SNR. We further observe that for this data the PCC and the classical cross-

correlation geometrically normalized (CCGN) without any pre-processing (1-bit normalization and spectral whitening) provide similar results. This depends on the data characteristics and can not be generalized as shown in D'Hour et al. (2015).

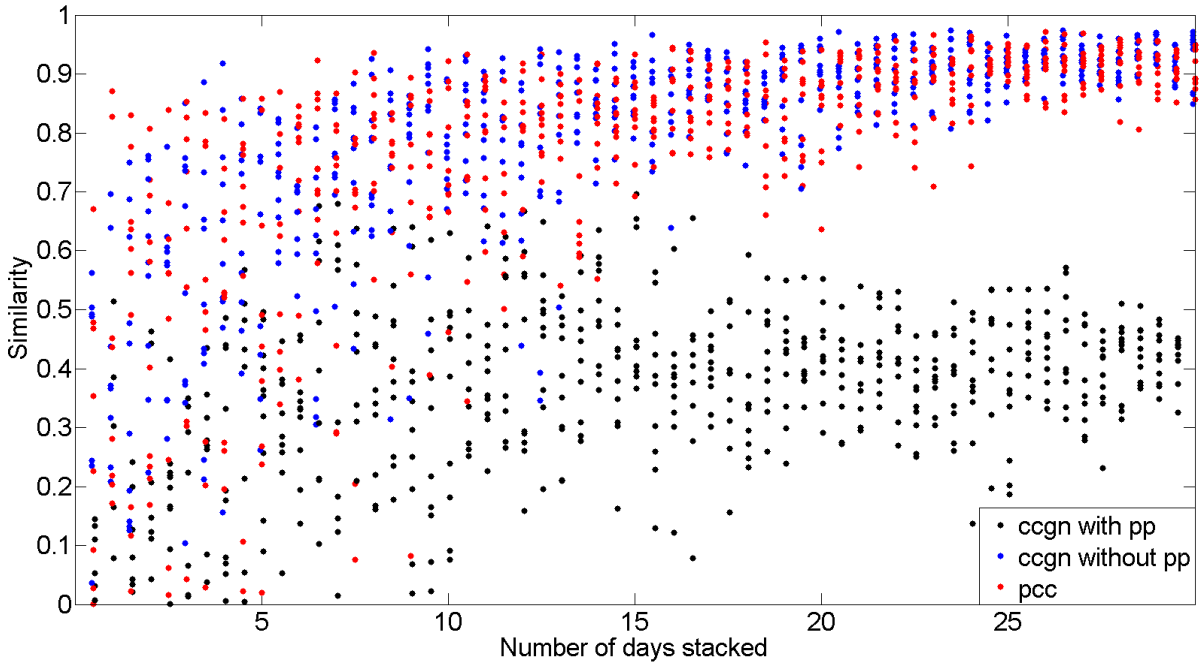

Figure 3.3: Waveform convergence of auto-correlation stacks as function of time, i.e., as function of data used in the stacks. The noise data used are from the pre-event period and have been selected randomly to show the robustness of the convergence to a stable reference waveform. The colours distinguish the three cases: CCGN with pre-processing in black, CC without pre-processing in blue and PCC without pre-processing in red. Pre-processing means 1-bit normalization and spectral whitening. A reference trace has been obtained for each method through stacking all available pre-event data.

3.4 Analysis and Results

Here, we analyzed the possibility of detecting structural changes caused by a m_b 4.9 seismic event that occurred at 32 km from the seismic station from 0.1-0.5 Hz band-passed auto-correlations.

Figure 3.4a shows the auto-correlograms' section of 5 months of data that were processed as previously described. Each auto-correlogram result from a 15 days linear stack with a step of one day. The correlograms have been plotted with respect to the center time of the 15-days window. The m_b 4.9 event is represented by an orange line. In this figure, the temporal changes of the auto-correlograms are not clear so we calculated the similarity as function of lag-time (Figure 3.4b).

Figure 3.4b shows the similarity between each auto-correlogram and the reference trace for 6 different lag-time windows (30-60s, 55-85s, 80-110s, 105-135s, 130-160s, 155-185s). In this figure, we can observe that the main similarity decrease starts at day 191 when the m_b 4.9 event occurred. This observation shows that a change in the auto-correlograms occurred simultaneously with our main seismic event. Also from this figure, it is important to note that the strongest similarity decrease is confined between the lag time 80-120 s. If we consider that the m_b 4.9 earthquake, located at about 32 km from the SPSPA seismic station, is responsible for this change then the corresponding apparent velocity of the scattered waves would be between 0.53 and 0.75 km/s. These apparent velocity values are lower by a factor of 3 or more than the fundamental mode Rayleigh wave group velocities which reflects the longer wave path due to scattering.

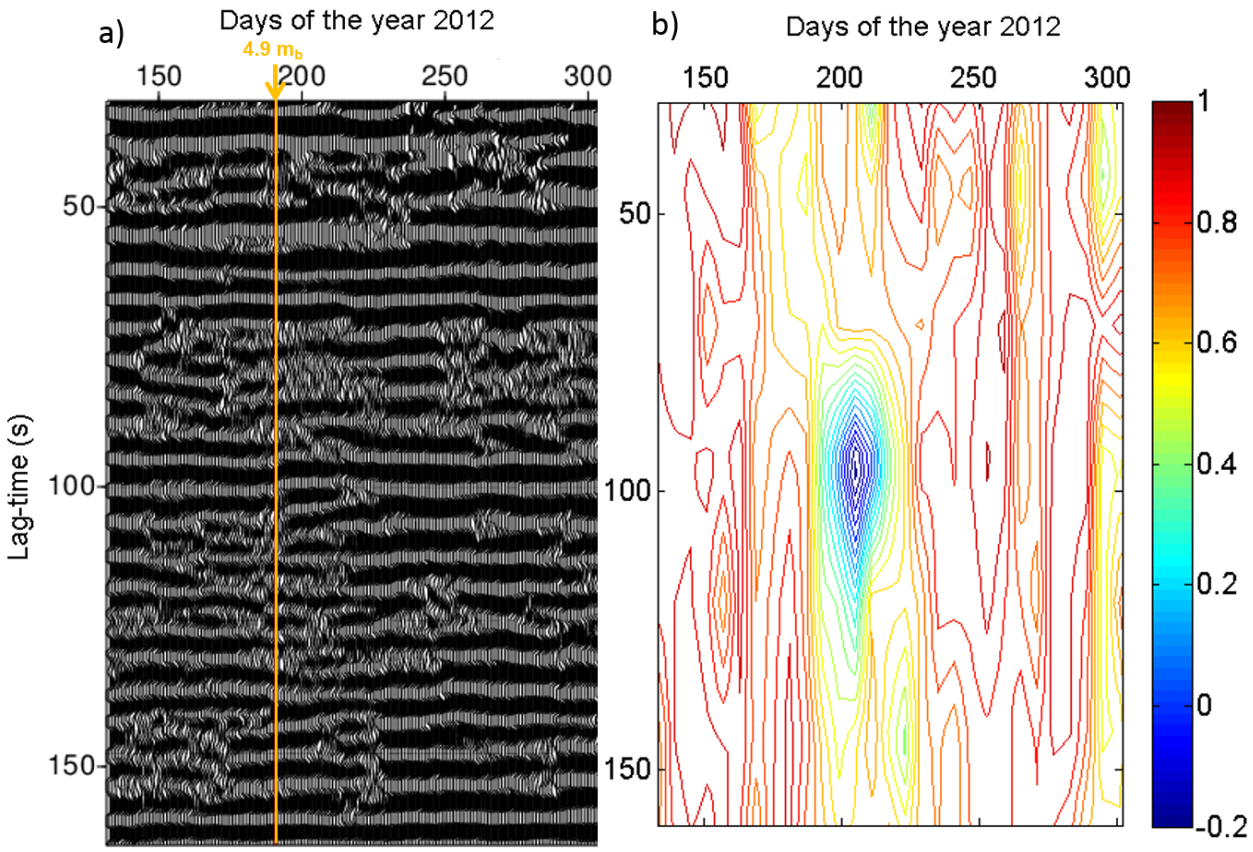

Figure 3.4: a) Record section of the auto-correlations using PCC. The correlograms have been stacked linearly using a 15-day moving window and have been plotted with respect to the window's center. The m_b 4.9 event is marked by the orange line. b) The contour plot shows the similarity of the auto-correlations from a) with respect to a reference trace (stack of all pre-event auto-correlations). The results are shown from 30 to 160 s to focus on the lag time of interest to display the main changes (80 to 120 s).

Next, we looked at the variation of the similarity with time for the lag time window 80-120 s that showed the strongest variation in Figure 3.4b. As the SPSPA is very isolated, we do not have an accurate catalogue of the regional seismicity. So, in order to have a measure of the seismic energy recorded on the vertical component, we plotted the daily cumulative squared amplitude of the 1-3 Hz band-passed raw data (Figure 3.5a). The result

of the similarity for the 80-120 s lag time window is shown in Figure 3.5b. On this figure, we can observe a co-seismic sharp decrease of the similarity on day 191 (red arrow) that continues until reaching a minimum 13 days later (day 204). We then observe a post-seismic recovery that reaches 77% of the pre-event levels (dashed red circle) 1 month after the earthquake (on day 221). Then, the recovery rate becomes slower and it needs one more month to reach a full recovery (on day 250).

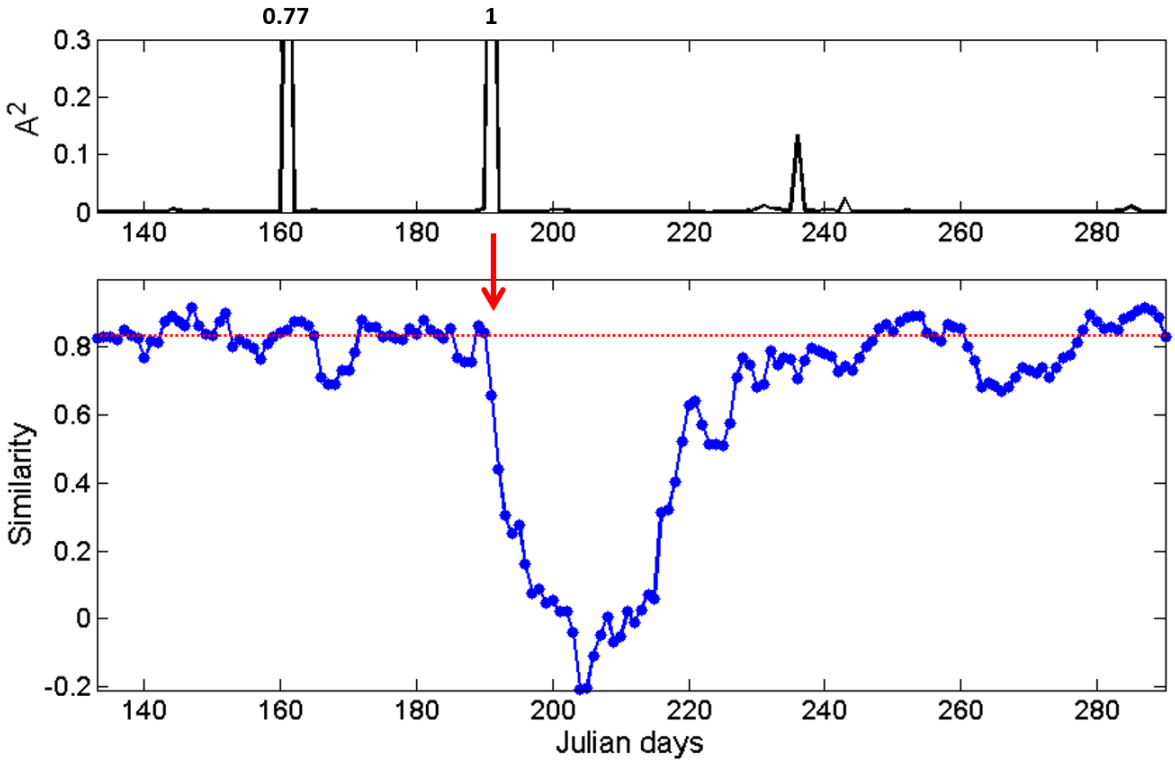

Figure 3.5: a) Normalized squared amplitude A (accumulative energy) per day. b) Study of the similarity evolution for the auto-correlograms from Figure 2a and a reference trace (stack of all the correlograms before the day 191) at 80s-120s lag time. The red arrow marks the occurrence of the 4.9 mb earthquake and the red dashed line shows the median similarity of the pre-event period.

Also, we can note that the relatively high seismic energies registered on days 161 and 236 do not have a discernible effect on the auto-correlograms. As their magnitudes are considerably smaller (m_b 3.1 and m_b 2.6, respectively) and at a similar distance than the one occurring on day 191 (m_b 4.9), they have a less important impact on the medium around and by extension on the auto-correlograms. In addition, as we stack over 15 days to get a good SNR, we do not have a high temporal resolution and our approach may become unable to detect small and short-duration changes.

We did the same analysis using, this time, the CCGN method (eq. 6 in Schimmel et al., 1999). We compared the results obtained previously with PCC to the one obtained with CCGN and used three different length of stacking windows (5, 15 and 30 days). We can see these comparisons on Figures 3.6 and 3.7. It can be highlighted that for this data CCGN gives the same results as PCC, although, it seems that the slow recovery after day 221 is more pronounced with PCC. Moreover, the results obtained after stacking 15 days and 30 days are very similar. Stacking only 5 days shows a similar trend but does not give a satisfactory SNR as the resulting auto-correlations are more variable. These observations show that our results are robust because they are equivalent for two independent methods (PCC and CCGN) and for different moving windows.

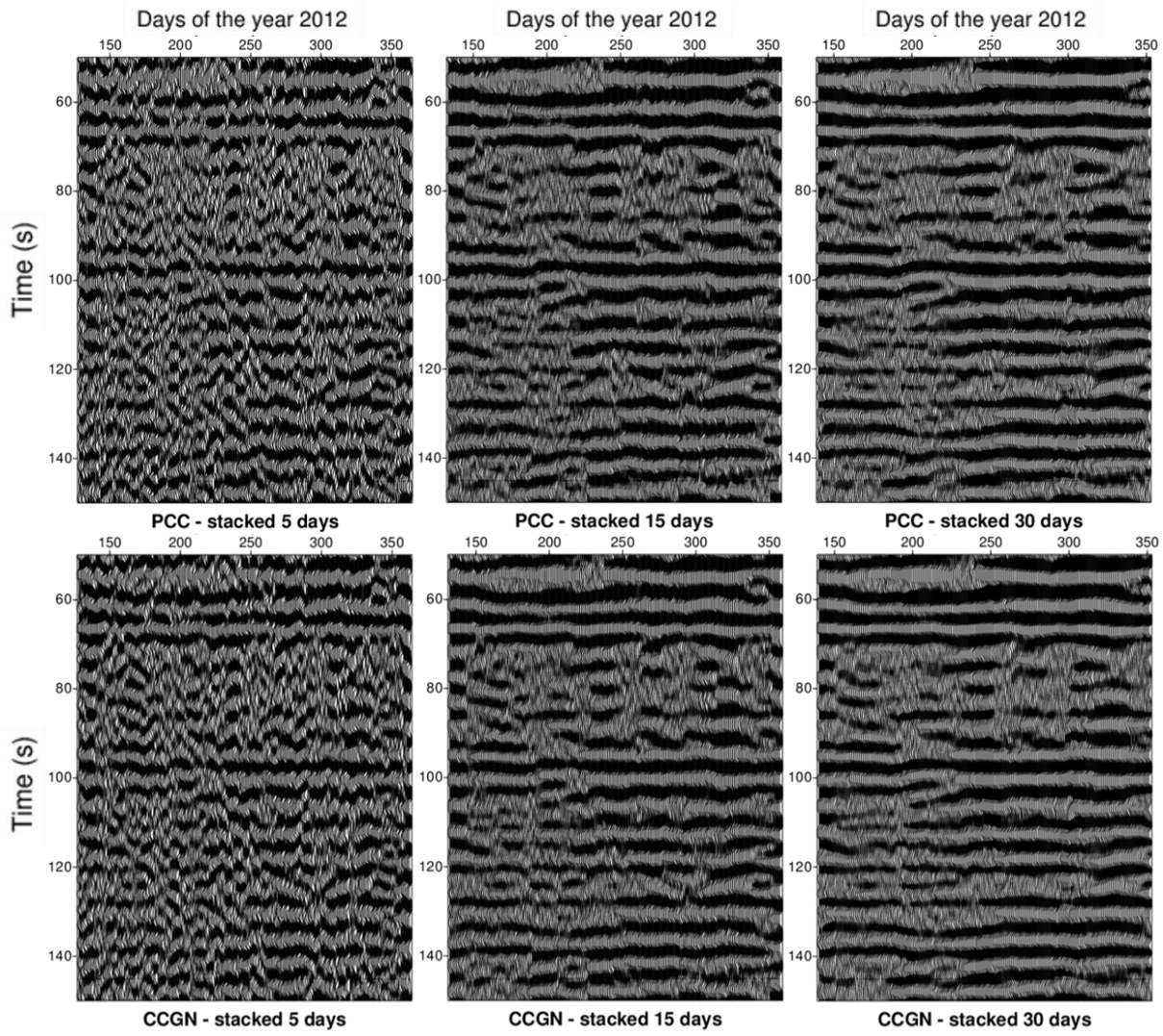

Figure 3.6: Section of auto-correlograms obtained by using PCC and stacked linearly using a 5-day (a), 15-day (b) and 30-day (c) moving window and by using CCGN and stacked linearly using a 5-day (d), 15-day (e) and 30-day (f) window for different time periods.

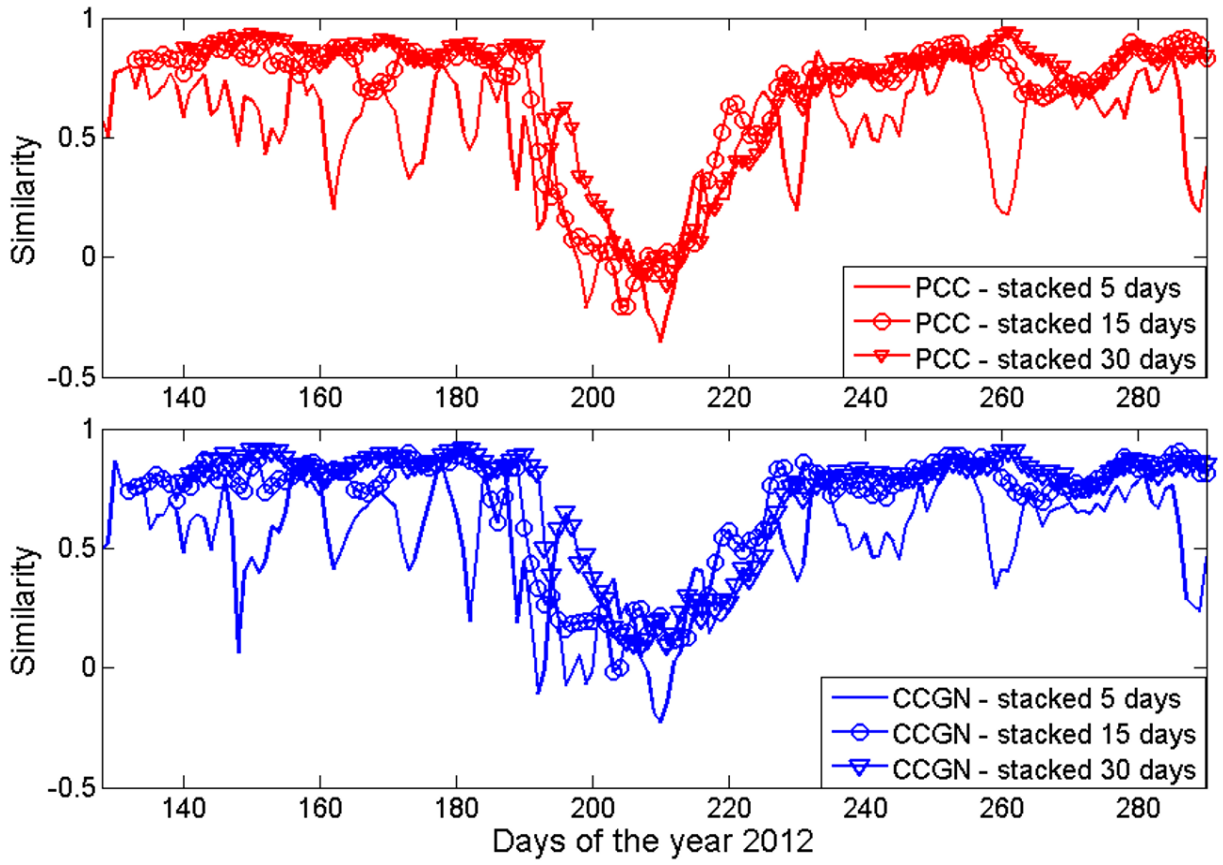

Figure 3.7: Similarity evolution between auto-correlograms obtained for a 5-day (-), 15-day (o) and 30-day (▲) moving data window with PCC (red) and CCGN (blue).

We also analyzed the influence of the reference trace when computing the similarity by using three other reference traces (Figure 3.8): (1) stack of all the pre-event auto-correlations (the one used in this study - red), (2) stack of all the post-event auto-correlations (black), (3) stack of all the auto-correlations except the most affected period by the m_b 4.9 event (blue). We can observe that for the three different reference traces, we obtain a sharp similarity decrease simultaneously to the main event. The overall results for the reference traces which include post-event data are quite similar. The results for the reference trace (1) uses only the pre-event autocorrelations so the similarity is less disturbed by incoherent signals from precursory events than the two other reference traces. As for our analysis we want to show co-seismic structural changes and post-seismic

recovery, we used the reference trace (1) which is not influenced by the post-seismic recovery to better detect when the similarity reaches pre-event values.

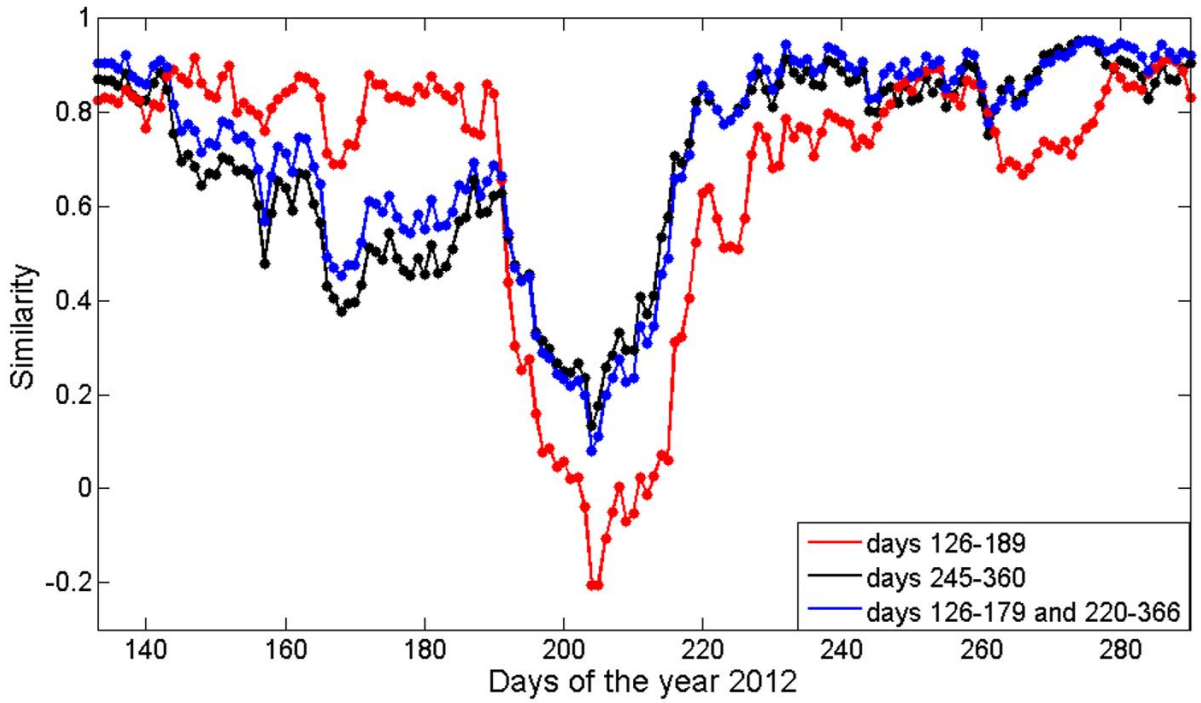

Figure 3.8: Study of the influence of the reference trace used to calculate the similarity evolution from the auto-correlograms. The reference traces are the stacks of auto-correlations calculated with PCC for the different time periods.

3.5 Discussion and Conclusion

With the only seismic station available in the Saint Paul transform fault region, we were able to detect waveform changes in the noise auto-correlograms related to a m_b 4.9 earthquake. Indeed, we could detect a similarity decrease when the m_b 4.9 earthquake occurred and then a fast recovery that slows down with the time. The same result has been

obtained using two different methods (PCC and CCGN) and three different moving time windows (5, 15 and 30 days), which shows the robustness of our observations.

The co-seismic similarity decrease indicates that the m_b 4.9 seismic event was responsible for a detectable change in the medium. This co-seismic change could be attributed to the opening of new fractures, cracks or the re-opening of pre-existing fractures, providing new pathways for groundwater flow (e.g., Toksöz et al., 1976; Rojstaczer et al., 1995; Poupinet et al., 1984; Baish and Bokelmann, 2001). These cracks are partially filled with water (Li and Vidale, 2001) and are meant to be transitory (Sibson, 1996).

The calculation of the zero-lag correlation between the auto-correlograms (stacked within a moving window of 15 days) and a reference trace allows us to obtain the approximate time necessary to reach a full similarity recovery, i.e., to come back to the seismic noise response of the pre-event period. The post-seismic recovery displays a fast recovery at the early post-seismic period followed by a relatively slow recovery. Only one month after the main event, we observe that the similarity has recovered 77% of the median pre-event value (dashed red line on Figure 3.5b) while another month is needed to reach a full recovery. Other studies showed, as well, that the recovery rate decreases with time (Li and Vidale, 2001; Schaff and Beroza, 2004; Sawazaki et al., 2009). They interpreted it as "a nonlinear response of the crust to the strong shaking of the main shock".

The healing process corresponds to the closure of the cracks that opened during the main shock, to come back to a similar configuration of the one prior the m_b 4.9 earthquake. Different process may contribute to the cracks closure as precipitation of secondary minerals (Sausse et al., 2001; Tenthorey and Fitz Gerald, 2006, Murakami et al., 2007) or compaction and pressure solution (Renard et al., 2000; Tenthorey et al., 2003). These healing process generally need years to be complete. In few studies (Li et al., 2006; Peng and Ben Zion, 2006; Minato et al., 2012), faster recovery (about 90% in a few months) have been observed. Sawasaki et al. (2009) highlights that the parameters responsible for the time recovery is not yet clear. However, the type of rocks seems to be an important factor.

The time necessary to reach a full recovery in this study is inferior to the one generally observed (e.g., Baish and Bokelmann, 2001; Roux and Ben-Zion, 2013). It can be due to the fact that in these previous studies the magnitudes of the analyzed earthquakes were stronger (m_b 6.9 and m_b 7.1 respectively) and therefore the medium would need more time to recover (Peng and Ben-Zion, 2006). The fact that we analyzed data from a region close to the MAR and in an aqueous environment may also influence the recovery rate and should be subject of further investigations.

From our study, we can conclude that it is possible to monitor the temporal evolution of the sub-surface related to a small magnitude earthquake (m_b <5.0) and in a rough geographic area such as the Saint Paul transform fault that cut the MAR. We further monitored the recovery, or healing process, in a pure ridge environment. We observe a fast recovery (~2 months) which might be related to the MAR spreading environment. These results are the first observation of a post seismic healing process in the MAR area and continuous monitoring, also at other ridge environments, would be important to further characterize the dynamic processes at Mid Ocean ridges.

3.6 Preliminary results for the 2013 and 2014 data*

This part shows the preliminary results and analysis obtained for the 2013 and 2014 data, as done previously. The purpose of this study is to improve our understanding of the behavior of the Saint Paul transform zone related to different earthquakes.

3.6.1 Data and processing

We used two set of data recorded by the broad band seismometer installed in the SPSPA. The first set of data were recorded from April (day 100) to June (day 183) 2013 and the second one from April (day 100) to November (day 332) 2014. We did a visual

*This section is not included in the submitted manuscript.

inspection of the data and we were able to detect approximately 30 seismic events during the 2013 period (83 days) and 70 during the 2014 period (232 days). We used the locations and magnitudes of the main earthquakes ($m_b > 4.0$) from the USGS website and of the smaller earthquakes ($m_b < 3.0$) from a local catalogue. The respective earthquakes' location are plotted proportionally to their magnitudes in Figure 3.9. For the 2013 period (circles), one m_b 4.1 earthquake occurred day 148 at 28 km from the SPSPA and two m_b 4.6 earthquakes on day 166 at 122 and 135 km. For the 2014 period (stars), four main events occurred: a m_b 5.9 on day 146 at 337 km, a m_b 5.0 day 183 at 177 km, a m_b 5.4 day 226 at 296 km and a m_b 4.3 day 228 at 37.81 km. Also, we highlight a m_b 2.8 event that occurred day 214 at 35 km from SPSPA.

As in the previous part, we used PCC on 0.1-0.5 Hz band passed data and then we stacked linearly the auto-correlations within 15 days. To analyze the temporal evolution of the auto-correlograms, we calculated two reference traces: one for 2013 and one for 2014. Here the reference traces correspond to the stack of the entire 2013 and 2014 data, respectively.

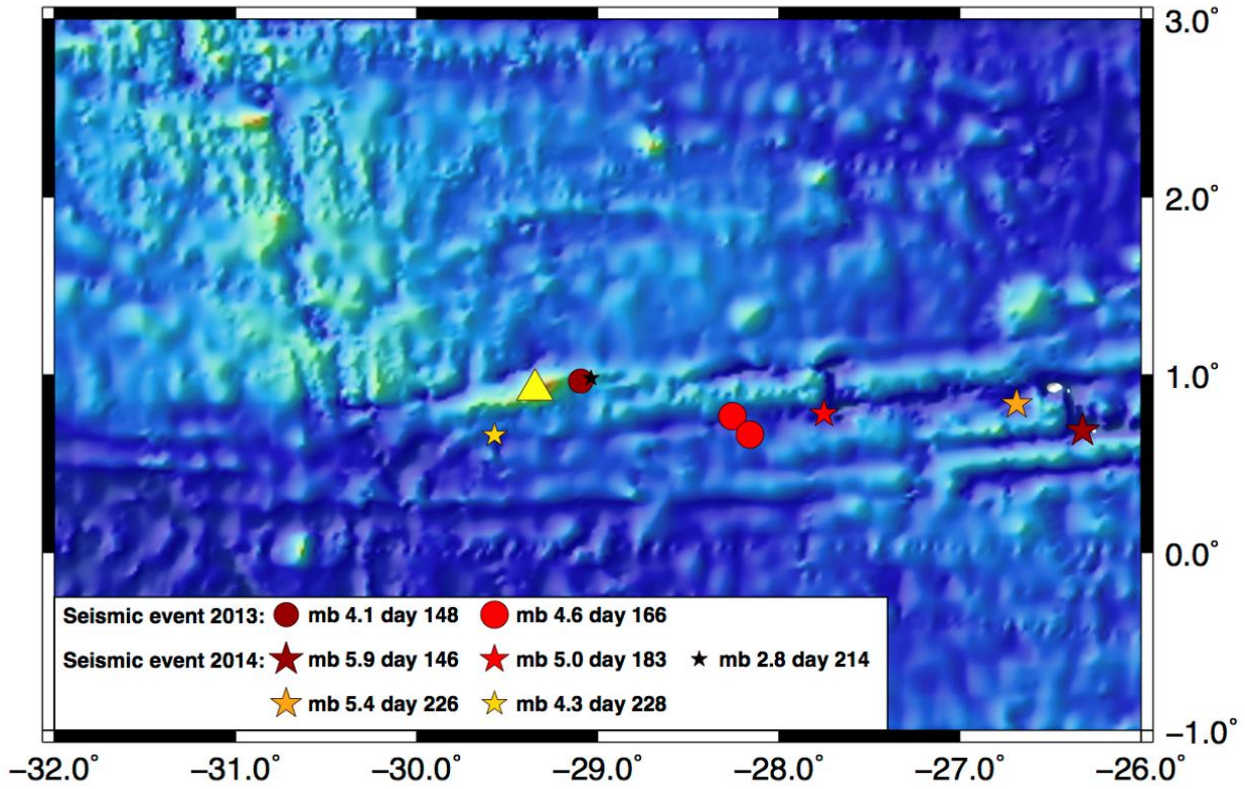

Figure 3.9: Map showing the location of the SPSPA seismic station (yellow triangle) and the earthquakes (circles and stars) within the period of interest. The circles show the seismic events from 2013 and the stars from 2014. They are sized proportionally with the magnitude and have different colors to distinguish the events occurring at different days.

3.6.2 Analysis and Results

In this part, we analyze the possibility of detecting structural changes caused by different earthquakes that occurred at less than 350 km from the SPSPA. This analysis is done using 0.1-0.5 Hz band-passed auto-correlations.

Figure 3.10 a and c represent the similarity between each auto-correlogram and the reference trace for 6 different lag-time windows (30-60 s, 55-85 s, 80-110 s, 105-135 s, 130-160 s, 155-185 s) for the years 2013 and 2014, respectively. Figure 3.10 b and d show

the strongest variations of the similarity with time occurring at the lag time windows 130-160 s for 2013 and 80-110 s for 2014.

Figure 3.10 a and b represent the results obtain for the year 2013. In this figure, we can observe that the main similarity decrease starts day 148 on the same day as the m_b 4.1 seismic event. Also from this figure, we can note that the similarity decrease occurs at all lag time even if the 130-160 s lag time shows a strongest decrease. Then, we observe a rapid recovery. Unfortunately, the data stopped before reaching a full recovery due to technical problems. However, we can observe that on the last recorded day (20 days after the main event) we already reached 62% of the median pre-event similarity value.

In Figure 3.10 c and d (year 2014), we can observe two main similarity decreases, the first one starting day 174 and the second one starting day 214. It is difficult to link the first one to a particular earthquake. The eventuality of smaller undetected earthquakes near the SPSPA could explain this similarity decrease. The second similarity decrease can be related to the m_b 2.8 occurring on day 214. Despite the small magnitude of this event, its close location to the SPSPA (~35 km) can justify its role in this similarity decrease. The m_b 5.3 and m_b 4.3 earthquakes occurring respectively on days 226 and 228 could also be related to the second decrease by increasing later on the damages created at first by the m_b 2.8 event. Moreover, these two similarity decreases seem to occur at all lag time even if the strongest decrease is observed for the lag time 80-110 s. At this lag time (Fig. 3.10d), we can observe a sharp similarity decrease followed by a relatively fast recovery. After about a month, the similarity recovery is interrupted by a second perturbation on day 214. On this day, the value of the similarity represented 83 % of the median pre-event similarity value. After this second sharp decrease, the similarity recovers rapidly to reach 78% of the previous in approximately 2 weeks and continues slower until reaching a full recovery 21 days later.

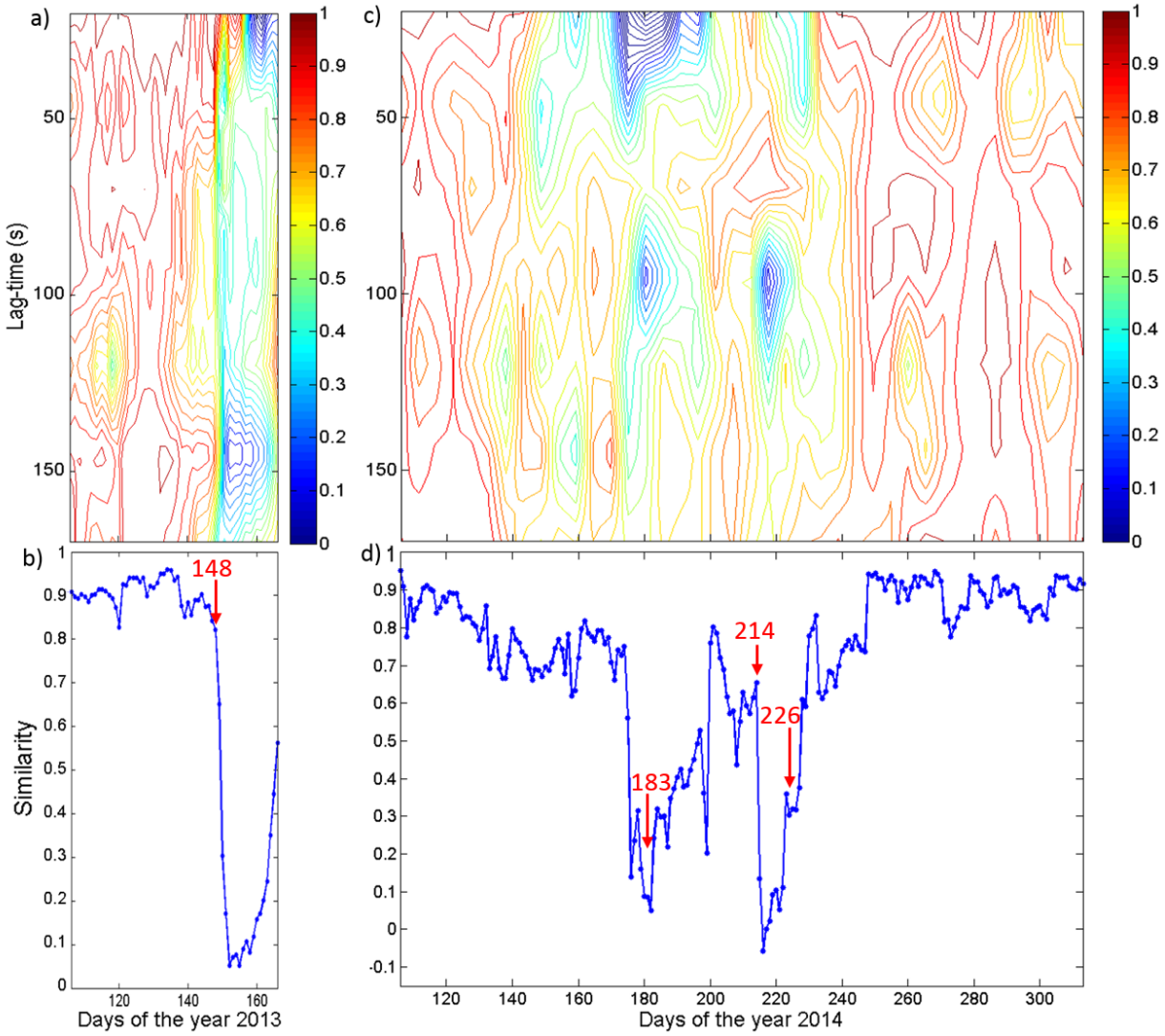

Figure 3.10: Study of the similarity temporal variations for the years 2013 (a and b) and 2014 (c and d). The contour plots (a and c) shows the similarity of the auto-correlations with respect to a reference trace (stack of all the auto-correlations per year) for different lag time. b) and d) show the similarity evolution for the lag times 130-160 s and 80-110 s, respectively. The red arrows show the occurrence of the earthquakes that might be related to the similarity decreases. The length of the arrows is proportional to the magnitudes of the events.

3.6.3 Comparison and conclusions on the three years of data

From the SPSPA seismic station, we were able to detect waveform changes in the noise auto-correlograms related to different earthquakes. For now, we did not establish a clear relation between each similarity decrease and a single earthquake.

The table 3.1 shows the distance to the SPSPA, the magnitude of the earthquakes associated to the four observed similarity decreases, as well as the time necessary for a partial or full recovery.

In 2012, the similarity decreases on the same day as a m_b 4.9 earthquake occurring at 42 km from the SPSPA. It is followed by a fast recovery that slows down with time. The auto-correlograms come back to the pre-event value after 2 months.

In 2013, we can observe a strong similarity decrease starting simultaneously with a m_b 4.1 seismic event at 28 km from the SPSPA. It is followed by a rapid recovery. After two weeks, we could observe a recovery of 62%. The data immediately after this two weeks were not available.

The results of the data from 2014 show a sharp similarity decrease followed by a rapid recovery, 83% in 23 days, which is interrupted by another strong similarity decrease. After this second similarity decrease, the healing process starts again and reaches 78% in 12 days and then 100% 21 days later.

	Distance to the SPSPA	Magnitude	Recovery
2012	42 km	4.9	100% in 2 months
2013	28 km	4.1	62% in 2 weeks
2014a	?	?	83% in 3 weeks
2014b	35 km	2.8	100% in 1 month

Table 3.1: Recapitulative table indicating the distance to the SPSPA, the magnitude of the earthquakes associated to the four observed similarity decreases. It shows as well the time necessary for a partial or full recovery.

From the study of these four earthquakes, we can note the difficulty to link entirely the similarity decreases with the occurrence of earthquakes above m_b 4.0. For the similarity decrease in 2014a, we did not find any significant earthquake that could explain it. Also, on the same day than the similarity decrease in 2014b a m_b 2.8 event has been recorded. We were not able to determine if this earthquake could be responsible for such an important medium change.

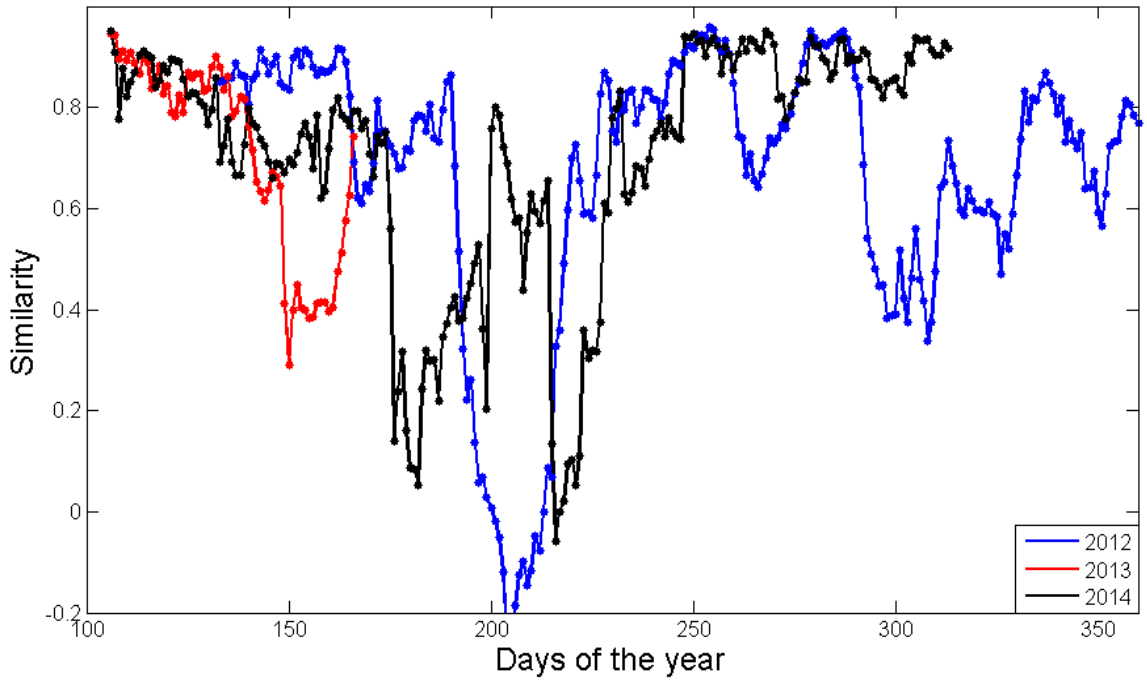

Figure 3.11: Study of the similarity evolution for the years 2012 (blue), 2013 (red) and 2014 (black).

Also, it is important to highlight that for the four studied earthquakes (Figure 3.11), we can observe a rapid recovery ($\leq$ 2 months). It could indicate that post seismic healing process in the MAR area is fast. However, it is not clear yet if we have systematically a fast recovery in the early post seismic period which rate decrease with the time. Nevertheless, we observe this pattern for the two post seismic healing processes that had

reached a full recovery. Other studies showed, as well, that the recovery rate decreases with time (Li and Vidale, 2001; Schaff and Beroza, 2004; Sawazaki et al., 2009) even if the geological context were different. These indications are in favor of our hypothesis.

Another interesting point is that the similarity decreases, observed in 2013 and 2014, are visible at all lag time contrary to the one in 2012 that was confined in a particular lag time. It shows that the structural changes are relatively homogeneous. They did not occurred in a localized area as observed previously.

In conclusion, this study is promising and gives several important information about the post seismic behavior in the MAR environment. We could learn that the healing process seems to be fast and to decrease with the time. In the future, we could use these data to characterize the parameters responsible for detectable medium changes such as magnitude and distance from the SPSPA and to confirm our hypothesis on the healing process in the MAR.

3.7 Acknowledgement

The data for this paper can be requested to aderson@geofisica.ufrn.br or virginie.dhour@gmail.com. The authors thank the Instituto Nacional de Ciência e Tecnologia - Estudos Tectônicos (INCT-ET/CNPq) and the Instituto Nacional de Ciência e Tecnologia – Geofísica do Petróleo (INCT-ET/CNPq). V. D'Hour thanks CAPES for her PhD grants and Science without Borders Programme for allowing the sponsored period of 1 year in Barcelona, Spain. M. Schimmel thanks the Science without Borders Programme for his PVE grant and CGL2013-48601-C2-1-R.A. Nascimento thanks CNPq for his PQ grants. V. D'Hour also thanks IPGP for the one year visit. The authors also thank Eduardo Menezes for his valuable work in the data acquisition period and Pascal Bernard for fruitful discussions.

Chapter 4

Test of the coda wave interferometry methods for a swarm of small magnitude earthquakes in NE Brazil.*

4.1 Abstract

Coda wave corresponds to a scattered seismic wave that passed several times by the same volume. For this reason, the coda (later part) of a seismic signal is more sensitive to small medium changes. Coda wave interferometry exploits this idea to measure time lags or waveform differences that give information on changes in the Earth's structure. In this work, we use coda wave interferometry to monitor temporal changes of the subsurface caused by an intraplate sequence of seismic events in North-East of Brazil. From February 2007 to July 2007, 214 events were detected and the main event, m_R 3.7, occurred on the 20/03/2007. We first validated our processing with synthetics data. We show that the processing we use for coda wave interferometry is able to detect a 1.1% change in the source position (compared to the distance source-receiver) and a 15% decrease of the scatterers' amount. We observed that these changes could not be detected by the first arrival waves. Then, from the real data, we observed a rapid decorrelation of the seismic coda after the m_R 3.7 seismic event. This indicates a rapid change of the subsurface in the fault's region induced by the earthquake. As we have a weak density of multiplets, we also use seismic ambient noise phase cross-correlation to confirm the results obtained with coda wave interferometry.

*The main content of this chapter is to be submitted for publication to *J. South Am. Earth Sci.*

4.2 Introduction

Coda wave interferometry (CWI) is a relatively recent technique, which is based on the interference pattern between the coda of two co-located events called multiplets (Snieder and Vrijlandt, 2005; Snieder, 2006). Coda waves have been first described by Aki (1969) as the late arriving waves of the seismogram that arise from scattering. Later studies showed that the coda waves are repeatable under the same conditions demonstrating that they carry information about the medium (Grêt, 2004; Snieder et al., 2007; Wapenaar et al., 2010a,b). Coda waves' creation are related to the complex wave propagation into a medium with heterogeneities, such as seismic discontinuities and volumetric scatterers (Groenenboom and Snieder, 1995). The presence of these heterogeneities causes a redistribution in time of the seismic energy which means that a main wave is partitioned into different waves which arrive after the main wave, i.e., in its coda. Hence, coda waves repeatedly sample the medium making them more sensitive to small changes which are not perceptible in the first arrival waves (Snieder, 2006). In addition, this method is advantageous because it is not invasive and needs only one station. Because of coda waves' high sensitivity, CWI has been used to determine seismic velocity changes in fault zones (Poupinet et al., 1984; Baisch and Bokelmann, 2001; Roux and Ben-Zion, 2013), in laboratory specimens (Snieder et al., 2002; Grêt et al., 2006), in volcanoes (Ratdomopurbo and Poupinet, 1995; Snieder and Hagerty, 2004; Grêt et al., 2005; Larose et al., 2010; Wegler et al., 2006), and as well for the monitoring of small stress changes (Grêt et al., 2006), CO2 sequestration (Khatiwada et al., 2012), nuclear waste (Grêt, 2004; Grêt et al., 2006; Snieder et al., 2007) and for the estimation of the separation between a pair of earthquakes (Robinson et al., 2011).

In this chapter, we focus on testing CWI efficiency for the detection of medium changes due to a m_R 3.7 (Brazilian earthquake magnitude scale as in Assumpção, 1983) intraplate earthquake. The main event in this study has a low magnitude and, therefore, a small impact on the medium is expected when compared to previous studies which use events with magnitude typically larger than m_b 6.0 (e.g., Baisch and Bokelmann, 2001;

Schaff and Beroza, 2004; Roux and Ben-Zion, 2013). The study uses an intraplate sequence of small magnitude events (m_R <3.7) occurring in São Caetano, NE Brazil.

This chapter is divided into four parts. Section 4.3 explains the CWI method and presents the processing steps. In the Section 4.4, we illustrate the method using synthetic data from the code developed by Groenenboom and Snieder (1995). Section 4.5 shows the analysis and the results obtained with CWI for data from NE Brazil. In this section, we also discuss the results. And finally, a conclusion is given in section 4.6.

4.3 Data processing

CWI uses co-located doublets events recorded by the same station. Since they have basically the same ray path, they ought to have very similar waveforms and arrival times. If we observe a travel-time difference between the two signals, we can assume that the medium has changed between the moment when the first event occurred and the moment the second event occurred.

So this travel-time perturbation (t_s) is the tool that we use to quantify a change in the medium. Also, we can calculate t_s by cross-correlating the data as following (Snieder, 2002; Grêt, 2004):

$$R^{(t,t_w)}(t_s) \equiv \frac{\int_{t-t_w}^{t+t_w} u_{unp}(t')u_{per}(t'+t_s)dt'}{(\int_{t-t_w}^{t+t_w} u_{unp}^2(t')dt' \int_{t-t_w}^{t+t_w} u_{per}^2(t')dt')^{1/2}} \qquad (4.1)$$

where the time window is centered at time t with duration $2t_w$. t_s is the time shifted used in the cross-correlation, u_{unp} is the unperturbed wave field and u_{per} is the perturbed wave field.

To analyze the data, we used a Matlab toolbox "GISMO suite" (www.giseis.alaska.edu/Seis/EQ/tools/GISMO/). The workflow is: 1) cross-correlation of all the first arrival waveforms between them in order to obtain a cross-correlation matrix, 2) determination of groups of similar events into different clusters, 3) cross-correlation of

the first arrival waveforms and coda waves, separately, with a master event from a same cluster.

4.4 Test of the method on synthetic data

In order to illustrate our procedure, we produced three set of synthetic data from the code developed by Groenenboom and Snieder (1995). The first set has been simulated for a source located at the origin (0,0), 96 receivers at the opposite side and 200 scatterers between them (Figure 4.1). Then, to create the second set we changed the relative position of the source by moving, in the y-axis, the receivers of 0.8, 1, 1.6 and 2 m, respectively. Finally, we simulated the third set of data with 15%, 10%, 8% and then 5% less scatterers than the initial setting. This last set mimics the medium changes caused by an earthquake followed by a progressive recovery.

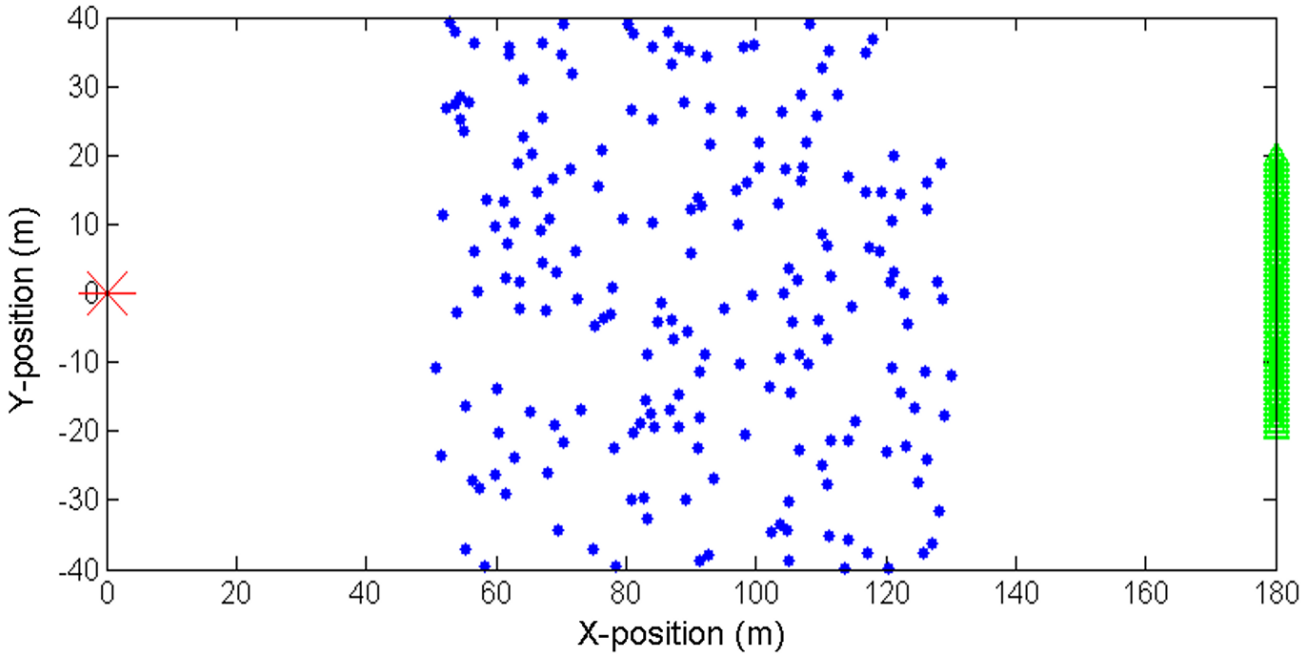

Figure 4.1: Configuration of the source (red star), the receivers (green triangles) and the scatterers (blue dots) for the creation of the synthetic data initial set.

From Figures 4.2a and 4.2b, we can observe the records from the second receiver from the top of the original configuration of Figure 4.1 (top seismogram) and after the several changes. It shows the traces recorded for different source positions (Figure 4.2a) and for different amount of scatterers in the medium (Figure 4.2b). For both cases, the first arrival waves (0-0.1 s) do not show any visible change (Figure 4.2c and 4.2d – black dots). It confirms that using the first arrival waves is not sensitive enough to detect small changes (Grêt et al., 2005; Snieder, 2006; Larose et al., 2010; among others).

In the case of a change of 2 m in the source position (the maximum in this study), a waveform difference is visually discernible in the coda wave trace (Figure 4.2a). This difference from the initial trace is measured by cross-correlating the coda waves (0.1-0.25 s) of all the traces with the initial one. We can observe that the coda waves' correlation coefficients decrease as the change of the source position increases (Figure 4.2c – red dot). For comparison purposes, we applied the same processing on the first arrival waves (Figure 4.2c – black dot) and the resulting correlation coefficient stays stable and high (>0.8).

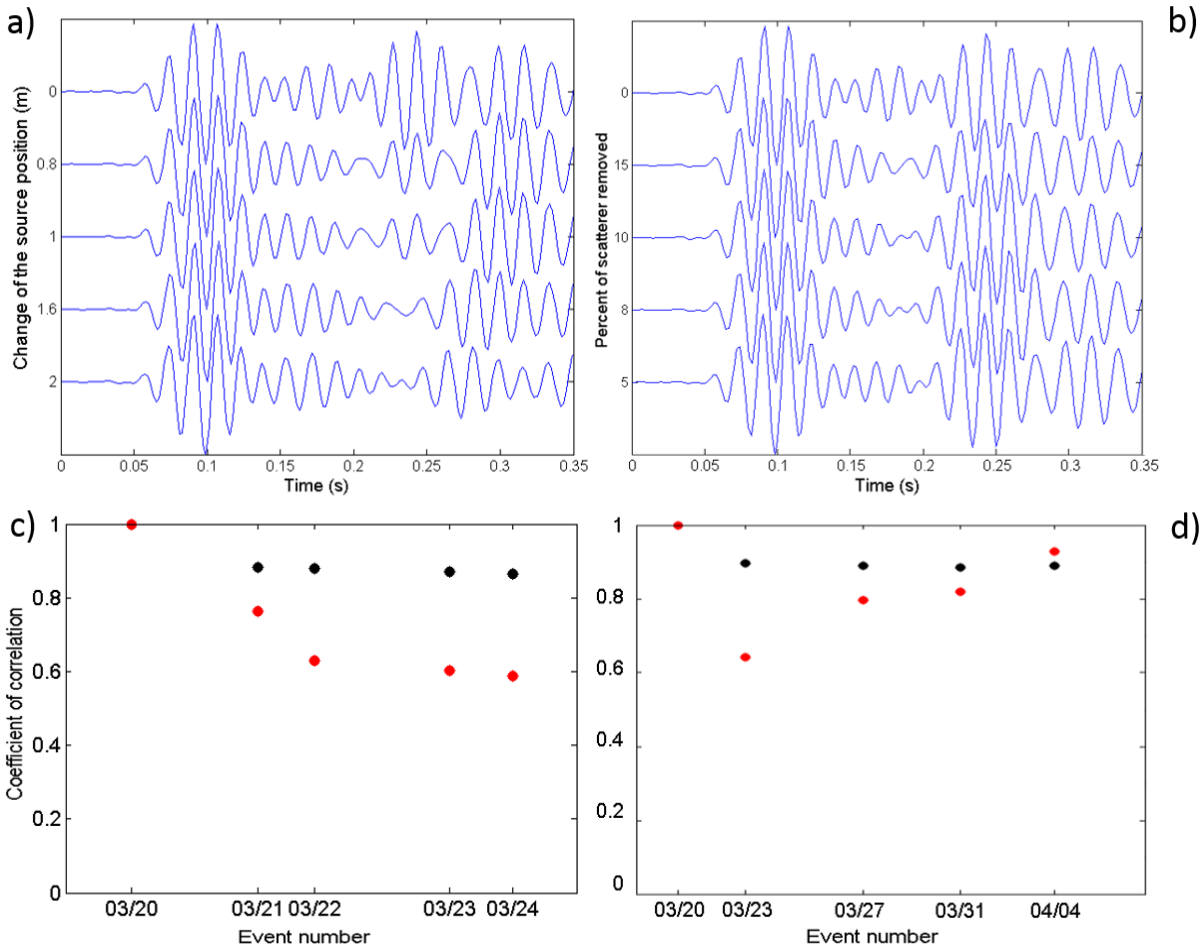

Figure 4.2: a) Traces from the initial configuration, a change of 0.8, 1.0, 1.6, 2.0 m in the source position. b) Traces from the initial configuration, 15%, 10%, 8% and 5% of scatterers removed. Analysis of the effect of the configuration changes by cross-correlating the first trace by the following ones for the P waves (black dots) and the coda waves (red dots): c) for a change of source position that increases with time and d) for a quantity of scatterers that decreases abruptly (-15%) to come back near the initial amount (-5%).

When 15% of the scatterers are removed (the maximum in this study), we can observe a slight decrease of the coda wave's amplitude compared to the initial waveform. It can be explained by the fact that the coda waves are the result of the scattering, so if we decrease

the scattering effect, we decrease the coda waves' amplitude. As for set changing the source position, we calculated the correlation coefficient for each amount of scatterers removed in respect to the initial trace for the first arrival waves (Figure 4.2d – black dot) and for the coda waves (in Figure 4.2d – red dot). We can observe that whilst the first arrival waves' correlation coefficient stays stable and high (>0.8), the coda waves correlation coefficient drops as the amount of scatterers decreases by 15% and then it recovers up to 0.9 as the amount of scatterers comes back close to the initial value (-5%).

This analysis on synthetic data shows, as expected, that the coda wave is sensitive enough to detect small changes as a slight change in the source position (1.1% of the distance source-receiver) or decrease of the amount of scatterers (15%), whilst the P phase does not show any changes. Also, one has to be aware that we can not discriminate between these two causes using the CWI method only.

4.5 Real data example

4.5.1 Data configuration and studied area

Here, we show an example of the CWI method in the case of an intraplate seismic swarm. This seismic swarm occurred in a NE-trending branch of the ductile Pernambuco shear zone, near São Caetano, state of Pernambuco, NE of Brazil (Figure 4.3).

After the occurrence of a m_R 4.0 event (May 2006), a local five-station network was deployed in the epicentral area for almost 6 months from 01/02/2007 until 21/07/2007. The stations were equipped with short period S13J three components sensors (with 1 Hz frequency) and SMART24® recorders. A total of 214 events were detected during this period (Lima Neto et al., 2013). The sampling rate of these data was 500 Hz. Lima Neto et al. (2013) determined that these seismic events spread over ~ 4 km long and within a depth between 2 and 8 km on the same plane as the dip of the original fault (60° south).

The event with the highest magnitude recorded (m_R 3.7) occurred on the 20/03/2007 and it is followed by aftershocks of lower magnitude. The red triangles correspond to the

stations that gave the best results, SOJO and SOLC, and whose results are represented next. Unfortunately, the data from the station SOJO has two time gaps from the 25/02/2007 to the 09/03/2007 and then from the 15/04/2007 to the 15/05/2007. This station is particularly important for our study because of its location close to the epicenter of the main event (Figure 4.3 – blue star).

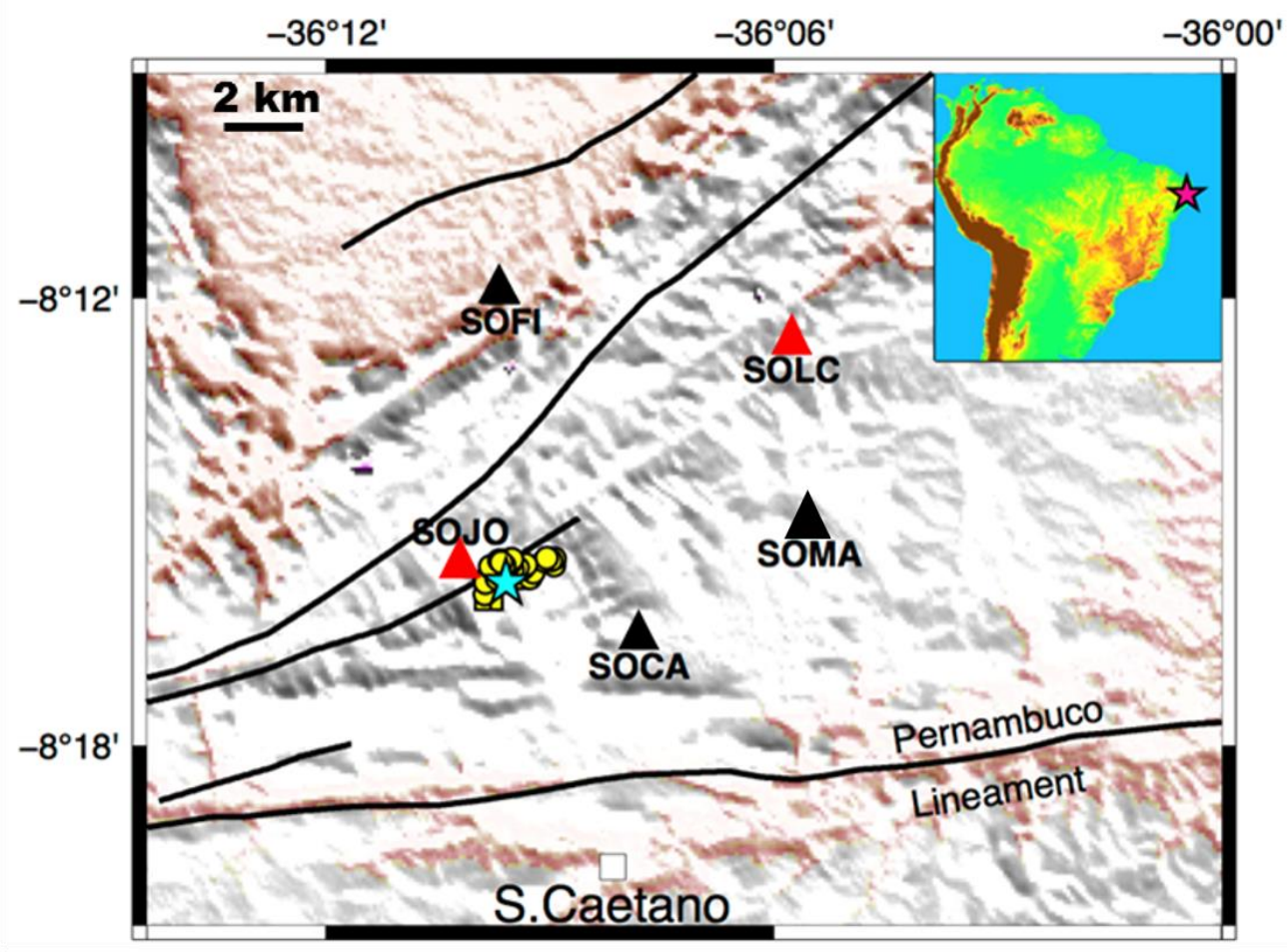

Figure 4.3: Map showing the fault system of the studied region, the location of the stations (triangles) and the distribution of the events occurring during the study (small yellow circles) including the major m_R 3.7 event (blue star). The red triangles show the stations that gave satisfactory results.

4.5.2 Results and discussion

We applied the CWI processing for the stations SOLC and SOJO separately. The following figures illustrate the result of the different processing steps for the station SOLC.

As for the synthetic data, we cross-correlated the first arrival wave (0-0.12s) for all the pairs of data recorded at the station SOLC to obtain a cross-correlation matrix (Figure 4.4). From this matrix, we could determine a main cluster (Figure 4.4 – red dotted squares) gathering a group of similar events. This cluster is formed by seven events, from 20/03/2007 until 12/04/2007, linked by a correlation coefficient, for the first arrival wave, equal or greater than 0.8. Then, we cross-correlated the coda waves of all the events with a chosen master event (first event chronologically) to obtain their waveform similarity represented by their correlation coefficient. We repeated the last step of the processing for different time windows (Figure 4.5 – blue, green and red bars) and for different frequencies to test the influence of these parameters.

Firstly, we compared the results obtained with the three time windows 0.2-0.5 s (Figure 4.6a – blue dot), 0.3-0.6 s (Figure 4.6a – green dot) and 0.4-0.7 s (Figure 4.6a – red dot). The three results follow the same general trend for the three different time windows even if it is less clear for the 0.4-0.7 s window. We can observe a decrease after the main event (20/03/2007) until reaching a minimum day 26/03/2007 (Figure 4.6a – green dot) or day 31/03/2007 (Figure 4.6a – blue dot) followed by a relative come back to the initial values. We can as well notice that more the time window is further in the coda, the maximum change occurs earlier and is less pronounced. Another test, not displayed here, with a 0.3 s length overlapping window has been calculated from 0.2 s to 1.25 s and the results confirm these observations. Another test with a longer window length (0.5 s) shows that if we take a longer time window, the correlation coefficient gets too averaged so we can not see the changes anymore.

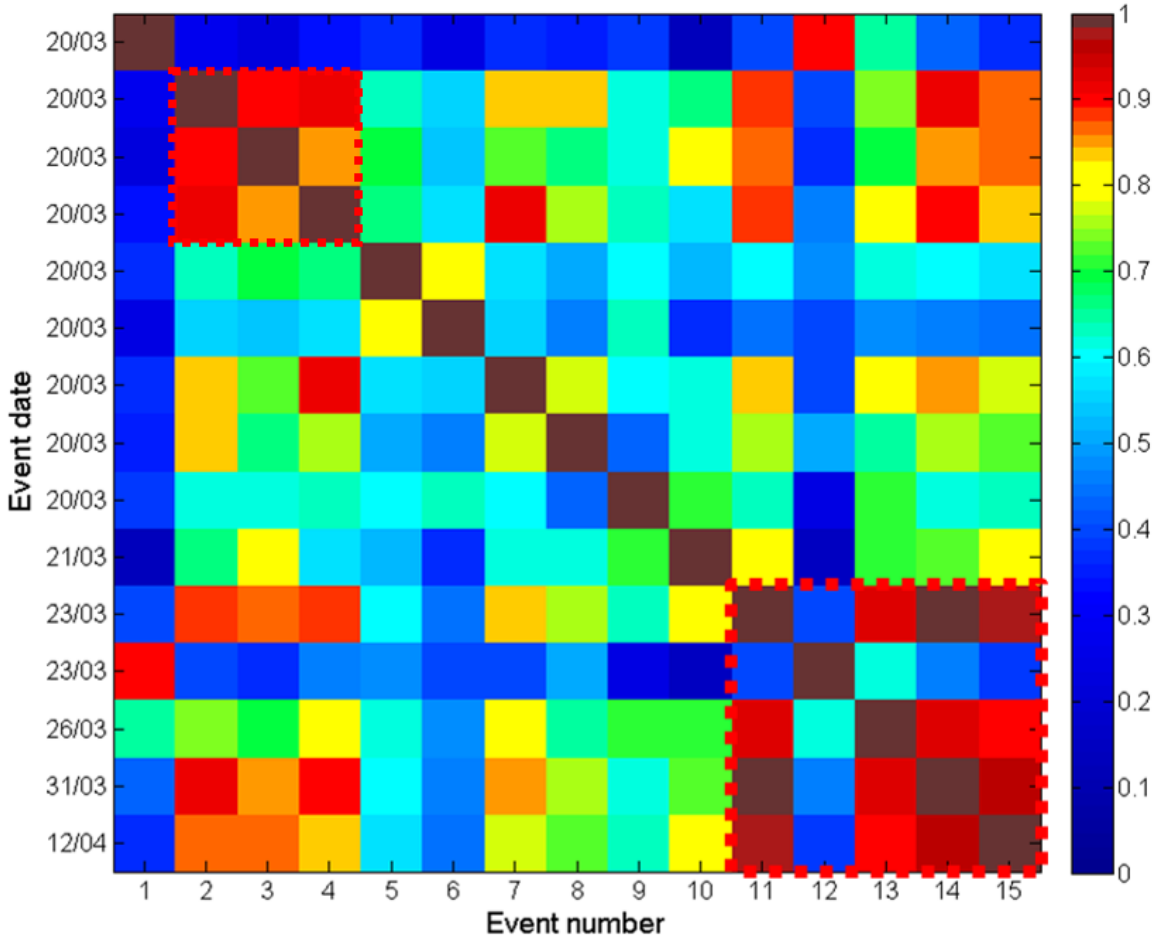

Figure 4.4: Matrix of correlation of the events recorded at station SOLC. The events for which the cross-correlation is marked from 0.8 (yellow) to 1 (red) are considered as well correlated. The red dotted squares show the main cluster (the second event from 23/03 is not included in this cluster).

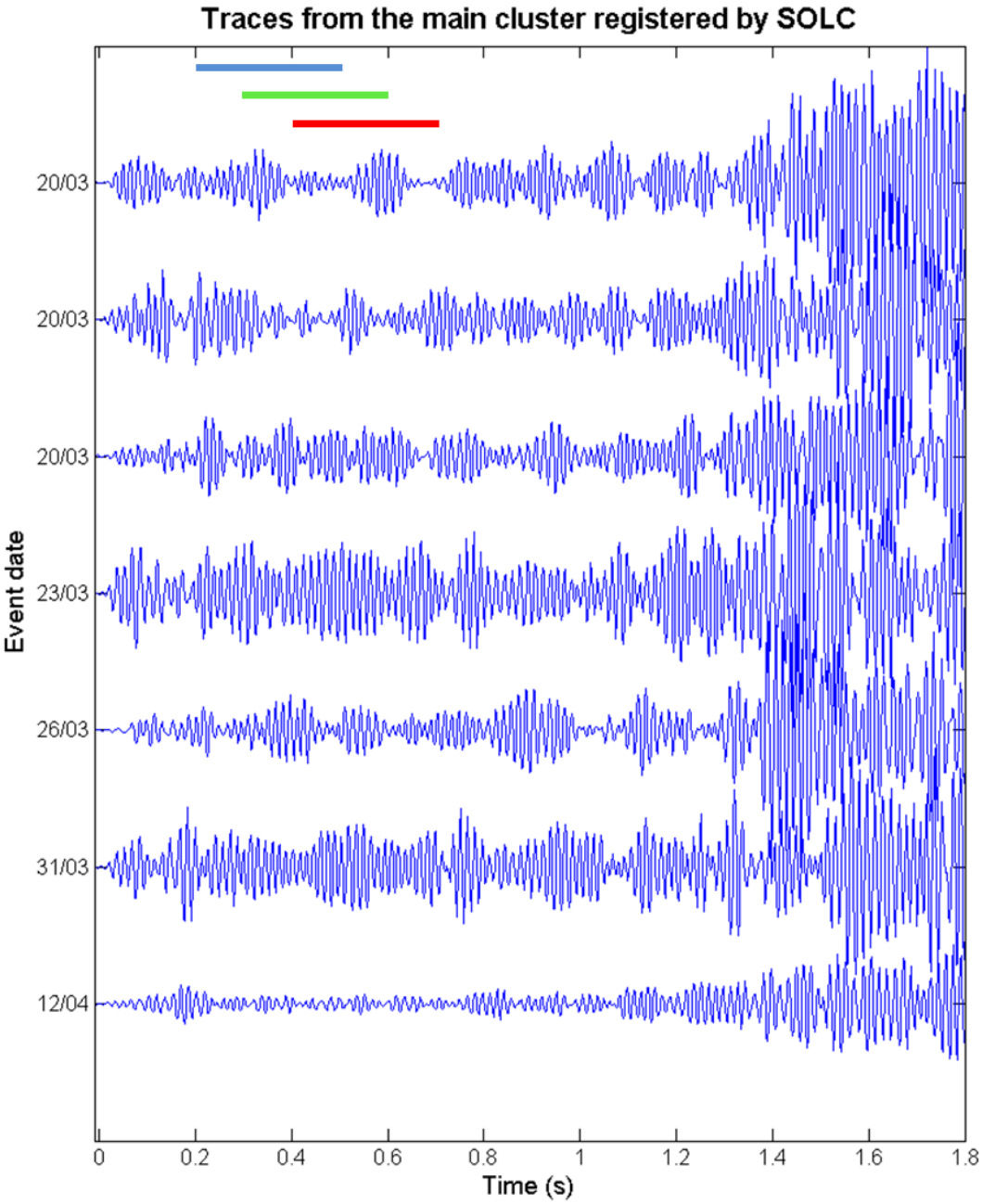

Figure 4.5: Plot of the traces from the main cluster at station SOLC. The blue, green and red bars on the top indicate the time windows used to calculate the coda waves' cross-correlation between the first trace and the following traces. The corresponding results are shown Figure 4.6.

Secondly, we tested the influence of the frequency band using four different frequency bands 5-10 Hz (Figure 4.6b – green dot), 20-40 Hz (Figure 4.6b – blue dot), 32-64 Hz (Figure 4.6b – black dot), 64-128 Hz (Figure 4.6b – red dot). We can observe that the result obtained with the 5-10 Hz band displays a different trend than the one using higher frequency bands. By consequence, this frequency band seems less robust. The three other frequency bands show a maximum decrease of the correlation coefficient 11 days after the main event (31/03/2007), then it increases until day 12/04/2007. The frequency band that accentuate the most this trend is 64-128 Hz.

Finally, considering the previous observations, we used the time window 0.2-0.5 s and the frequency band 64-128 Hz to obtain the temporal evolution of the medium measured at stations SOLC and SOJO (Figure 4.7).

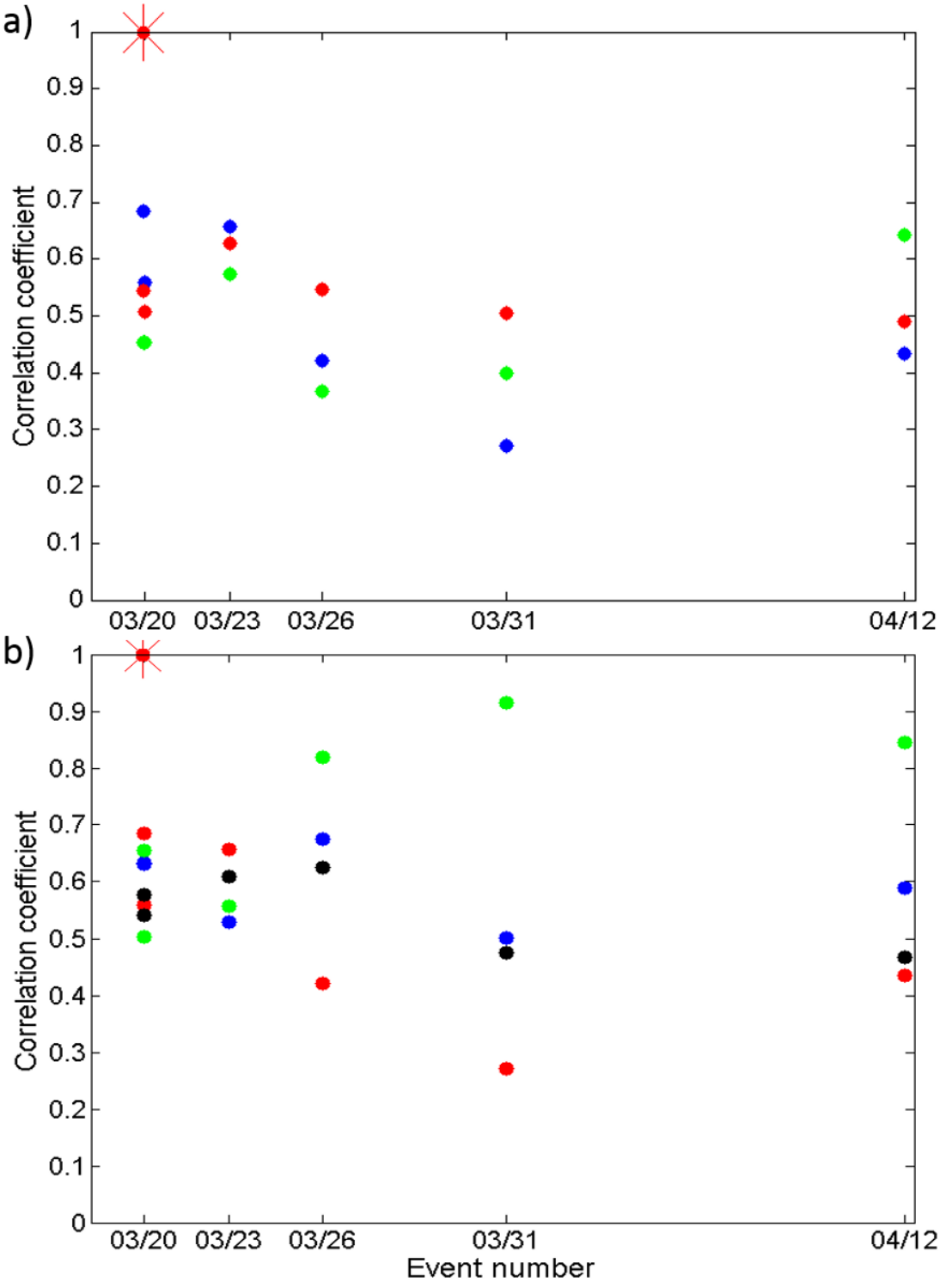

Figure 4.6: Results of the coda wave's cross-correlation of the main SOLC cluster. a) represents the results for the different windows shown in Figure 4.5 (0.2-0.5 blue, 0.3-0.6 green and 0.4-0.7 red). b) represents the results for different frequency bands (5-10 green, 20-40 blue, 32-64 black, 64-128 red).

In Figure 4.7, we can observe a similar temporal variation for both stations, the correlation coefficient decreases until six days after the event and increases again to come back again at almost the same level than the first correlated event on 04/12/2007. This temporal variation can be interpreted by a continuous change of the medium due to the main event occurring on 20/03/2007 (e.g., Poupinet, 1984; Snieder, 2002; Schaff and Beroza, 2004; Grêt et al., 2005). Even if we have only seven (SOLC) and six (SOJO) events to analyze, our result and corresponding interpretation seems to be relatively robust because we could observe a systematic variation of the coefficient of correlation independently of the time window in the coda and of the frequency band.

Also, to strengthen these results, we analyzed the ambient seismic noise recorded at stations SOJO and SOLC. We used phase cross-correlation (PCC – Schimmel, 1999), which is based on the instantaneous phase coherence concept used in phase-weighted stacks (Schimmel and Paulssen, 1997). Then, we stacked linearly the cross-correlations within a 3-day moving window to obtain a cross-correlogram for every averaged day. Finally, we compared the cross-correlograms to a reference trace (stack of the pre-event period). Figure 4.8 shows the result of the PCC analysis for our period of interest (17/03/2007 – 12/04/2007). In order to compare the CWI and PCC results we plot in red the days used for the CWI. The ambient seismic noise analysis shows a decrease from the 24/03/2007 and reach a minimum on the 28/03/2007. This result is coherent to the one obtained using CWI which strengthens our hypothesis of a medium change induced by an intraplate m_R 3.7 earthquake. However, the relative recovery seems rather to correspond to temporary variations than an actual medium recovery (D'Hour et al., 2015).

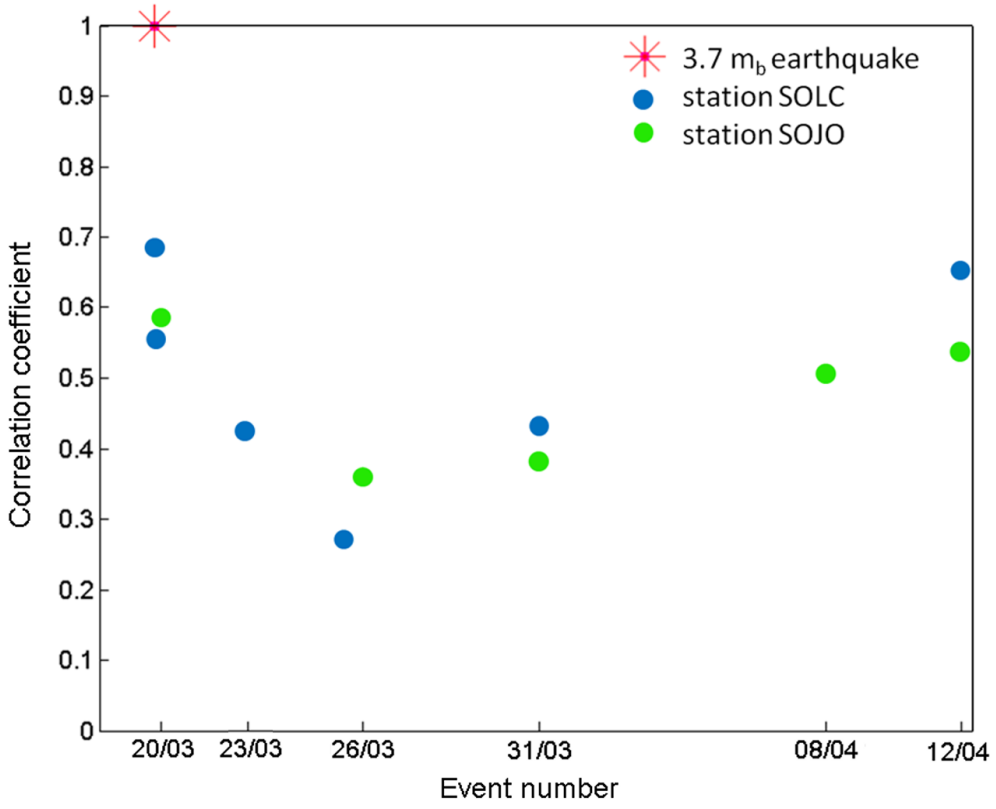

Figure 4.7: Result of the coda wave's cross-correlation obtained for the main clusters of the stations SOJO (green dot) and SOLC (blue dot). The red star mark the main m_R 3.7 event that occurred on 20/03/2007.

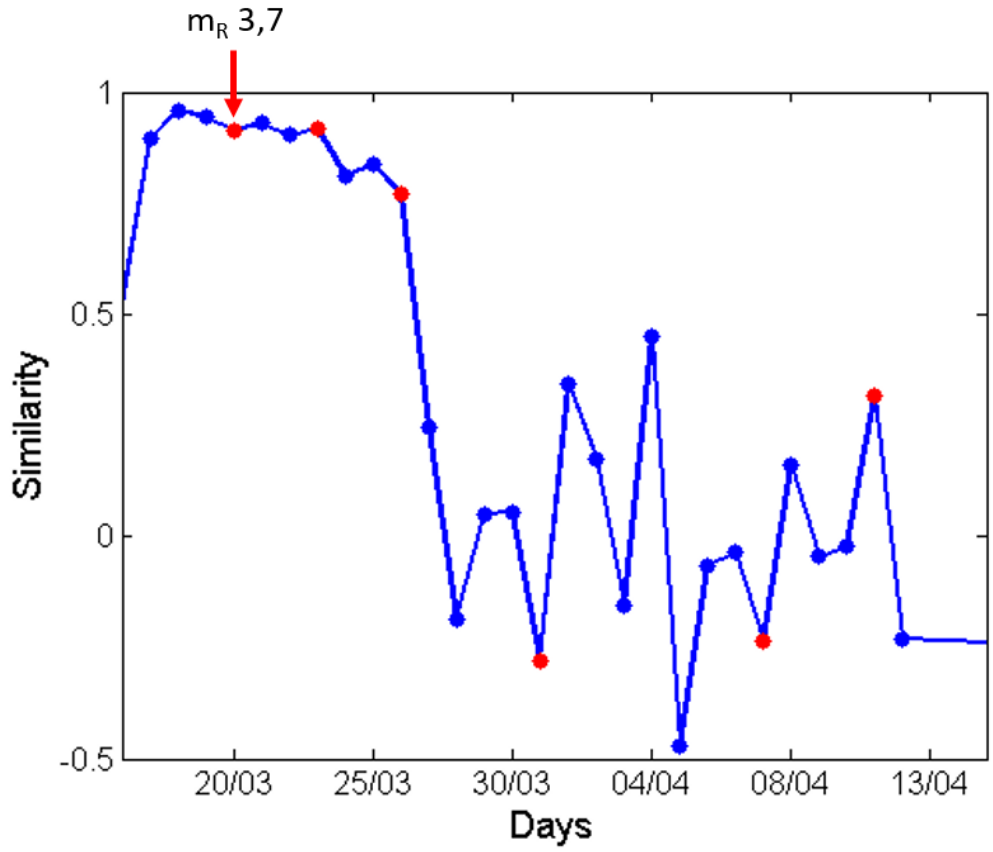

Figure 4.8: Result of the ambient noise cross-correlation for the stations pair SOJO-SOLC from 17/03/2007 to 12/03/2007. The red dots mark the days from the SOLC and SOJO clusters. The red arrow mark the day when the m_R 3.7 event occurred.

The reason why this change can be detected by the coda wave interferometry and not by the first arrival waves is that the coda waves spend more time in the medium which makes them more sensitive to small changes. The results obtained with CWI (Figure 4.7) show a decrease of the similarity after the main event but this method does not allow us to determine if this change is due to a structural medium changes or to a change in the source position (Figure 4.2). Using ambient seismic noise, we were able to detect a similar decrease than with CWI that would mean that this change could be interpreted as structural changes. These changes could be due to a change in the amount and/or strength of the scatterers provoked by fluid migration or opening and closing of fractures and pre-existing faults (Niu et al., 2003; Snieder and Page, 2007).

4.6 Conclusion

This work shows that coda wave interferometry is a sensitive tool to detect small medium changes related to intraplate seismic sequence of events, whose main event is m_R 3.7, near São Caetano, NE of Brazil. Indeed, the results of our processing show a decrease of the correlation coefficient occurring after the main event. This decrease was observed for the largest cluster recorded by two different stations, for different time windows and for different frequency bands.

However, because of the lack of data (the largest cluster contains only seven events), it appears necessary to complement CWI with ambient seismic noise correlation in order to validate the results.

Finally, the results of our study show that it is possible to use CWI for the monitoring of an intraplate medium changes related to small magnitude events. If the density of data is insufficient, it might be necessary to combine CWI with ambient seismic noise correlation.

4.7 Acknowledgements

We thank Martin Schimmel for his help and advice. We also thank Jeroen Groenenboom, and Roel Snieder for letting us use their code to calculate the synthetic data. The authors thank the Instituto Nacional de Ciência e Tecnologia - Estudos Tectônicos (INCT-ET/CNPq) and the Instituto Nacional de Ciência e Tecnologia – Geofísica do Petróleo (INCT-ET/CNPq). V. D'hour thanks CAPES for her PhD grant. A. Nascimento thank CNPq for their PQ grants. M. Schimmel thanks the Science without Borders Programme for his PVE grant and CGL2013-48601-C2-1-R. V. D'hour also thanks the Science without Borders Programme for allowing the sponsored period of 1 year in Barcelona, Spain. The authors also thank Eduardo Menezes for this valuable work in the data acquisition period.

Chapter 5

Conclusion

The work shown in this thesis represents a contribution to the field of monitoring. We demonstrate that ambient seismic noise monitoring might be used in intraplate and Mid-Atlantic Ridge context. Coda wave interferometry was also tested for the intraplate area but its results seems less robust and needs to be reinforced by the ambient seismic noise results.

The study of the intraplate settings, in São Caetano, using ambient seismic noise correlation (Chapter 2) gave satisfactory results and manage to get through some data restrictions as:

- a low density of data, only 6 months including 36 days of gap for the station SOJO;
- the recording of the data stopped before the end of the seismic activity preventing us from observing any relaxation of the medium;
- no access to drills, neither to meteorological data to check the level of water in order to confirm our theory of fluid migration and to explain some discrepancy (severe decrease of the similarity over only one day).

Despite these difficulties, we were able to detect localized structural changes related to a m_R 3.7. An earthquake of this magnitude provoke small damages in a restricted area. Generally, the study the earthquakes' effects uses seismic events of at least magnitude 6 (Wegler et al., 2009; Wegler & Sens-Schönfelder, 2007; Obermann et al., 2008; Zaccarelli et al., 2011, among others). In these cases of higher magnitude events, they were able to show sharp time shifts corresponding to a co-seismic velocity decrease. In our case of lower magnitude events, the medium changes are slighter and more difficult to detect. As the damaged area is spatially localized (as proposed in Chapter 2), we cannot perform an analysis of seismic velocity changes that require a homogeneous change.

In the Mid-Atlantic Ridge study, in Saint Peter and Saint Paul Archipelago (Chapter 3), we were able to detect four different medium changes related to different earthquakes. From this analysis, we could determine that the post-seismic recovery tends to be fast in

the Mid-Atlantic Ridge environment. Indeed, we observe a full recovery in approximately 1 to 2 months for the data in 2012 and 2014. For the 2013 data, we do not observe a full recovery because of technical problem but in 2 weeks, we could already observe a 87% recovery. We also observe, for the events of 2012 and 2014, that the medium recovers rapidly in the early stage of the post-seismic period and then takes a longer time to fully recover as also observed in previous studies (Li and Vidale, 2001; Schaff and Beroza, 2004; Sawazaki et al., 2009). A full study of the three years of available data at SPSPA could give some more information about the healing process near the Mid-Atlantic Ridge. That is why the preliminary results shown in Chapter 3.6 seems important and that it is worth to continue into this research.

References

Aki, K. (1969), Analysis of seismic coda of local earthquakes as scattered waves, *J. Geophys. Res.*, 74, 615–631.

Assumpção, M. (1983), A regional magnitude scale for Brazil, *Bull. Seism. Soc. Am.* 73, 237-246.

Assumpção, M., G. Suárez, and J.A.V. Veloso (1985), Fault plane solutions of intraplate earthquakes in Brazil: Some constraints on the regional stress field, *Tectonophysics* 113, 283–293.

Baisch, S., and G.H.R. Bokelmann (2001), Seismic waveform attributes before and after the Loma Prieta earthquake: Scattering change near the earthquake and temporal recovery, *J. Geophys. Res.* 106, 16323– 16337.

Bensen, G.D., M.H. Ritzwoller, M.P. Barmin, A.L. Levshin, F. Lin, M.P. Moschetti, N.M. Shapiro, and Y. Yang (2007), Processing seismic ambient noise data to obtain reliable broad-band surface wave dispersion measurements, *Geophys. J. Int.* 169, 1239–1260.

Bensen, G.D., M.H. Ritzwoller, M.P. Barmin, A.L. Levshin, F. Lin, M.P. Moschetti, N.M. Shapiro, and Y. Yang (2008), Broad-band ambient noise surface wave tomography across the United States, *J. Geophys. Res. 113*, B05306, doi: 10.1029/2007JB005248.

Bensen, G.D., M.H. Ritzwoller, and Y. Yang (2009), A 3-D shear velocity model of the crust and uppermost mantle beneath the United States from ambient seismic noise, *Geophys. J. Int.* 117, 1177-1196, doi: 10.1111/j.1365-246X.2009.04125.x.

Berrocal, J., M. Assumpção, R. Antezana, C.M. Dias Neto, R. Ortega, H. França, and J.A.V. Veloso (1984), Seismicity of Brazil. *Brazilian Commission of Nuclear Energy*.

Bezerra, F.H.R., A.F. do Nascimento, J.M. Ferreira, F.C. Nogueira, R.A. Fuck, B.B Brito Neves, and M.O.L. Sousa (2011), Review of active faults in the Borborema Province, Intraplate South America - Integration of seismological and paleoseismological data, *Tectonophysics* 510, 269–290.

Bonatti, E. (1990), Subcontinental mantle exposed in the Atlantic Ocean on St Peter-Paul islets, *Nature* 345, 800-802.

Bosl, W.J., and A. Nur (2002), Aftershocks and pore fluid diffusion following the 1992 Landers earthquake, *J. Geophys. Res.* 107, 2366–2368.

Brenguier, F., N.M. Shapiro, M. Campillo, V. Ferrazzini, Z. Duputel, O. Coutant, and A. Nercessian (2008a), Towards forecasting volcanic eruptions using seismic noise, *Nat. Geosci.* 1, 126–130.

Brenguier, F., M. Campillo, C. Hadziioannou, N.M. Shapiro, R. Nadeau, and E. Larose (2008b), Postseismic relaxation along the San Andreas fault at Parkfield from continuous seismological observations, *Science* 321, 1478–1481.

Brito Neves, B.B., E.J. Santos, and W.R. Van Schmus (2000), Tectonic history of the Borborema Province, northeastern Brazil. In: Cordani, U., Milani, E.J., Thomaz Filho, A., Campos, D.A. (Eds.), Tectonic Evolution of South America: Proceedings of the 31st International Geological Congress, Rio de Janeiro, pp. 151–182.

Campillo, M., and A. Paul (2003), Long-range correlations in the diffuse seismic coda, *Science* 299, 547–549.

Campos, T. F. C., F. H.R. Bezerra, N. K. Srivastava, M. M. Vieira, and C. Vita-Finzi (2010), Holocene tectonic uplift of the St Peter and St Paul Rocks (Equatorial Atlantic) consistent with emplacement by extrusion, *Marine Geology* 271, 177-186, doi: 10.1016/j.margeo.2010.02.013

Cho, K., R.B. Herrmann, C.J. Ammon, and K. Lee (2007), Imaging the upper crust of the korean peninsula by surface-wave tomography, *Bull. seism. Soc. Am.* 67, 198–207.

Chen, J.H., B. Froment, Q.Y. Liu, and M. Campillo (2010), Distribution of seismic wave speed changes associated with the 12 May 2008 Mw 7.9 Wenchuan earthquake, *Geophys. Res. Lett.*, 37(18), doi:10.1029/2010GL044582.

Claerbout, J.F. (1968), Synthesis of a layered medium from its acoustic transmission response, *Geophysics* 33, 264–269.

D'Hour, V., M. Schimmel, A. F. Do Nascimento, J.M. Ferreira, and H.C. Lima Neto

(2015), Detection of subtle hydromechanical medium changes caused by a small magnitude earthquake swarm in NE Brazil, *Pure Appl. Geophys.*, in press.

Derode, A., E. Larose, M. Tanter, J. de Rosny, A. Tourin, M. Campillo, and M. Fink (2003), Recovering the Green's function from field-field correlations in an open scattering medium, *J. acoust. Soc. Am.* 113, 2973–2976.

Dias, R.C., J. Julià, and M. Schimmel (2014), Rayleigh-Wave, Group-Velocity Tomography of the Borborema Province, NE Brazil, from Ambient Seismic Noise, *Pure Appl. Geophys*. 172, 1429-1449, doi: 10.1007/s00024-014-0982-9.

Do Nascimento, A.F., P.A. Cowie, R.J. Lunn, and R.G. Pearce (2004), Spatio-temporal evolution of induced seismicity at Acu reservoir, NE Brazil, *Geophys. J. Int.* 158, 1041-1052.

Do Nascimento, A.F., R.J. Lunn, and P.A. Cowie (2005), Modeling the heterogeneous hydraulic properties of faults using constraints from reservoir-induced seismicity, *J. Geophys. Res.* 110, B09201.

Do Nascimento, A.F., R.J. Lunn, and P.A. Cowie (2005), Numerical modelling of pore-pressure diffusion in a reservoir-induced seismicity site in northeast Brazil. *Geophys. J. Int.* 160, 249-262.

Ferreira, J.M., R.T. Oliveira, M.K. Takeya, and M. Assumpção (1998), Superposition of local and regional stresses in northeast Brazil: evidence from focal mechanisms around the Potiguar marginal basin, *Geophys. J. Int.* 134, 341–355.

Ferreira, J.M., F.H.R. Bezerra, M.O.L Sousa, A.F. Do Nascimento, J.M. Sá, and G.S. França (2008), The role of Precambrian mylonitic belts and present-day stress field in the coseismic reactivation of the Pernambuco lineament, Brazil, *Tectonophysics* 456, 111–126.

Gavrilenko, P. (2005), Hydromechanical coupling in response to earthquakes : on the possible consequences for aftershocks, *Geophys. J. Int.* 161, 113–129.

Gavrilenko, P., C. Singh, and R.K. Chadha (2010), Modelling the hydromechanical response in the vicinity of the Koyna reservoir (India): Results for the initial filling period, *Geophys. J. Int.* 183, 461–477.

Grêt, A. (2004), Time-Lapse Monitoring with Coda Wave Interferometry, Doctoral

Thesis Geophysics, Center for Wave Phenomena, Colorado School of Mines Golden, Colorado, USA.

Grêt, A., R. Snieder, R.C. Aster, and P.R. Kyle (2005), Monitoring rapid temporal changes in a volcano with coda wave interferometry, *Geophys. Res. Lett.* 32, L06304, doi: 10.1029/2004GL021143.

Grêt, A., R. Snieder, and U. Ozbay (2006), Monitoring in situ stress changes in a mining environment with coda wave interferometry, *Geophys. J. Int.* 167, 504–508, doi:10.1111/j.1365-246X.2006.03097.x.

Groenenboom, J., and R. Snieder (1995), Attenuation, Dispersion and Anisotropy by Multiple Scattering of Transmitted Waves Through Distributions of Scatterers, *J. Acoust. Soc. Am.* 98, 3482–3492.

Hadziioannou, C., E. Larose, A. Baig, P. Roux, and M. Campillo (2011), Improving temporal resolution in ambient noise monitoring of seismic speed, *J. geophys. Res.* 116, B07304.

Hobiger, M., U. Wegler, K. Shiomi, and H. Nakahara (2012), Coseismic and postseismic elastic wave velocity variations caused by the 2008 Iwate-Miyagi Nairiku earthquake, Japan, *J. Geophys. Res.* 117, B09313, doi:10.1029/2012JB009402.

Hobiger, M., Wegler, U., Shiomi, K., and Nakahara, H. (2014), Single-station cross-correlation analysis of ambient seismic noise: application to stations in the surroundings of the 2008 Iwate-Miyagi Nairiku earthquake, *Geophys. J. Int.* 198.

Khatiwada, M., L. Adam, M. Morrison, and K. van Wijk (2012), A feasibility study of time-lapse seismic monitoring of CO2 sequestration in a layered basalt reservoir, *J. Appl. Geophys.* 82, 145–152. doi:10.1016/j.jappgeo.2012.03.005.

Larose, E., P. Roux, M. Campillo, and A. Derode (2008), Fluctuations of correlations and Green's function reconstruction: role of scattering, *J. Appl. Phys.* 103 (11), 114907–1114907

Larose, E., T. Planès, V. Rossetto, and L. Margerin (2010), Locating a small change in a multiple scattering environment, *Appl. Phys. Lett.* 96, 1-3.

Li, Y., and J. Vidale (2001), Healing of the shallow fault zone from 1994-1998 after the

1992 M7.5 landers, california, earthquake, *Geophys. Res. Lett.*, 28, 2999-3002, doi: 10.1029/2001GL012922.

Li, Y., P. Chen, E. S. Cochran, J. E. Vidale, and T. Burdette (2006), Seismic Evidence for Rock Damage and Healing on the San Andreas Fault Associated with the 2004 M 6.0 Parkfield Earthquake, *Bull. Seismol. Soc. Am.* 96, S349-S363, doi: 10.1785/0120050803.

Lima Neto, H.C., J.M. Ferreira, F.H. Bezerra, M. Assumpção, A.F. Do Nascimento, M. Sousa, and E. Menezes (2013), Upper crustal earthquake swarms in São Caetano: Reactivation of the Pernambuco shear zone and trending branches in intraplate Brazil, *Tectonophysics* 608, 804–811.

Lin, F., M.H. Ritzwoller, J. Townend, M. Savage, and S. Bannister (2007), Ambient noise Rayleigh wave tomography of New Zealand, *Geophys. J. Int.* 170, 649–666, doi:10.1111/j.1365-246X.2007.03414.x.

Liu, Z.K.., and J.L. Huang (2010), Temporal changes of seismic velocity around the Wenchuan earthquake fault zone from ambient seismic noise correlation, *Chinese Journal of Geophysics* 53, 853-863, doi: 10.3969/j.issn.0001-5733.2010.04.010.

Liu, Z., J. Huang, Z. Peng, and J. Su (2014), Seismic velocity changes in the epicentral region of the 2008 Wenchuan earthquake measured from three-component ambient noise correlation techniques, *Geophys. Res. Lett.* 41, 37–42, doi:10.1002/2013GL058682.

Lobkis, O.I., and R.L. Weaver (2001), On the emergence of the Green's function in the correlations of a diffuse field, *J. acoust. Soc. Am.* 110, 3011–3017.

Lopes, A.E.V., M. Assumpção, A.F. Do Nascimento, J.M. Ferreira, E.a.S. Menezes, and J.R. Barbosa (2010), Intraplate earthquake swarm in Belo Jardim, NE Brazil: reactivation of a major Neoproterozoic shear zone (Pernambuco Lineament), *Geophys. J. Int.* 180, 1303-1312.

Maeda, T., K. Obara, and Y. Yukutake (2010), Seismic velocity decrease and recovery related to earthquake swarms in a geothermal area, *Earth, Planets and Space* 62, 685-691.

Meier, U., N. Shapiro, and F. Brenguier (2010), Detecting seasonal variations in seismic

velocities within Los Angeles Basin from correlations of ambient seismic noise, *Geophys. J. Int.* 181, 985–996.

Michelson, A.A. and E.W. Morley (1987), On the Relative Motion of the Earth and the Luminiferous Ether, *Amer. J. Sci.* 34, 333-345.

Miguens, A.P. (1995), Navegação Costeira, Estimada e em Águas Restritas. Volume I. Diretoria de Hidrografia e Navegação da Marinha, Rio de Janeiro.

Miller, S.A., C. Collettini, L. Chiaraluce, M. Cocco, M. Barchi, and B.J.P. Kaus (2004), Aftershocks driven by a high-pressure CO2 source at depth, *Nature* 427, 724-27.

Minato, S., T. Tsuji, S. Ohmi, and T. Matsuoka (2012), Monitoring seismic velocity change caused by the 2011 Tohoku-oki earthquake using ambient noise records, *Geophys. Res. Lett.* 39, L09309.

Mordret, A., A. Jolly, Z. Duputel, and N. Fournier (2010), Monitoring of phreatic eruptions using Interferometry on Retrieved Cross-Correlation Function from Ambient Seismic Noise: Results from Mt. Ruapehu, New Zealand, *J. Vol. Geotherm. Res.* 191, 46–59.

Moschetti, M.P., M.H. Ritzwoller, and N.M. Shapiro (2007), Surface wave tomography of the western United States from ambient seismic noise: Rayleigh wave group velocity map, *Geochemistry, Geophysics, Geosystems* 8, Q08010, doi:10.1029/2007GC001655.

Motoki, A., S.E. Sichel, T.F. da Costa Campos, N.K. Srivastava, and R. Soares (2009), Taxa de soerguimento atual do arquipélago de São Pedro e São Paulo, Oceano Atlântico Equatorial, *REM: R. Esc. Minas*, Ouro Preto, 62(3): 331-342.

Murakami, H, N. Oshiman, S. Yamaguchi, T. Hashimoto, and R. Yoshimur (2007), Time evolution of hydraulic and electrokinetic parameters around the Nojima fault, Japan, estimated by an electrokinetic method, *Tectonophysics*, 443, 200-208.

Nakahara, H. (2015), Auto Correlation Analysis of Coda Waves from Local Earthquakes for Detecting Temporal Changes in Shallow Subsurface Structures: the 2011 Tohoku-Oki, Japan Earthquake, *Pure Appl. Geophys.* 172, 213–224.

Nishida, K., J. Montagner, and H. Kawakatsu (2009), Global surface wave tomography

using seismic hum, *Science* 326 (5949), 112.

Niu, F., P. Silver, R. Nadeau, and T. McEvilly (2003), Migration of seismic scatterers associated with the 1993 Parkfield aseismic transient event, *Nature* 426, 544-548.

Nur, A., and J.R. Booker (1972), Aftershocks caused by pore fluid flow?, *Science* 175, 885-887.

Obermann, A., T. Planès, E. Larose, and M. Campillo (2013), Imaging preeruptive and coeruptive structural and mechanical changes of a volcano with ambient seismic noise, *J. Geophys. Res.*, 118, 6285-6294, doi:10.1002/2013JB010399.

Ohmi, S., K. Hirahara, H. Wada, and K. Ito (2008), Temporal variations of crustal structure in the source region of the 2007 Noto Hanto earthquake, central Japan, with Passive Image Interferometry, *Earth Planets Space* 60, 1069–1074.

Palmiotto, C., L. Corda, M. Ligi, A. Cipriani, H.J.B. Dick, E. Douville, L. Gasperini, P. Montagna, F. Thil, A.M. Borsetti, B. Balestra, and E. Bonatti (2013), Nonvolcanic tectonic islands in ancient and modern oceans, *Geochemistry, Geophysics, Geosystems* 14, 4698-4717, doi:10.1002/ggge.20279.

Peng, Z., and Y. Ben-Zion (2006), Temporal changes of shallow seismic velocity around the Karadere-Duzce Branch of the North Anatolian Fault and strong ground motion, *Pure Appl. Geophys.*, 163, 567–600, doi:10.1007/s00024-005-0034-6.

Poupinet, G., W.L. Ellsworth, and J. Frechet (1984), Monitoring velocity variations in the crust using earthquake doublets: an application to the Calaveras fault, California, *J. Geophys. Res.* 89, 5719–5731.

Pytharouli, S.I., R.J. Lunn, Z.K. Shipton, J.D. Kirkpatrick, and A.F. Do Nascimento (2011), Microseismicity illuminates open fractures in the shallow crust, *Geophys. Res. Lett.* 38, L02402.

Ratdomopurbo, A., and G. Poupinet (1995), Monitoring a Temporal Change of Seismic Velocity in a Volcano: Application to the 1992 Eruption of Mt. Merapi (Indonesia), *Geophys. Res. Lett.* 22, 775–778.

Renard, F., J. P. Gratier, and B. Jamtveit (2000), Kinetics of crack-sealing, intergranular

pressure solution, and compaction around active faults, *Journal of Structural Geology* 22, 1395-1407.

Rickett, J., and J. F. Claerbout (1996), Passive seismic imaging applied to synthetic data, *Stanford Exploration Project Report* 92, 87–94.

Roberts, P. M., W. S. Phillips, and M. C. Fehler (1992), Development of the active doublet method for measuring small velocity and attenuation changes in solids, *J. Acoust. Soc. Am.*, 91(6), 3291–3302.

Robinson, D. J., M. Sambridge, and R. Snieder (2011), A probabilistic approach for estimating the separation between a pair of earthquakes directly from their coda waves, *J. Geophys. Res.*, 116, B04309, doi:10.1029/2010JB007745.

Rojstaczer, S., S. Wolf, and R. Michel (1995), Permeability enhancement in the shallow crust as a cause of earthquake-induced hydrological changes, *Nature* 373, 237-239.

Roux, P., K.G. Sabra, P. Gerstoft, W.A. Kuperman, and M.C. Fehler (2005), P-waves from cross-correlation of seismic noise, *Geophys. Res. Lett.* 32, L19303.

Roux, P., and Y. Ben-Zion (2013), Monitoring fault zone environments with correlations of earthquake waveforms, *Geophys. J. Int.* 196, 1073-1081.

Rubinstein, J. L., and G. C. Beroza (2004), Evidence for widespread non-linear strong ground motion in the Mw 6.9 Loma Prieta earthquake, *Bull. Seismol. Soc. Am.* 94(5), 1595–1608.

Sabra, K. G., P. Gerstoft, P. Roux, and W. A. Kuperman (2005), Surface wave tomography from microseisms in Southern California, *Geophys. Res. Lett.* 32, L14311, doi:10.1029/2005GL023155.

Sausse, J., E. Jacquot, B. Fritz, J. Leroy, and M. Lespinasse (2001), Evolution of crack permeability during fluid-rock interaction Example of the Brézouard granite (Vosges, France), *Tectonophysics* 336, 199-214.

Sawazaki, K., H. Sato, H. Nakahara, and T. Nishimura (2009), Time-lapse changes of

seismic velocity in the shallow ground caused by strong ground motion shock of the 2000 Western-Tottori earthquake, Japan, as revealed from coda deconvolution analysis, *Bull. Seismol. Soc. Am.* 99(1), 352.

Saygin E., and B.L.N. Kennett (2010), Ambient noise tomography for the Australian Continent, *Tectonophysics* 481, 116-125. doi:10.1016/j.tecto.2008.11.013.

Scales, J.A. and R. Snieder (1998), What is noise?, *Geophys*. 63, 1122–1124.

Schaff, D. P., and G. C. Beroza (2004), Coseismic and postseismic velocity changes measured by repeating earthquakes, *J. Geophys. Res.* 109, B10302, doi:10.1029/2004JB003011.

Schaff, D. P. (2012), Placing an upper bound on preseismic velocity changes measured by ambient noise monitoring for the 2004 Mw 6.0 Parkfield earthquake (California), *Bull. Seismol. Soc. Am.* 102(4), 1400–1416, doi:10.1785/0120110342.

Schimmel, M., and Paulssen, H. (1997), Noise reduction and detection of weak, coherent signals through, Geophys. J. Int. 130, 497–505.

Schimmel, M. (1999), Phase Cross-Correlations : Design, Comparisons, and Applications, *Bull. Seismol. Soc. Am.* 89, 5, 1366–1378.

Schimmel, M., and J. Gallart (2007), Frequency-dependent phase coherence for noise suppression in seismic array data, *J. Geophys. Res.* 112, B04303.

Schimmel, M., E. Stutzmann, and J. Gallart (2011), Using instantaneous phase coherence for signal extraction from ambient noise data at a local to a global scale, *Geophys. J. Int.* 184, 494–506.

Sens-Schönfelder, C., and U. Wegler (2006), Passive image interferometry and seasonal variations of seismic velocities at Merapi Volcano, Indonesia, *Geophys. Res. Lett.* 33, L21302.

Shapiro, N.M., M. Campillo, L. Stehly, and M.H. Ritzwoller M.H. (2005), High resolution surface wave tomography from ambient seismic noise, *Science* 307, 1615–1618.

Sibson, R. (1996) Structural permeability of fluid-driven fault-fracture meshes, *J. Struct. Geol.* 18, 1031-1042.

Sichel, S.E., S. Esperança, A. Motoki, M. Maia, S.L.M. Mello, and M.F. Horan (2008), Geophysical and geochemical indications for existence of cold upper mantle beneath the Equatorial Atlantic Ocean, *Revista de Sociedade Brasileira de Geofísica* 26, 69-86.

Simão, N., J. Escartin, J. Goslin, J. Haxel, M. Cannat, and R. Dziak (2010), Regional seismicity of the Mid-Atlantic Ridge: Observations from autonomous hydrophone arrays, *Geophys. J. Int.* 183,1559–1578.

Smith, D.K., J. Escartin, M. Cannat, M. Tolstoy, C.G. Fox, D.R. Bohnenstiehl, and S. Bazin (2003), Spatial and temporal distribution of seismicity along the northern Mid-Atlantic Ridge (15–35N), *J. Geophys. Res.* 108(B3), 2167, doi:10.1029/2002JB001964.

Snieder, R. (2002), Coda wave interferometry and the equilibration of energy in elastic media, *Physical Review* 66, 046615, doi: 10.1103/PhysRevE.66.046615.

Snieder, R., Grêt, A., Douma, H., and Scales, J. (2002), Coda wave interferometry for estimating nonlinear behaviour in seismic velocity, Science 295, 2253-2255.

Snieder, R. (2004a), Coda wave interferometry, in "2004 McGraw-Hill Yearbook of Science &Technology", 54-56, McGraw-Hill, New York.

Snieder R. (2004b), Extracting the Green's function from the correlation of coda waves: a derivation based on stationary phase, *Phys. Rev. E* 69:046610.

Snieder, R., and M. Hagerty (2004), Monitoring change in Volcanic Interiors using Coda Wave Interferometry: Application to Arenal Volcano, Costa Rica, *Geophys. Res. Lett.* 31, L09608, doi:10.1029/2004GL019670.

Snieder, R., and M. Vrijlandt (2005), Constraining the source separation with coda wave interferometry: Theory and application to earthquake doublets in the Hayward fault, California, *J. Geophys. Res.*, 110, B04301, doi:10.1029/2004JB003317.

Snieder, R. (2006), The Theory of Coda Wave Interferometry, *Pure Appl. Geophys.* 163, 455-473. doi:10.1007/s00024-005-0026-6

Snieder, R., and J. Page (2007), Multiple scattering in evolving media, *Phys. Today*, 60(5), 49–55, doi:10.1063/1.2743124.

Snieder, R., S. Hubbard, M. Haney, G. Bawden, P. Hatchell, A. Revil, and DOE Geophysical Monitoring Working Group (2007), Advanced Noninvasive Geophysical Monitoring Techniques, *Annu. Rev. Earth Planet. Sci.* 35, 653-83.

Soden, A.M., Z.K. Shipton, R.J. Lunn, S.I. Pytharouli, J.D. Kirkpatrick, A.F. Do Nascimento, and F.H.R. Bezerra (2014), Brittle structures focused on subtle crustal heterogeneities: implications for flow in fractured rocks, *Journal of the Geological Society* 171, 509-524.

Sykes, L.R. (1978), Intraplate seismicity, reactivation of preexisting zones of weakness, alkalinemagmatism, and other tectonism postdating continental fragmentation, *Rev. Geophys. Space Phys.* 16, 621-688.

Takagi, R., T. Okada, H. Nakahara, N. Umino, and A. Hasegawa (2012), Coseismic velocity change in and around the focal region of the 2008 Iwate-Miyagi Nairiku earthquake, *J. geophys. Res.* 117, B06315, doi:10.1029/2012JB009252.

Tenthorey, E., S. F. Cox, and H. F. Todd (2003), Evolution of strength recovery and permeability during fluid-rock reaction in experimental fault zones, *Earth and Planetary Science Letters* 206, 161-172.

Tenthorey, E., and J. Gerald (2006), Feedbacks between deformation, hydrothermal reaction and permeability evolution in the crust: Experimental insights, *Earth and Planetary Science Letters* 247, 117-129, doi:10.1016/j.epsl.2006.05.005

Terakawa, T., A. Zoporowski, B. Galvan, and S. Miller (2010), High- pressure fluid at hypocentral depths in the L'Aquila region inferred from earthquake focal mechanism, *Geology* 38,995-998.

Toksöz, M. N., C. H. Cheng, and A. Timur (1976), Velocities of seismic waves in porous rocks, *Geophysics* 41(4), 621–645, doi:10.1190/ 1.1440639.

Trompette, R. (1994), Geology of Western Gondwana (2000-500 Ma): Pan-African-Brasiliano Aggregation of South America and Africa, Brookfield, A.A. Balkema, Rotterdam.

Villaseñor, A., Y. Yang, M.H. Ritzwoller, and J. Gallart (2007), Ambient noise surface

wave tomography of the Iberian Peninsula: Implications for shallow seismic structure, *Geophys. Res. Lett.* 34, L11304, doi: 10.1029/2007GL030164.

Wapenaar, K. (2004), Retrieving the elastodynamic Green's function of an arbitrary inhomogeneous medium by cross correlation, *Phys. Rev., Lett.* 93, 254301.

Wapenaar, K., D. Draganov, R. Snieder, X. Campman, and A. Verdel (2010a), Tutorial on seismic interferometry. Part 1- basic principles and applications, *Geophysics* 75, 75A 195–75A 209.

Wapenaar, K., E. Slob, R. Snieder and A. Curtis (2010b), Tutorial on seismic interferometry. Part 2 - underlying theory and new advances, *Geophysics* 75, 75A211–75A227.

Wästeby, N., A. Skelton, E. Tollefsen, M. Andrén, G. Stockmann, L. C. Liljedahl, E. Sturkell, and M. Mörth (2014), Hydrochemical monitoring, petrological observation, and geochemical modeling of fault healing after an earthquake, *J. Geophys. Res.*, 119, 5727-5740, doi:10.1002/2013JB010715.

Weaver, R.L., and O.I. Lobkis (2001), Ultrasonics without a source: Thermal fluctuation correlations at MHz frequencies, *Phys. Rev. Lett.* 87, 134301.

Weaver, R.L., and O.I. Lobkis (2002), On the emergence of the Green's function in the correlations of a diffuse field: Pulse-echo using thermal phonons, *Ultrasonics* 40, 435-439, doi:10.1016/S0041-624X(02)00156-7.

Wegler, U., B.G. Lühr, R. Snieder, and A. Ratdomopurbo (2006), Increase of shear wave velocity before the 1998 eruption of Merapi volcano (Indonesia), *Geophys. Res. Lett.* 33, L09303, doi:10.1029/2006GL025928.

Wegler, U., and C. Sens-Schönfelder (2007), Fault zone monitoring with passive image interferometry, *Geophys. J. Int.* 168, 1029–1033.

Wegler, U., H. Nakahara, C. Sens-Schönfelder, M. Korn, and K. Shiomi (2009), Sudden drop of seismic velocity after the 2004 M w 6.6 mid-Niigata earthquake, Japan, observed with Passive Image Interferometry, *J. Geophys. Res.* 114, B06305.

Yang, Y., M.H. Ritzwoller, A.L. Levshin, and N.M. Shapiro (2007), Ambient noise Rayleigh wave tomography across Europe, *Geophys. J. Int.* 168, 259–274.

Yang, Y., M.H. Ritzwoller, F.C. Lin, M. Moschetti, and N.M. Shapiro (2008), Structure

of the crust and uppermost mantle beneath the western United States revealed by ambient noise and earthquake tomography, *J. Geophys. Res.: Solid Earth*, 113(B12).

Yang, Y., Y. Zhen, J. Chen, S. Zhou, S. Celyan, E. Sandvol, F. Tilmann, K. Priestley, T.M. Hear, J.F. Ni, L.D. Brown, and M.H. Ritzwoller (2010), Rayleigh wave phase velocity maps of Tibet and the surrounding regions from ambient seismic noise tomography, *Geochemistry, Geophysics, Geosystems* 11, Q08010, doi:10.1029/2010GC003119

Yao, H., R. Van Der Hilst, and M. De Hoop (2006), Surface-wave array tomography in SE Tibet from ambient seismic noise and two-station analysis: Phase velocity maps, *Geophys. J. Int.* 166(2), 732–744.

Zaccarelli, L., N.M. Shapiro, L. Faenza, G. Soldati, and A. Michelini (2011), Variations of crustal elastic properties during the 2009 l'aquila earthquake inferred from cross-correlations of ambient seismic noise, *Geophys. Res. Lett.* 38, L24304, doi:10.1029/2011GL049750.

Zhao, P., Z. Peng, and K. Sabra (2010), Detecting remotely triggered temporal changes around the Parkfield section of the San Andreas Fault, *Earthquake Sci*. 23, 497-509, doi:10.1007/s11589-010-0748-0.

Zhan, Z., V.C. Tsai, and R.W. Clayton (2013), Spurious velocity changes caused by temporal variations in ambient noise frequency content, *Geophys. J. Int.* 194, 1574–1581.

Annex A

Ambient seismic noise in São Caetano.

This annex complements the results of Chapter 2. It includes a full record section of the auto-correlations obtain for station SOMA, which is similar to Figure 2.4 for station SOJO. Then, we show the similarity for station SOJO, as in Figure 2.8 c, calculated for different lag time. Finally, we included two entire cross-correlograms for the pair of stations SOJO-SOMA and SOJO-SOLC in order to show the similarity and differences between a cross-correlogram before and after the main event.

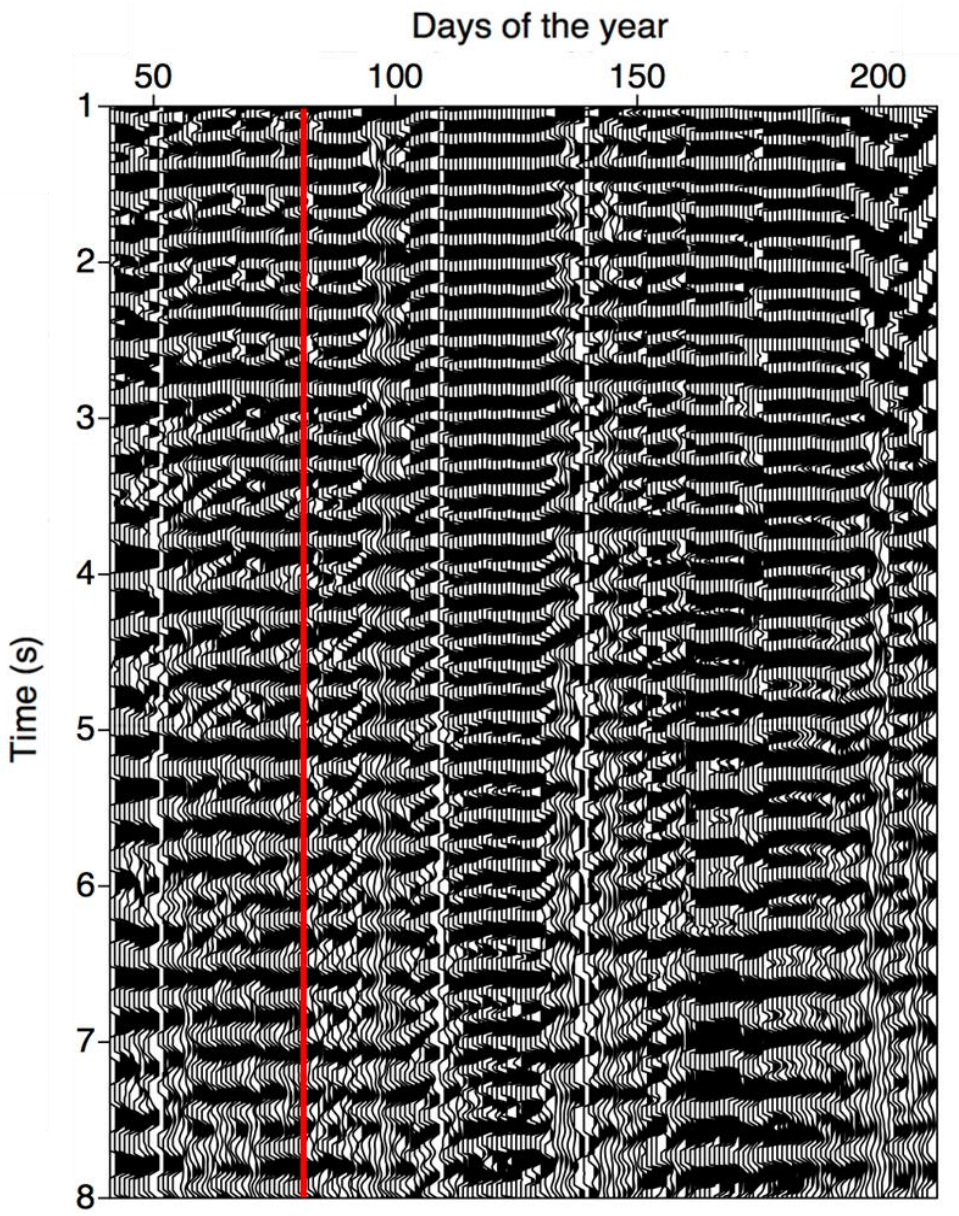

Figure A1: Full record section of the auto-correlations using PCC for the station SOMA from 1 to 9 s. The correlograms have been stacked linearly using a 3-day moving window. The main event is marked by the red line.

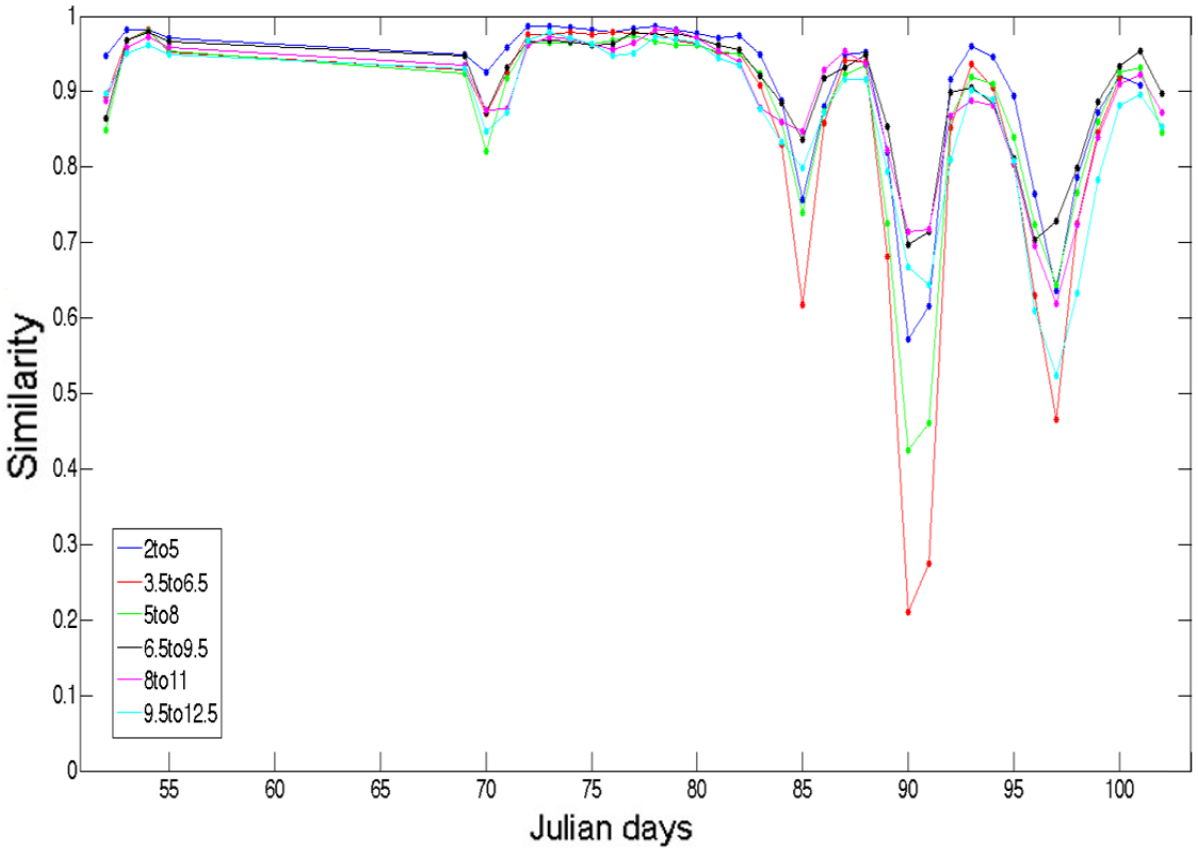

Figure A2: Temporal evolution of the similarity in respect to a reference trace (stack of all the data before the main event) for different lag time window for the station SOJO. It shows that the results is coherent for all the lag time proving that our previous result (Figure 2.8 c) does not depend on the chosen lag time.

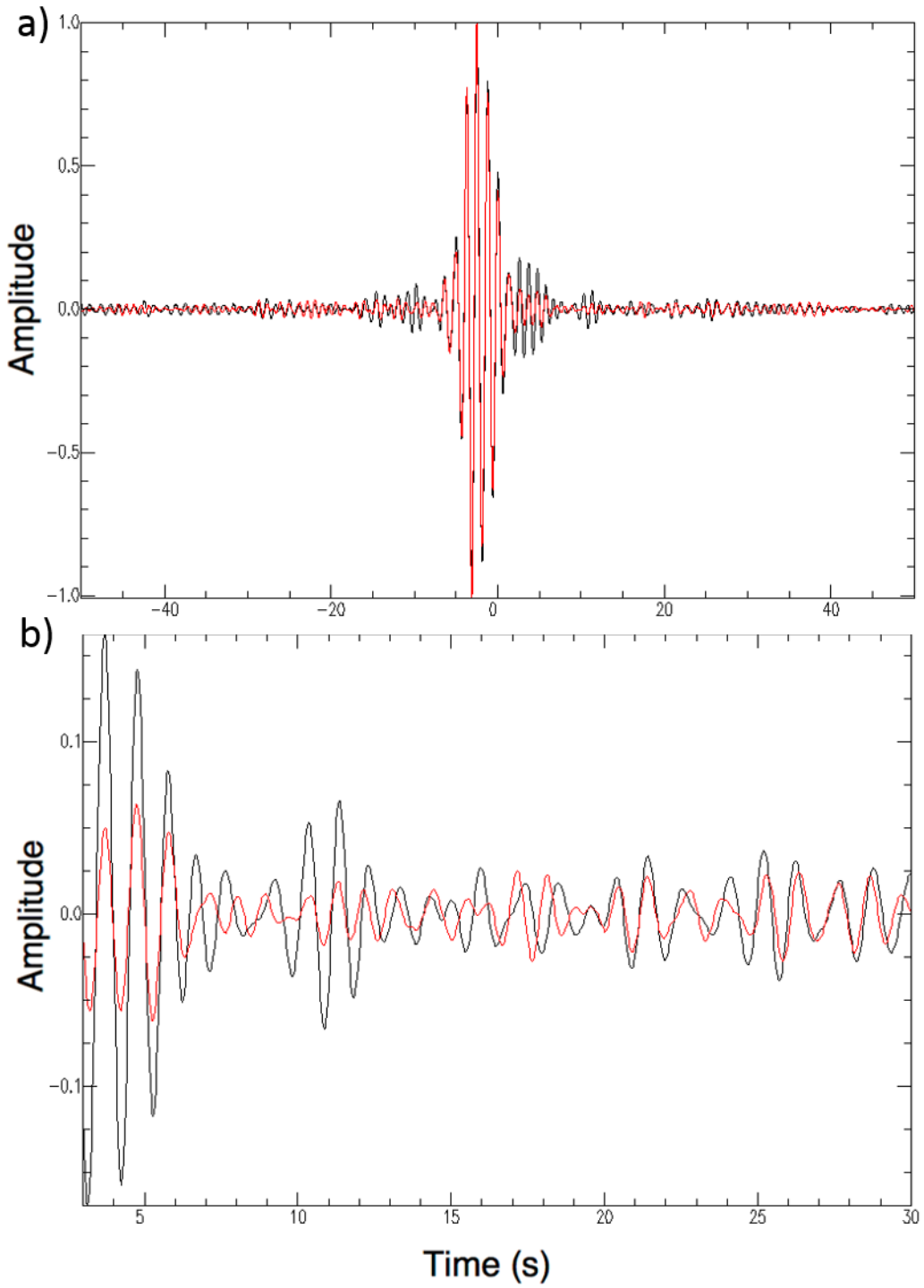

Figure A3: Example of two entire (a) cross-correlograms of the stations SOJO-SOMA. One before (black) the main m_R 3.7 event and the other one after (red). Then we did a zoom (b) to visualize better the difference between the signal before and after the main event.

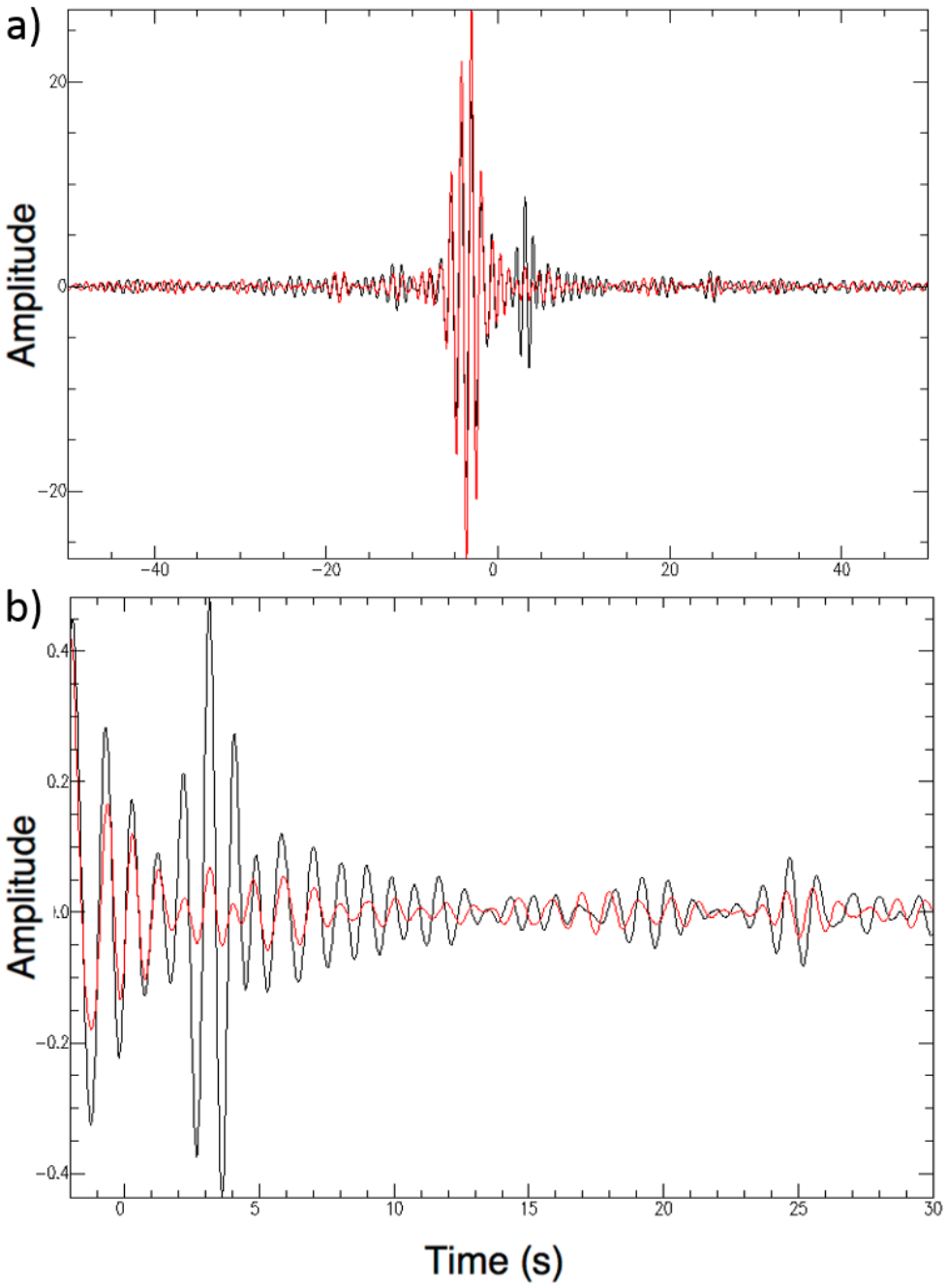

Figure A4: Example of two entire (a) cross-correlograms of the stations SOJO-SOLC. One before (black) the main m_R 3.7 event and the other one after (red). Then we did a zoom (b) to visualize better the difference between the signal before and after the main event.

Annex B

Ambient seismic noise in SPSPA.

This annex complements the results of Chapter 3. It includes an analysis of the seismicity by calculating the kurtosis of 1-3 Hz data. Then, we plotted the spectrograms of some 1-3 Hz data in order to check the results of the kurtosis. After, we complement the results of Figure 3.5, which shows the similarity of the vertical component, by adding the results for the horizontal components. Finally, we show an analysis showing the temporal evolution of the seismic events' location in order to understand better the type of seismicity found in Saint Peter transform fault.

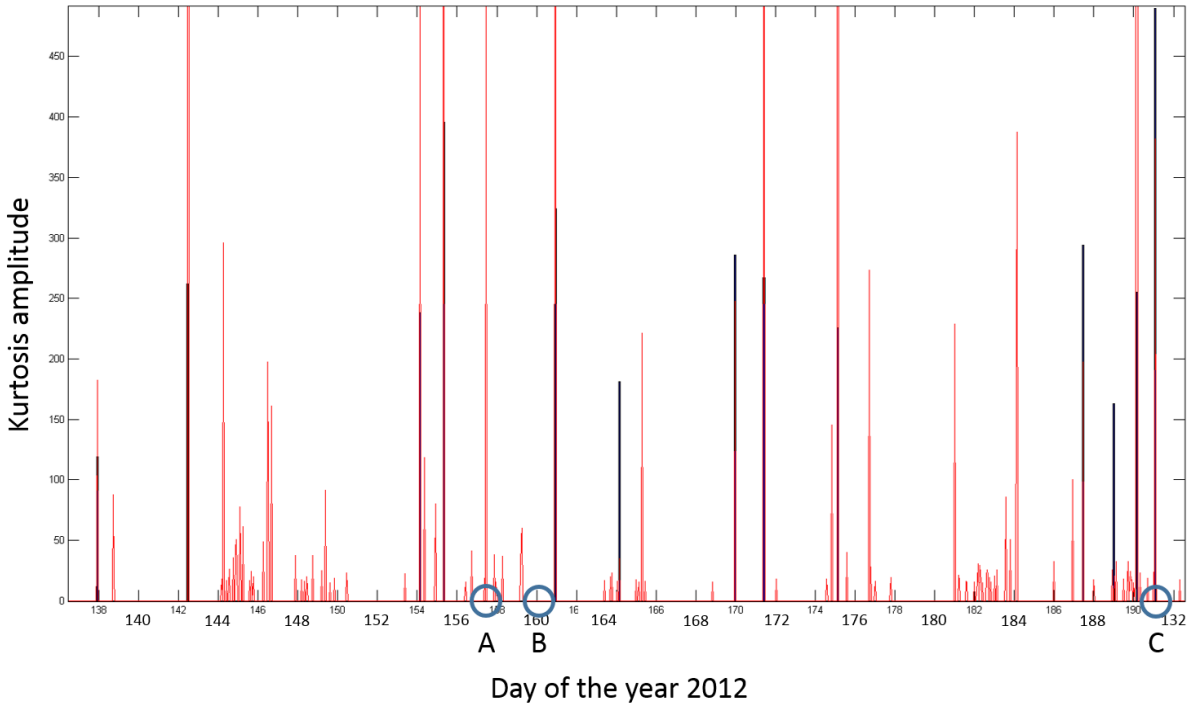

Figure B1: Events (from day 138 to 192) included in the catalogue (black bars) and the one detected with the kurtosis (red) of 1-3 Hz data. Circle A shows an event detected only by the kurtosis. Circle B shows no detected events. Circle C shows an event detected by kurtosis and catalogue.

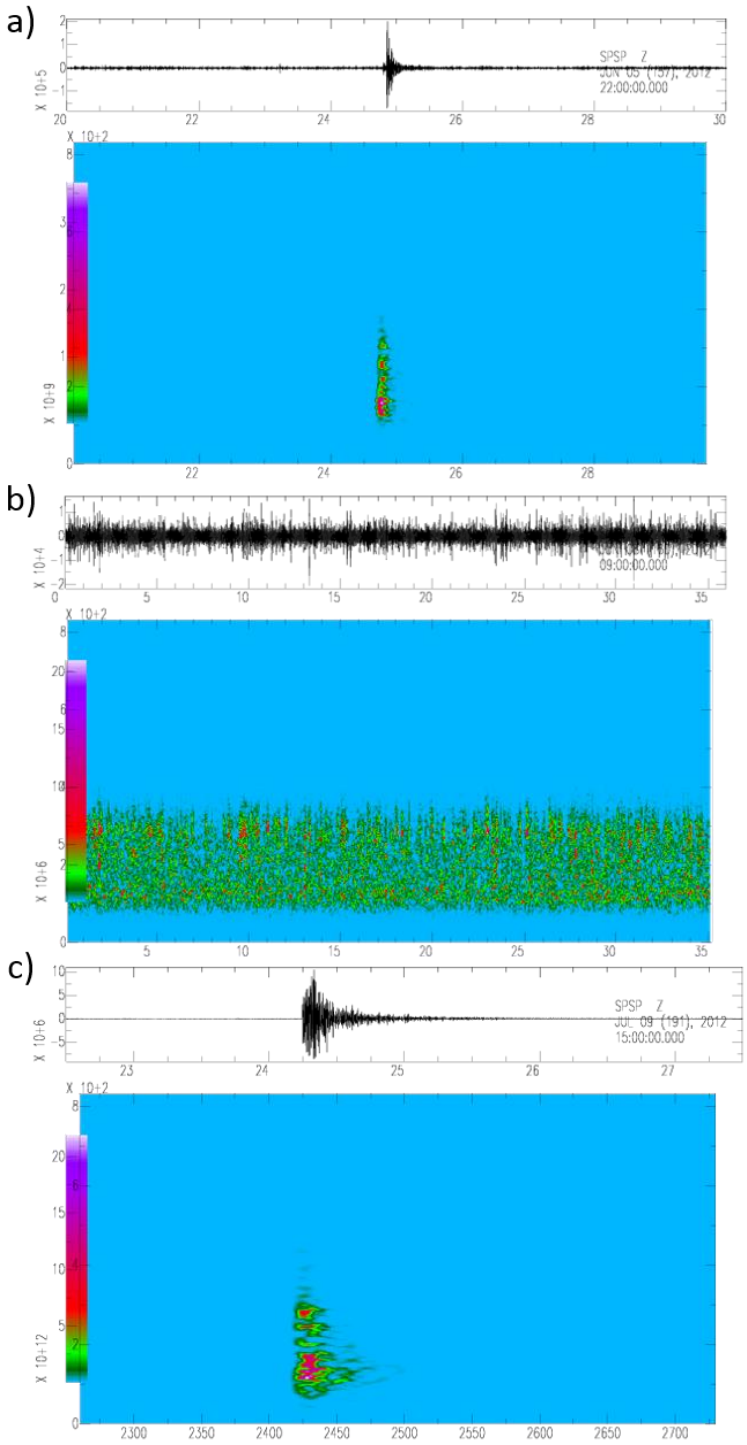

Figure B2: Spectrograms of the events of the circle A (a), circle B (b) and circle C (c) represented in Figure B1. The data have before been filtered 1-3 Hz. It shows that the kurtosis detect accurately the seismic event and is more precise than the catalogue.

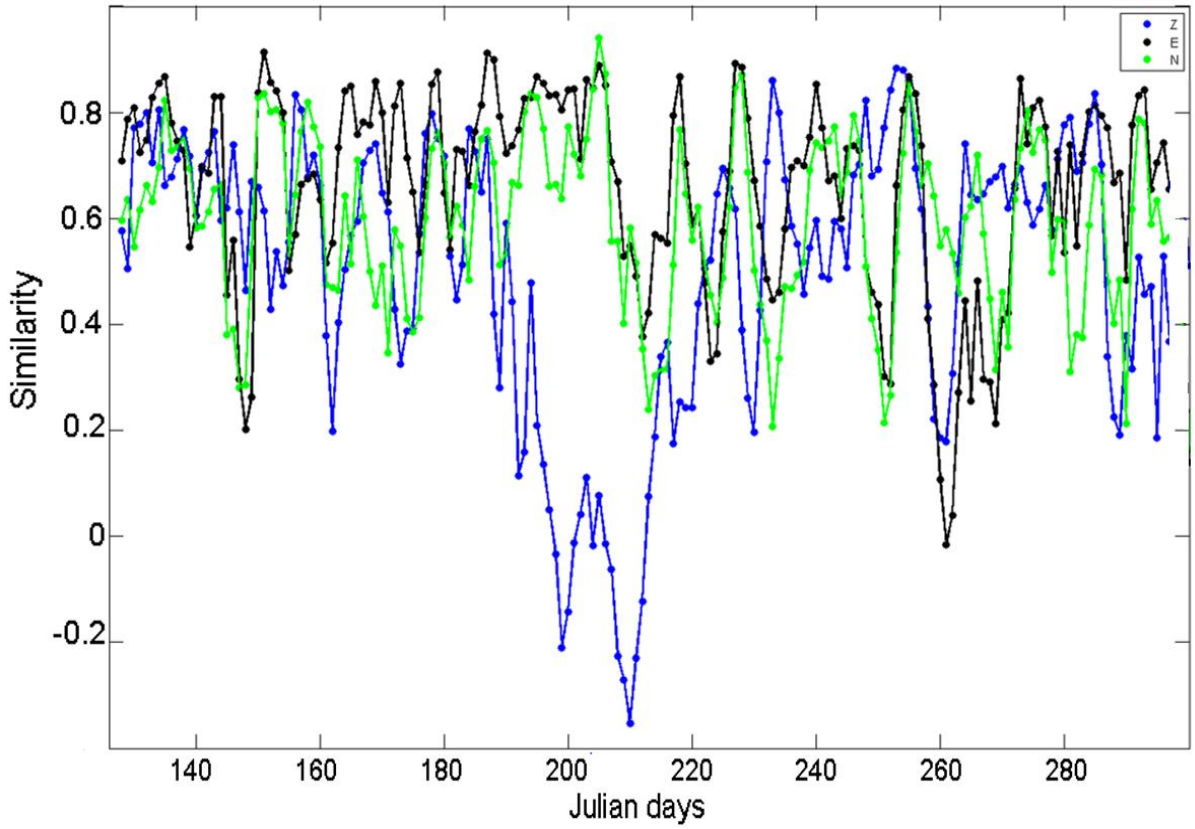

Figure B3: Temporal evolution of the similarity for the vertical (blue) and horizontal (black and green) components. The similarity drop is visible only for the vertical component. For this reason, we did not continue further the investigation of the horizontal component.

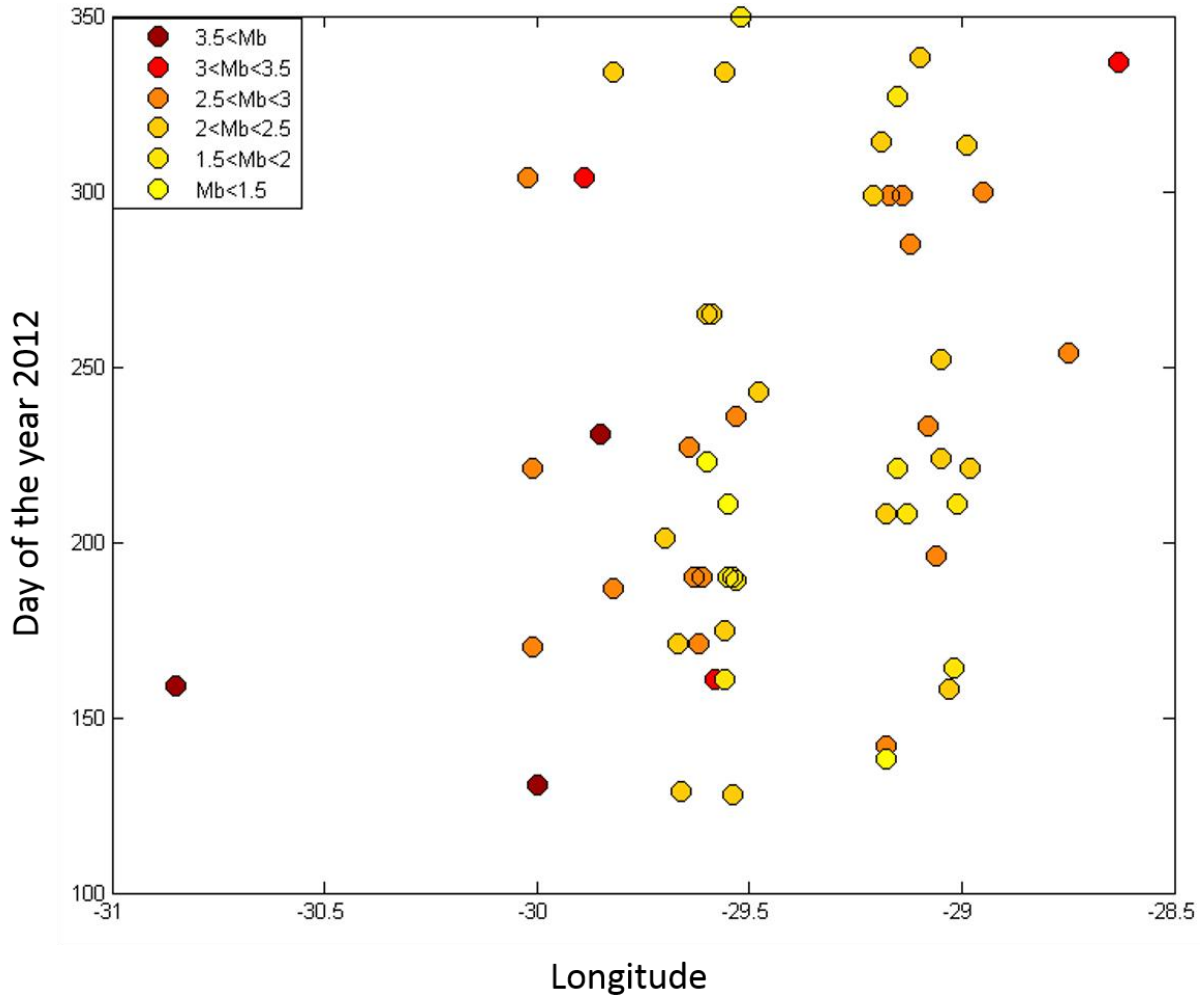

Figure B4: Location of the events along the Saint Paul transform fault as function of their day of occurrence and magnitude. There are no apparent trend. It shows that it is no directionality of the fault growth.

Annex C
Coda wave interferometry in São Caetano.

This annex complements the results of Chapter 5. It shows results for station SOLC evoked in the text page 78 as: a linking tree used to determine the events of a cluster, the result of coda wave's cross-correlation obtain with a 0.3 s and 0.5 s length overlapping window calculated from 0.2 s to 1.2 s. It includes also two figures that are similar to Figures 5.5 and 5.6a obtain for station SOLC, but this time for station SOJO.

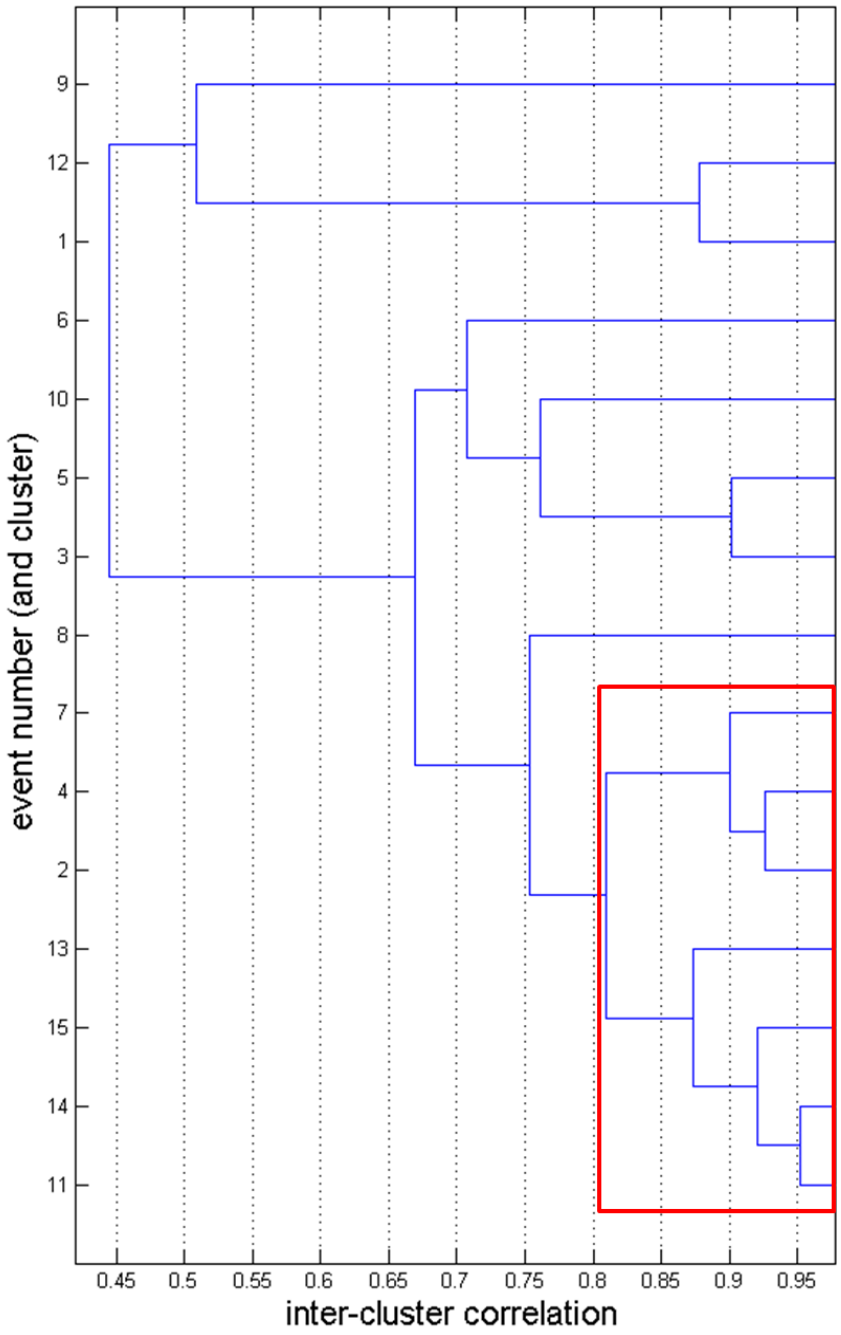

Figure C1: Linking tree showing the link between the events in function of their correlation coefficient. The red square shows the main cluster with P wave correlation coefficient superior at 0.8.

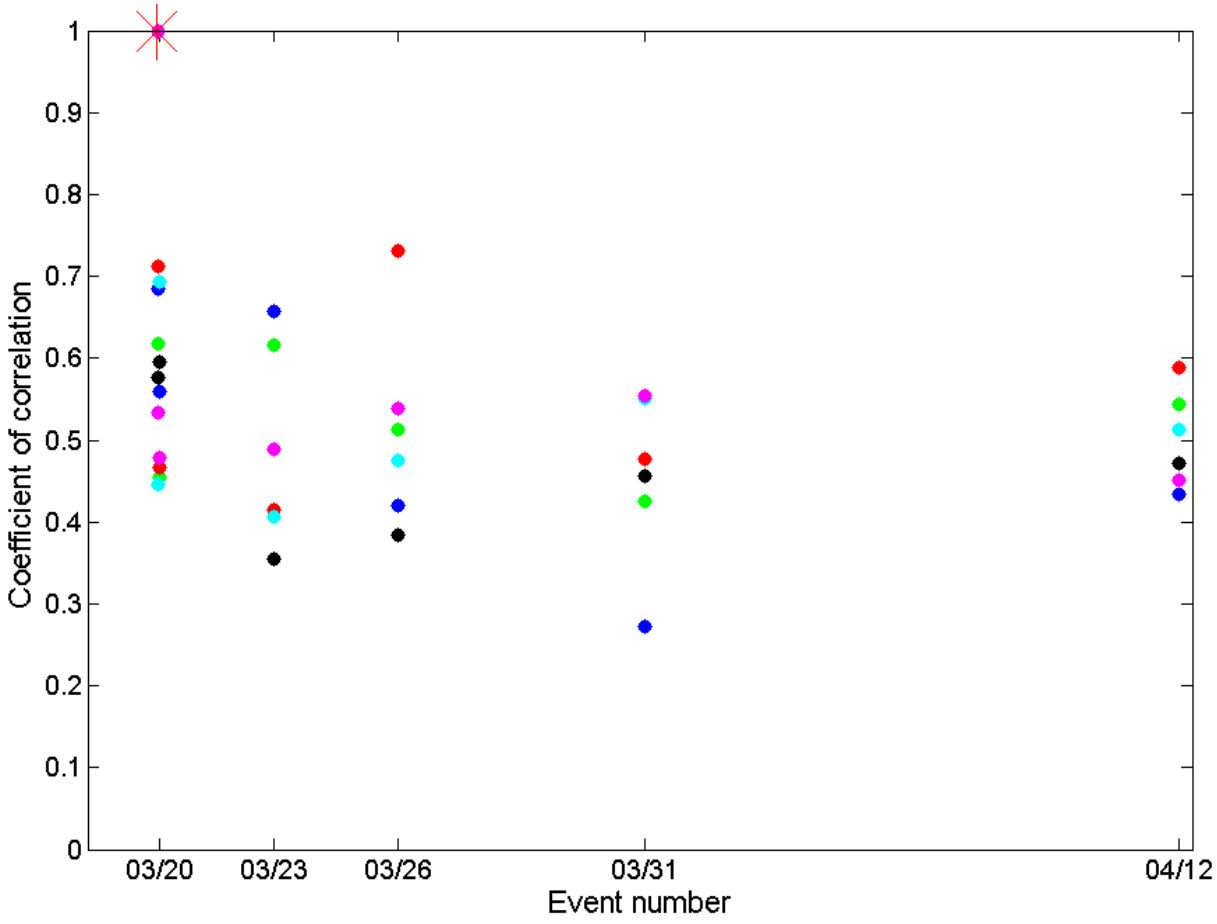

Figure C2: Results of the coda wave's cross-correlation of the main SOLC cluster for different 0.3 s length windows (0.2-0.5 blue, 0.35-0.65 green, 0.5-0.8 red, 0.65-0.95 black, 0.8-1.1 cyan, 0.95-1.25 magenta). It seems that when we use a window further in the coda, the maximum change appears earlier and is less pronounced.

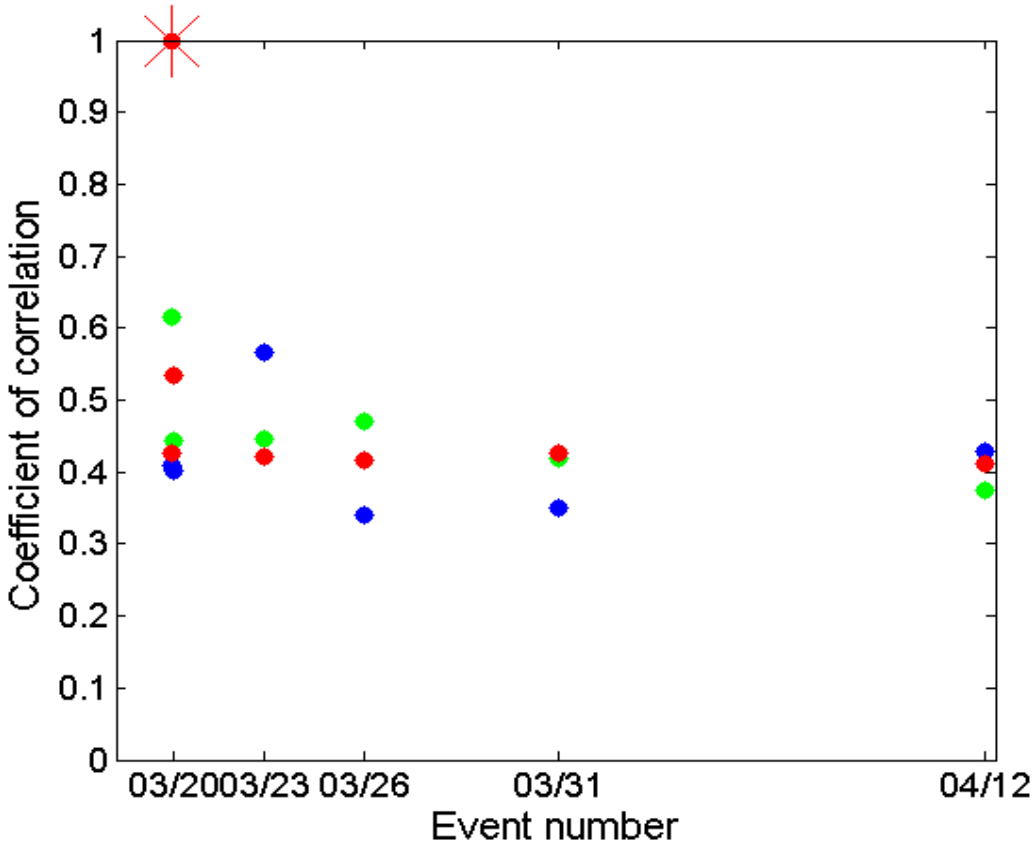

Figure C3: Results of the coda wave's cross-correlation of the main SOLC cluster for different 0.5 s length windows (0.2-0.7 blue, 0.45-0.95 green and 0.7-1.2 red). No trend can be distinguish. A 0.5 s length windows is too long to detect small changes.

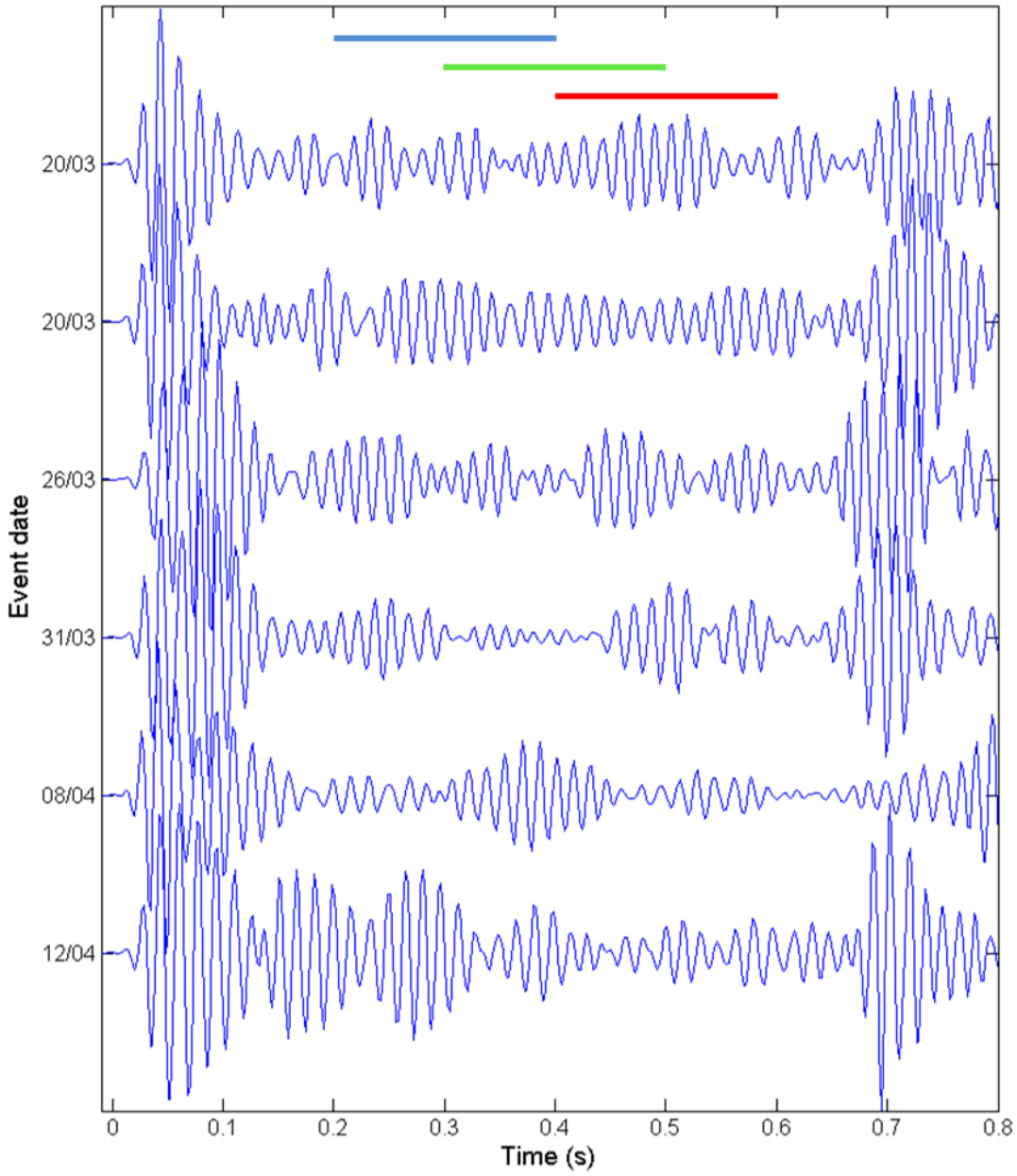

Figure C4: Plot of the traces from the main cluster at station SOJO. The blue, green and red bars on the top indicate the time windows used to calculate the coda waves' cross-correlation between the first trace and the following traces. The corresponding results are shown Figure C5.

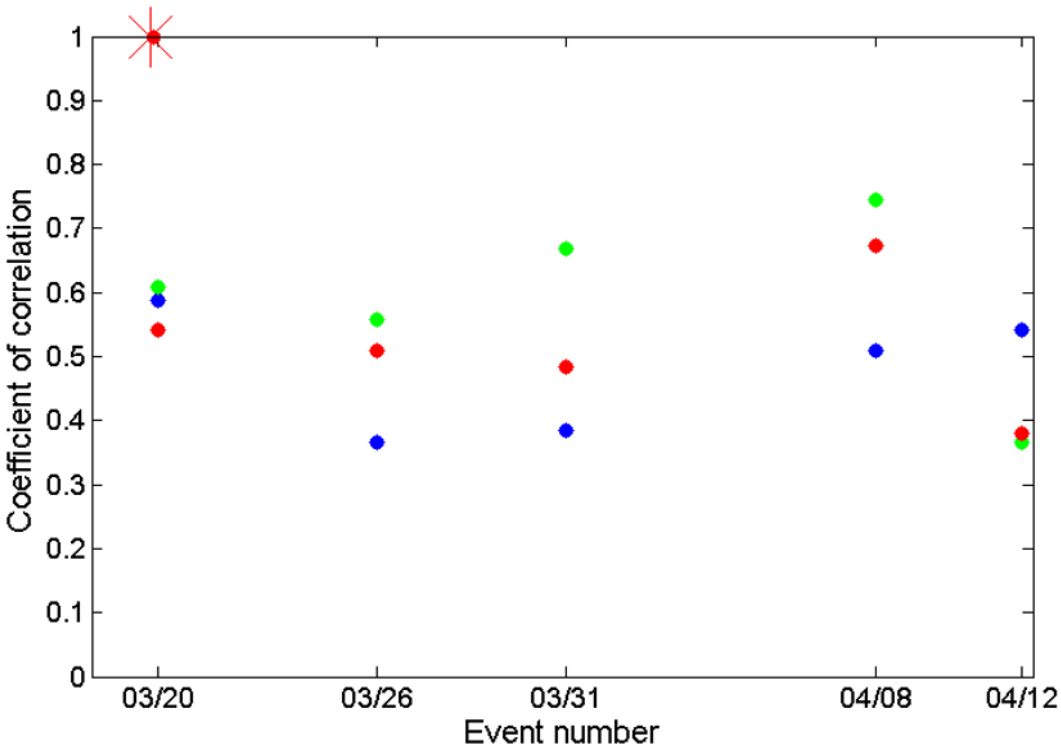

Figure C5: Results of the coda wave's cross-correlation of the main SOJO cluster for the different windows shown in Figure C4 (0.2-0.5 blue, 0.3-0.6 green and 0.4-0.7 red).